AD-A063 487 SRI INTERNATIONAL MENLO PARK CA F/G 13/13
THEORETICAL AND LABORATORY STUDY OF DEEP-BASED STRUCTURES. VOLU--ETC(U)
DEC 77 P E SENSENY, H E LINDBERG DNA001-75-C-0245
UNCLASSIFIED DNA-4425F-1 NL

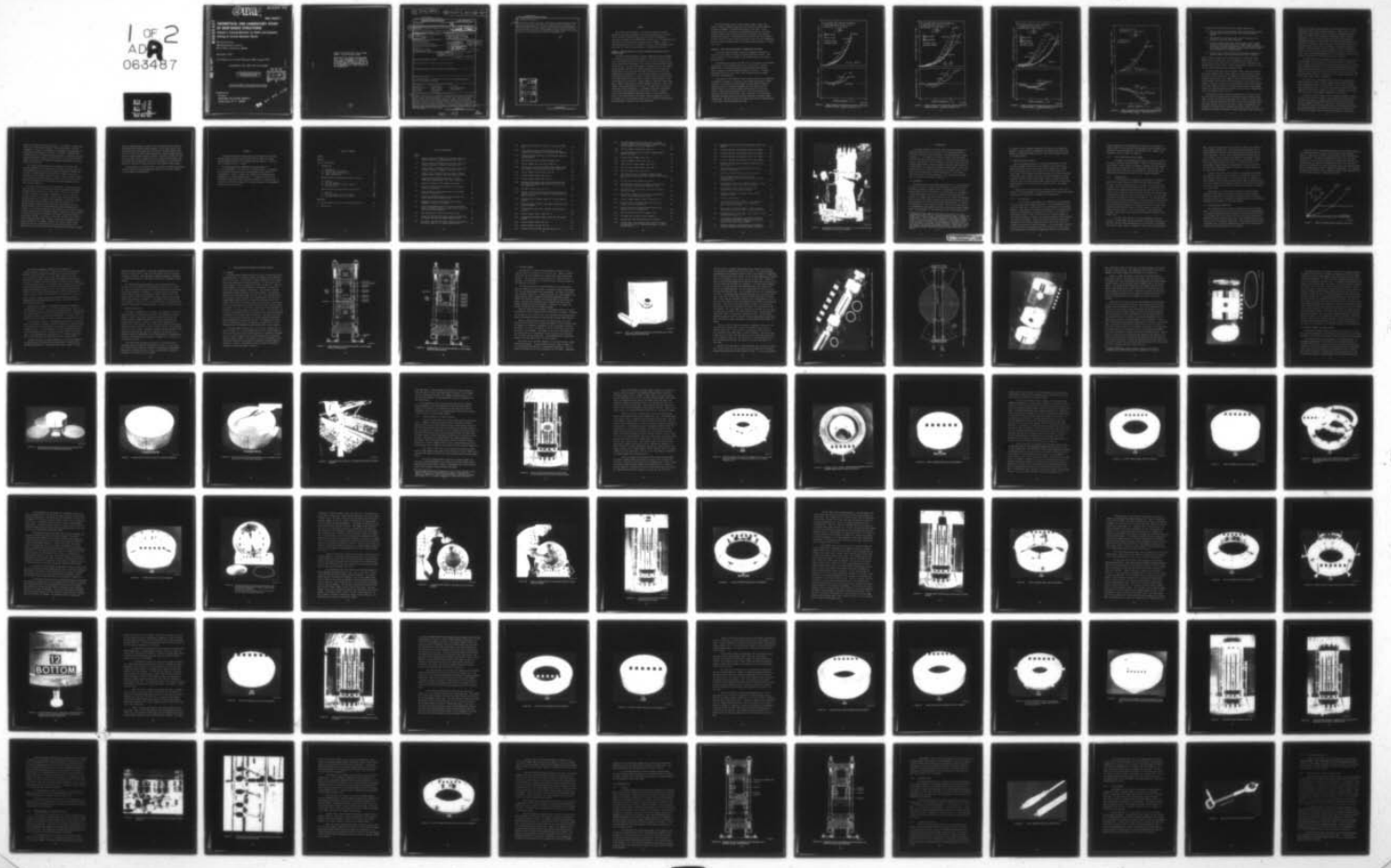

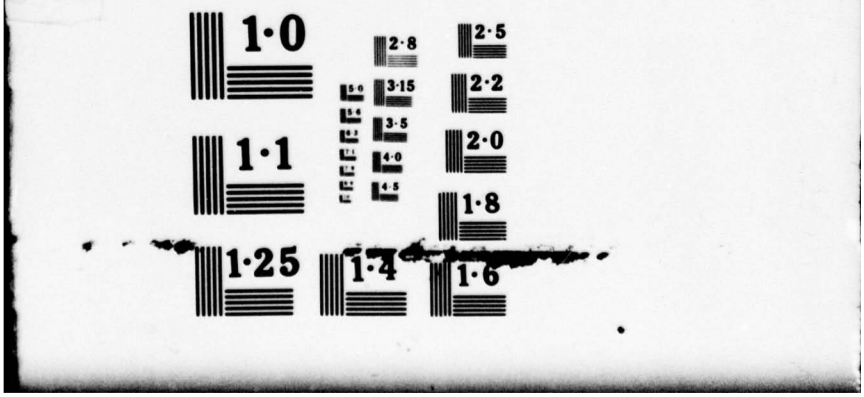

(12) LEVEL II

DNA 4425F-1

THEORETICAL AND LABORATORY STUDY OF DEEP-BASED STRUCTURES

Volume I–Triaxial Machine for Static and Dynamic Testing of 12-inch Diameter Rocks

SRI International
333 Ravenswood Avenue
Menlo Park, California 94025

December 1977

Final Report for Period February 1975—August 1977

CONTRACT No. DNA 001-75-C-0245

THIS WORK SPONSORED BY THE DEFENSE NUCLEAR AGENCY
UNDER RDT&E RMSS CODE B344075462 J34EAXSX31102 H2590D.

Prepared for
Director
DEFENSE NUCLEAR AGENCY
Washington, D. C. 20305

78 11 27 068

Destroy this report when it is no longer needed. Do not return to sender.

PLEASE NOTIFY THE DEFENSE NUCLEAR AGENCY, ATTN: TISI, WASHINGTON, D.C. 20305, IF YOUR ADDRESS IS INCORRECT, IF YOU WISH TO BE DELETED FROM THE DISTRIBUTION LIST, OR IF THE ADDRESSEE IS NO LONGER EMPLOYED BY YOUR ORGANIZATION.

(18) DNA, SBIE

(19) 4425F-1, AD-E300 404

UNCLASSIFIED

SECURITY CLASSIFICATION OF THIS PAGE (When Data Entered)

REPORT DOCUMENTATION PAGE

READ INSTRUCTIONS BEFORE COMPLETING FORM

1. REPORT NUMBER: DNA 4425F-1	2. GOVT ACCESSION NO. (9)
3. RECIPIENT'S CATALOG NUMBER	
4. TITLE (and Subtitle): (6) THEORETICAL AND LABORATORY STUDY OF DEEP-BASED STRUCTURES. Volume I. Triaxial Machine for Static and Dynamic Testing of 12-inch Diameter Rocks.	5. TYPE OF REPORT & PERIOD COVERED: Final Report. Feb 1975—Aug 1977.
	6. PERFORMING ORG. REPORT NUMBER: SRI PYU-4121
7. AUTHOR(s): (10) P.E. Senseny; H.E. Lindberg (Supervisor)	8. CONTRACT OR GRANT NUMBER(s): (15) DNA 001-75-C-0245
9. PERFORMING ORGANIZATION NAME AND ADDRESS: SRI International, 333 Ravenswood Avenue, Menlo Park, California 94025	10. PROGRAM ELEMENT, PROJECT, TASK AREA & WORK UNIT NUMBERS: NWET Subtask J34EAXSX311-02 (16) (17) X311
11. CONTROLLING OFFICE NAME AND ADDRESS: Director, Defense Nuclear Agency, Washington, D.C. 20305	12. REPORT DATE: (11) December 1977 13. NUMBER OF PAGES: 140 (12) 139p. 627104
14. MONITORING AGENCY NAME & ADDRESS (if different from Controlling Office)	15. SECURITY CLASS (of this report): UNCLASSIFIED 15a. DECLASSIFICATION DOWNGRADING SCHEDULE

16. DISTRIBUTION STATEMENT (of this Report)

Approved for public release; distribution unlimited.

17. DISTRIBUTION STATEMENT (of the abstract entered in Block 20, if different from Report)

18. SUPPLEMENTARY NOTES

This work sponsored by the Defense Nuclear Agency under RDT&E RMSS Code B344075462 J34EAXSX31102 H2590D.

19. KEY WORDS (Continue on reverse side if necessary and identify by block number)

Deep Basing	Rock Response	Rock Cavity
Laboratory Testing	Dynamic Testing	Tunnel Reinforcement
Scale Models	Static Testing	Testing Machine
MIGHTY EPIC	DIABLO HAWK	

20. ABSTRACT (Continue on reverse side if necessary and identify by block number)

Design and fabrication of a large-scale testing machine for static and dynamic testing of rock cavity reinforcement is described. The machine is patterned after a smaller prototype developed previously for DNA. The larger-scale machine can be used to apply static and dynamic triaxial loads on specimens that are 12 inches (0.3 m) in diameter and 12 to 18 inches (0.3 to 0.45 m) high, with rock cavities 2 inches in diameter. A variety of triaxial loadings are possible which permit laboratory simulation of different loadings imposed on (over)

DD FORM 1 JAN 73 1473 EDITION OF 1 NOV 65 IS OBSOLETE

UNCLASSIFIED

SECURITY CLASSIFICATION OF THIS PAGE (When Data Entered)

410 281

20. ABSTRACT (Continued)

deep-based structures in the field. The machine can apply vertical pressures up to 2 kbar (0.2 GPa) statically and to 1 kbar (0.1 GPa) dynamically. The maximum lateral pressure is 1.5 kbar (0.15 GPa) statically or dynamically. The testing machine can also be used to apply dynamic loading superimposed on a static preload. The static preload pressures can be as large as 0.2 kbar (0.02 GPa). The tunnel cavity is maintained at ambient pressure, with access at both ends for photography and electrical instrumentation.

1473B

SUMMARY

This project had two goals: (1) develop a large-scale testing machine for laboratory experiments on scale model deep-based structures, and (2) perform a theoretical and laboratory study of deep-based structures in support of the MIGHTY EPIC structures test. Paralleling these these goals, the final report is divided into two volumes: Volume I: Triaxial Machine for Static and Dynamic Testing of 12-Inch-Diameter Rocks, and Volume II: Model Tests and Analysis of MIGHTY EPIC Structures.

Volume I: Triaxial Machine for Static and Dynamic Testing of 12-Inch Diameter Rocks

The first volume describes the design, fabrication, and development of a large-scale testing machine capable of testing specimens 12 inches (0.3 m) in diameter and 12 to 18 inches (0.3 to 0.45 m) in height, three times larger than the specimens for the smaller testing machine developed for DNA at SRI. The large-scale machine incorporates most of the design and operational features of the smaller prototype, but its larger size permits study of more detailed scale model structures and use of more comprehensive instrumentation. Like the small machine, the large-scale testing machine consists of a series of stacked rings and plates secured by 12 high-strength studs that span the distance between plates at the bottom and top of the machine. Using a number of rings and plates rather than a single chamber gives the machine maximum flexibility: static and dynamic testing configurations make use of the same parts in both isotropic and triaxial configurations, although the functions and location of the parts in the machine stack may be quite different. Another feature, also developed with the small prototype, is the provision of ports in the testing machine that permit visual and physical access to the tunnel in the rock specimen during the test, allowing instrumentation and photographic coverage of the tunnel deformation.

The testing machine may be used to apply a range of static and dynamic triaxial loadings, among which are those that simulate symmetric and side-on loadings of deep-based structures in the field. Static loading pressures are applied by two independently operated, air-driven hydraulic pumps; dynamic loading pressures are applied by two separate explosive gas sources. The maximum vertical pressure that can be applied is about 2 kbar (0.2 GPa) statically and about 1 kbar (0.1 GPa) dynamically. For both static and dynamic tests, the maximum lateral pressure is 1.5 kbar (0.15 GPa).

Volume II: Model Tests and Analysis of Mighty Epic Structures

The second volume describes laboratory experiments performed on 4-inch- (0.1-m) diameter specimens containing reinforced tunnels. Theoretical analyses are also included to aid interpretation of the experimental results.

The specimens were made of SRI RMG 2C2, a tuff simulant, and included scale models of five different direct-contact structures fielded in MIGHTY EPIC. The pressures applied to the specimens simulated both side-on (uniaxial strain) loading and symmetric (isotropic) loading of deep-based structures in the field. Both loading types were applied statically and dynamically.

The results of the laboratory tests for each structure are summarized in Figures S.1 through S.4 The first three figures give plots of tunnel closure as a function of applied pressure for three 6061-TO aluminum monocoque liners of different strengths; the fourth gives a plot of tunnel closure as a function of applied pressure for two 1015 steel liners of equal radius-to-thickness ratio. One steel structure was a monocoque liner and the other was a liner stiffened to resist buckling. Specimens containing steel structures were subjected to uniaxial strain loading only. The data in these four figures show that the reproducibility of the tunnel closure measurements is good.

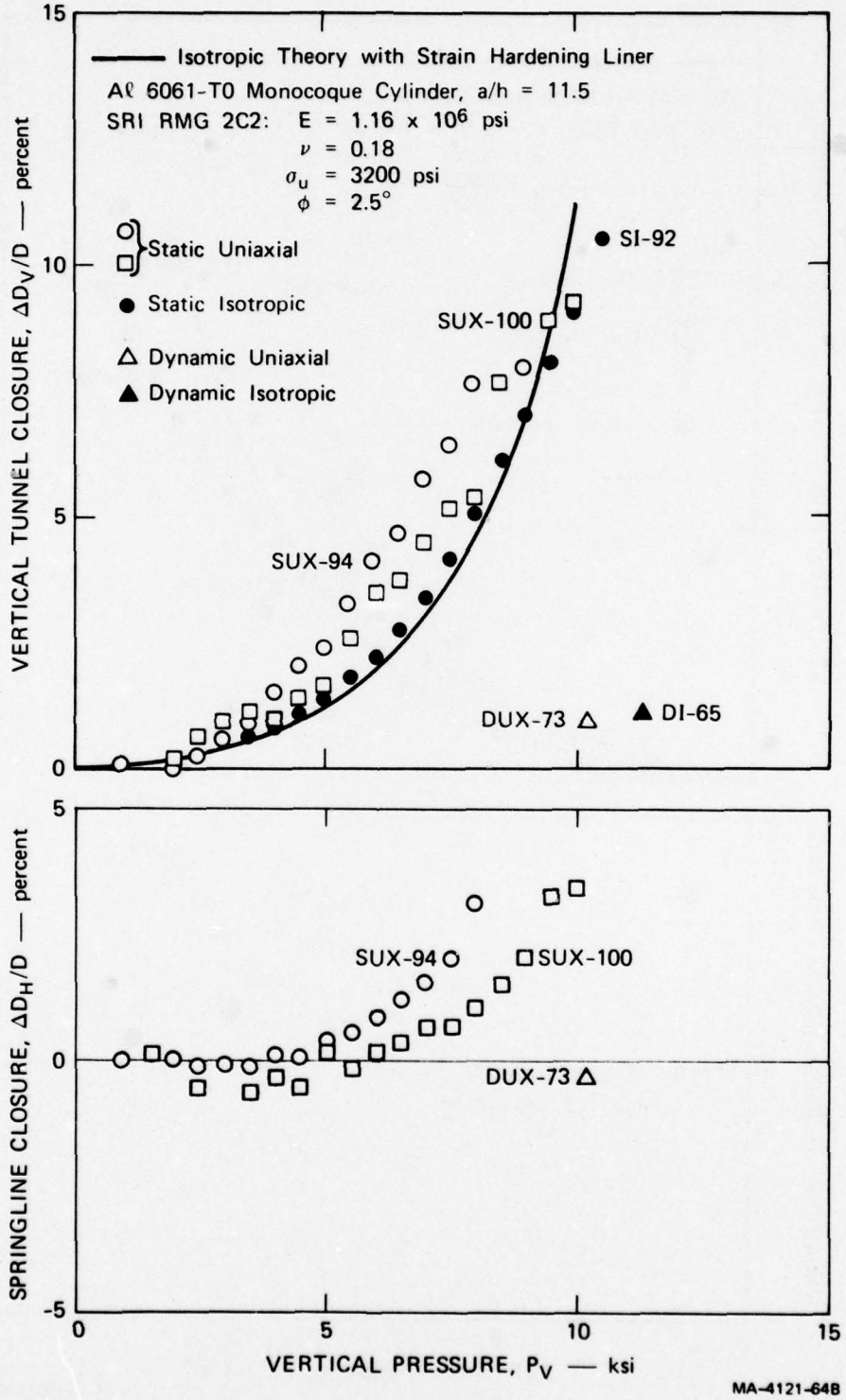

FIGURE S.1 TUNNEL CLOSURE IN SRI RMG 2C2 FOR UNIAXIAL STRAIN AND ISOTROPIC LOADING – Aℓ 6061-T0 LINER, a/h = 11.5

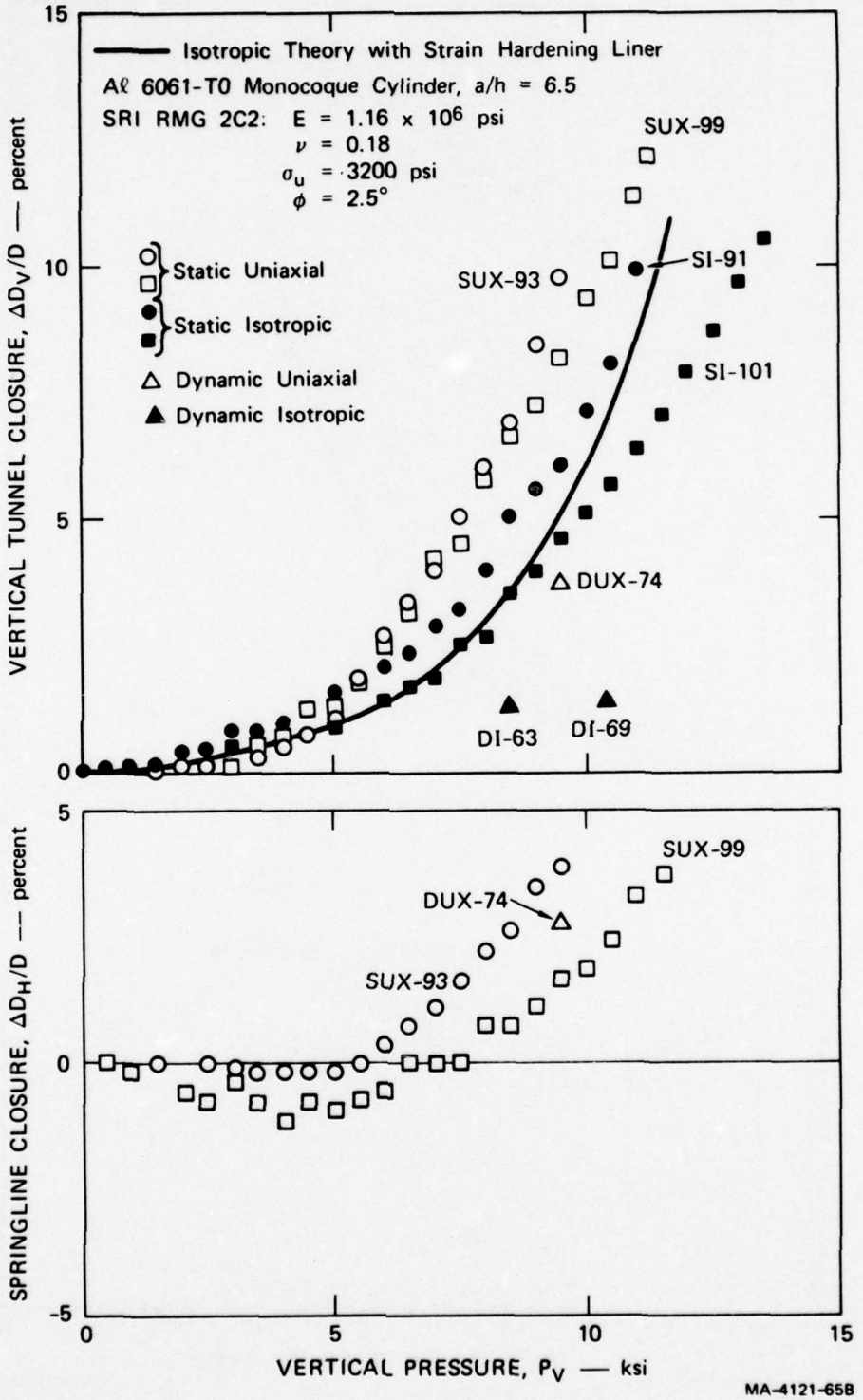

FIGURE S.2 TUNNEL CLOSURE IN SRI RMG 2C2 FOR UNIAXIAL STRAIN AND ISOTROPIC LOADING — Aℓ 6061-T0 LINER, a/h = 6.5

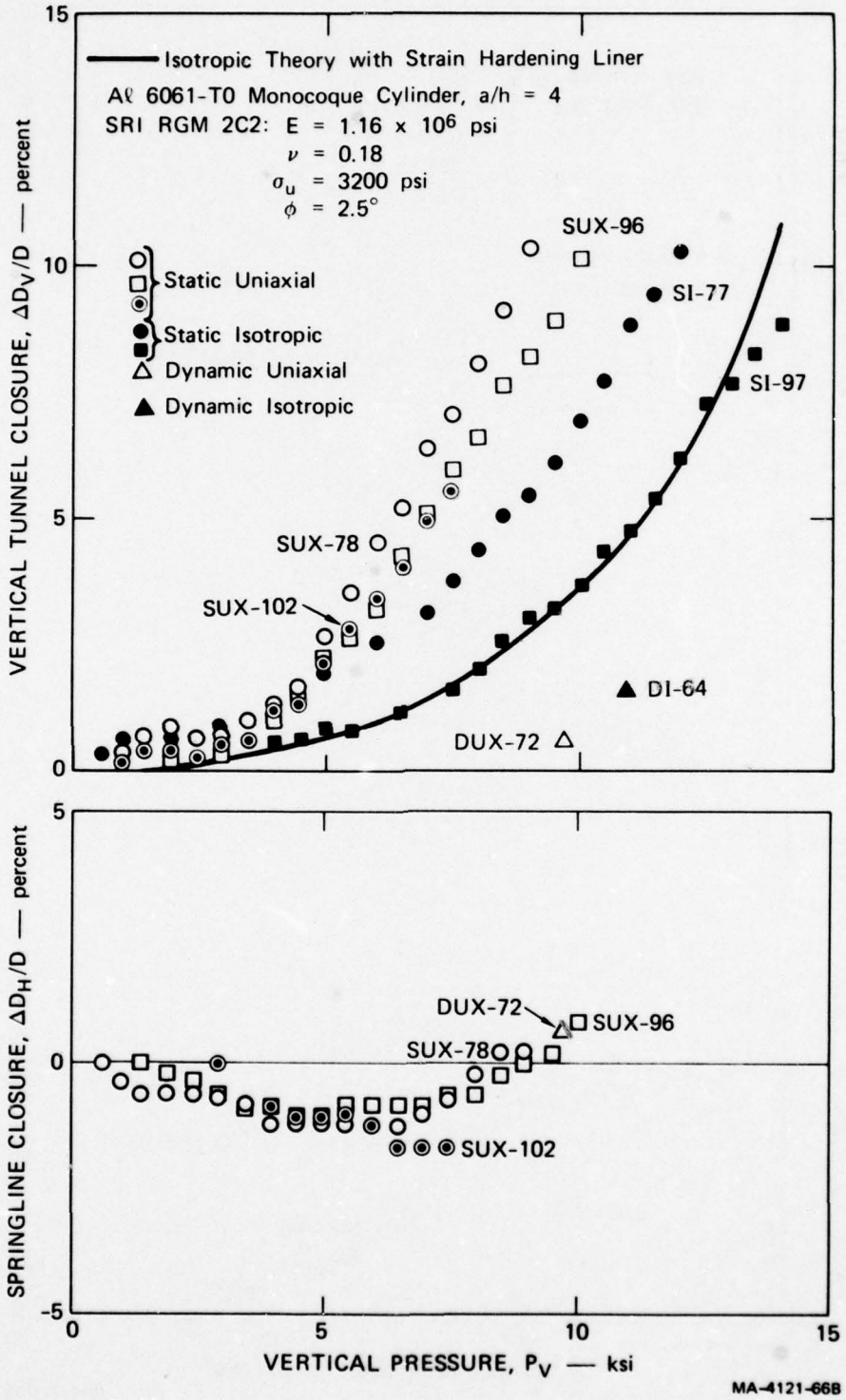

FIGURE S.3 TUNNEL CLOSURE IN SRI RMG 2C2 FOR UNIAXIAL STRAIN AND ISOTROPIC LOADING — Aℓ 6061-T0 LINER, a/h = 4.0

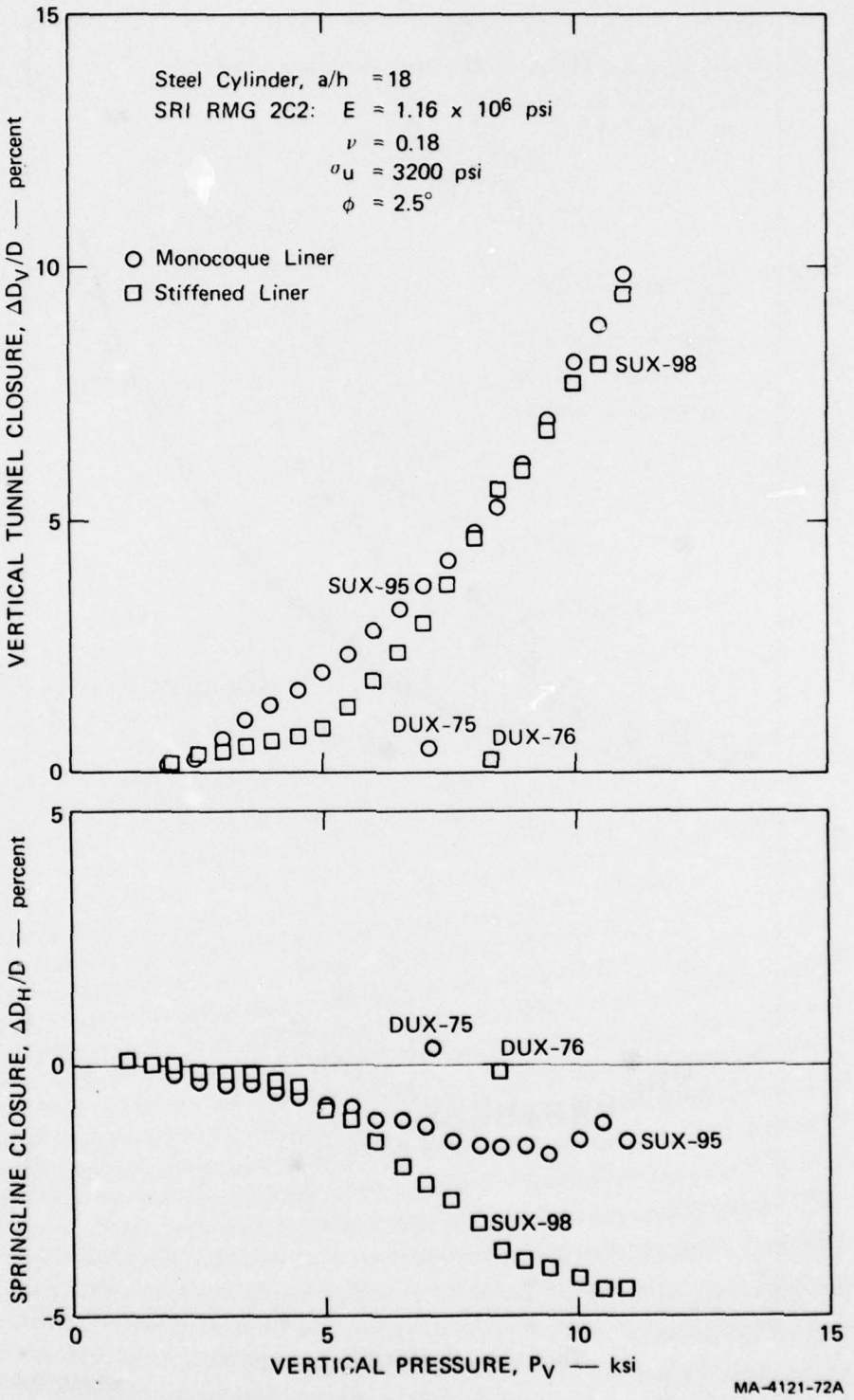

FIGURE S.4 TUNNEL CLOSURE IN SRI RMG 2C2 FOR STATIC AND DYNAMIC UNIAXIAL STRAIN LOADING — 1015 STEEL LINER, a/h = 18

Results of the tests on the Al 6061-TO liners indicate that:

(1) Vertical tunnel closures measured under static isotropic loading are less than those measured under static uniaxial strain loading.

(2) This difference in vertical tunnel closure increases as the strength of the tunnel liner increases.

(3) Tunnel springline motion under static uniaxial strain loading is outward at low pressures and then becomes inward at higher pressures, eventually crossing over to give a final inward closure. The pressure at which springline closure changes sign increases as the strength of the liner increases.

(4) Vertical tunnel closures obtained under dynamic loading are considerably smaller than those obtained under static loading.

Results from the uniaxial strain loading tests with 1015 steel liners support this last observation. Also, springline tunnel motion in the static tests on steel liners tend to follow the pattern observed for the aluminum liners, but the loads at which outward motion ceased are so large that the final springline motion remained outward.

The first result, that static isotropic tunnel closures are smaller than static uniaxial strain tunnel closures, is expected because closure is resisted more efficiently by the symmetric stress field produced by isotropic loading than by the asymmetric stress field produced by uniaxial strain loading. Also, because of the low strength of tuff and the tuff simulant, yielding occurred in the free-field for uniaxial strain loading. This further reduced resistance to closure under uniaxial strain loading because the confining pressure provided by the liner did not significantly control the plastic flow of the rock.

Pursuing this further provides an explanation for the second result, that the difference between static isotropic and static uniaxial strain tunnel closures increases with increasing liner strength. Analysis shows that, for isotropic loading, plastic flow in the rock is localized around the tunnel and that the size of the plastic region is determined by the strength of the tunnel liner; stronger liners better confine the rock, increase its strength, and therefore, permit less plastic flow and closure.

However, for uniaxial strain loading of weak materials like tuff, free-field yield occurs at relatively low pressure. Tunnel closure is still dominated by plastic flow, but since flow is not localized around the tunnel, the role of liner strength in controlling closure is greatly diminished. In fact, our test results show that liner strength has negligible influence on tunnel closure for uniaxial strain loading of the weak tuff-like simulant. This is in contrast with uniaxial strain tests performed on the stronger 6B rock simulant in the previous laboratory program, in which increases in liner strength resulted in systematic reductions in tunnel closure because the material in the free-field did not yield. Thus, in deep basing applications it is important to select a site material strong enough to remain elastic in the free field.

The third result, that springline motion is outward at low pressures and then inward at high pressures, and that the pressure at which this motion changes sign increases as the liner strength increases, is in agreement with NONSAP calculations for uniaxial strain loading of tunnels with various internal pressures. The steel liners tend to follow this same pattern, but the load at which the outward motion ceases is so large that net motion remains outward. The reason for the different behavior of the steel liners needs further investigation.

The fourth result, that dynamic tunnel closures are significantly smaller than static tunnel closures, suggests that porewater pressure has a significant influence on the amount of tunnel closure obtained in tests on saturated rocks. The static tests were performed under drained conditions (zero porewater pressure), while in the dynamic tests loading times are so short that porewater drainage can be neglected.

A theoretical tunnel closure curve for isotropic loading is plotted in each of the first three figures. These curves were calculated with the closed form symmetric loading solution worked out by Hendron and used in designing the MIGHTY EPIC structures. Yielding in the theory is treated with the Mohr-Coulomb yield function and associated flow rule, and strain hardening of the aluminum liner material is accounted for. The theory also assumes that the out-of-plane (along the tunnel axis)

plastic and elastic strains are both zero. It is shown in the main text that, for the low friction angles of tuff-like materials, this last assumption is violated. Nevertheless, the reasonably good agreement between theory and experiment in Figures S.1 through S.3 supports use of the simple theory for preliminary design analysis. Comparisons with more elaborate theoretical results that take account of out-of-plane plastic strain and also model the laboratory experiment loading more closely are given in the main text.

The results relating tunnel liner strength to the static load-carrying capability of the combined rock and tunnel structure, and also the agreement between theory and experiment for symmetric loading, are the same as results obtained from the previous program at SRI with a stronger rock having higher internal friction. These consistent results, over a range of material parameters, indicate that we are correctly relating the response and the most important strength properties of the liner and rock materials.

A series of special tests was also performed. The loading in these tests was static, but it differed from the static monotonic, isotropic, or uniaxial strain loading of the other tests. Results of these tests are shown in Section 6 of Volume II (Figures 6.1, 6.2, 6.3, and 6.6). In two of the tests, one isotropic and the other uniaxial strain, the loading pressures were removed and then reapplied. The results of these two tests show that the reinforced rock cavity shakes down, i.e., during subsequent loading, tunnel closure does not increase until the applied pressure exceeds the maximum pressure applied during previous loadings. In the third special test, the specimen was subjected to uniaxial strain loading followed by isotropic loading to simulate the repeat loading of structures fielded in both MIGHTY EPIC (side-on loading) and DIABLO HAWK (end-on loading). The results of this test show that the structure's load-carrying capability under isotropic loading is not degraded by the initial uniaxial strain loading. Further, the vertical tunnel closure during the isotropic loading portion of the test does not exceed the maximum vertical tunnel closure achieved during the uniaxial strain loading

until the loading pressure is greater than the maximum vertical pressure applied during the uniaxial strain loading. In the fourth special test, a uniaxial strain-like loading test, the lateral confining pressure was held at 0.5 ksi (3.45 MPa) and the specimen was allowed to expand radially until the lateral strain reached 0.1 percent. Results from this test show that the tunnel closure is greater than for uniaxial strain loading, and we conclude that the magnitude of the tunnel closure for a given vertical pressure is sensitive to small deviations from uniaxial strain loading.

We also report on the fabrication of four tunnel reinforcing structures that were tested at Waterways Experiment Station in the static, 30-inch-(0.76-m) diameter testing machine.

PREFACE

The program described in this report was performed for the Defense Nuclear Agency during the period February 1975 to August 1977 under Contract DNA001-75-C-0245. The technical monitors were Dr. K. Goering, LTC D. Burgess, and LTC J. Galloway.

The authors gratefully acknowledge the contributions of Dr. G. R. Abrahamson, J. V. Zaccor, T. D. Witherly, and G. S. Cartwright to the design of the large-scale testing machine and the efforts of W. Wilkinson, J. Busma, T. Henry, and H. Hanna in its fabrication and development. We also acknowledge Drs. L. E. Schwer and K. Preiss for providing the numerical results reported in Volume II. Thanks are due to E. Eckert, L. Dary and W. Heckman for technical support in the experiments reported in the second volume.

TABLE OF CONTENTS

LIST OF ILLUSTRATIONS

MP-4121-100

FIGURE 1.1 LARGE-SCALE TESTING MACHINE LOCATED AT THE SRI CORRAL HOLLOW EXPERIMENTAL SITE, TRACY, CALIFORNIA

1. INTRODUCTION

This report describes the design, fabrication and operation of a large-scale machine which can be used to test large-scale models of deep based structures in the laboratory. The testing machine is shown in Figure 1.1. It consists of a series of stacked rings and plates, which are secured by tightening the nuts on the studs at the bottom and the top of the machine. Use of a number of rings and plates rather than a single chamber gives the machine maximum versatility and flexibility for improvement: by adding and removing a limited number of parts, the machine can be used to perform either static or dynamic tests. In the static tests the specimen is loaded hydraulically. In the dynamic tests the specimen is loaded explosively. The difference in loading rates is more than five orders of magnitude.

1.1 BACKGROUND

For dynamic testing, the design and operation of the testing machine is similar to those of a smaller testing machine in current use in the deep-basing laboratory program at SRI. The development of the small machine demonstrated the feasibility of techniques that are fundamental to performing dynamic tests on rock specimens containing reinforced tunnels. For example, such tests require ports for visual and instrumentation access to the tunnel during the test and sealing systems at these ports and between the vertical and lateral loading fluids. In addition to development of these sealing techniques, work with the small machine also demonstrated that explosive gas sources can provide adequate dynamic loads.* The development of the prototypical small testing machine gave

*Testing machine rise times can be as short as 0.1 msec, close to an appropriately scaled value for modeling underground tests. However, with a model rock of finite length, loading times are increased to several milliseconds in order to eliminate overshoot and oscillations through the column of oil used to apply lateral pressures. This produces psuedo-static response of the tunnel, but at appropriate high strain rates (up to 10 per second at the tunnel boundary) and short loading times to produce dynamic rock skeleton and porewater behavior. Discussions of how this provides adequate simulation are given in references 1 and 2 of Volume I.

us a means to test scale-model deep-based structures in the laboratory. However, to obtain realistic modeling in more complex scale model tests requires rock specimens larger than the 4-inch (0.1-m) diameter possible in the small machine.

1.2 NEED FOR THE LARGE MACHINE

The rock specimens tested in the small testing machine are right circular cylinders 4 inches (0.1 m) in diameter, and 4 inches (0.1 m) high, whereas those tested in the large testing machine are 12 inches (0.3 m) in diameter and 12 to 18 inches (0.3 to 0.45 m) high, three times larger. Data obtained from tests performed on the smaller specimens is limited because the small size limits the kind and amount of instrumentation that can be used to obtain data. Also, the small-scale structures that line the tunnel must be fairly simple because to include great detail in models of this size would be expensive and for some designs impractical.

A large scale testing machine was therefore needed to reduce size effects in the rock specimen, to improve modeling of the tunnel reinforcing structure, and to permit more comprehensive instrumentation.

1.2.1 Rock Specimen

The 12-inch (0.3-m) diameter rock specimen has three advantages over the 4-inch (0.1-m) diameter specimens. First, developmental tests can be performed with a reduced ratio of tunnel diameter to rock specimen diameter. This allows us to examine the influence of the specimen boundaries on the deformation of the rock in the vicinity of the tunnel by performing a series of tests in which the ratio of tunnel diameter to rock specimen diameter is varied. The second advantage is that any grain-size effects are reduced. Because the grain size does not scale, when testing with real rock, any influence of grain size on the tunnel deformation is reduced with larger specimens. A third advantage of testing with the larger rock specimens, and the most important, is that joints and bedding planes surrounding an underground structure can be modeled.

Accurate simulation of the deformation of a structure in jointed rock requires that the joint spacing in the specimen be small compared to the tunnel size but large compared to the rock grain size. Clearly, these constraints require a large rock specimen.

1.2.2 Tunnel Reinforcing Structure Model

The larger rock specimens permit study of large-scale tunnels and tunnel reinforcing structure models. Tunnels in these specimens can be as much as 2 inches (50 mm) in diameter, allowing structural elements such as joints and stiffeners to be incorporated into the model. The larger scale models also admit the possibility of modeling structures fabricated from reinforced concrete or other composite materials.

1.2.3 Instrumentation

In the 4-inch (0.1-m) diameter rock specimens of the smaller machine, the tunnel diameter is 5/8 inch (16 mm), which precludes the use of extensive instrumentation. At present, data collected from a dynamic test on these small specimens consists of measurements of the crown-invert and springline diameters before and after the test, and records of the vertical and lateral pressures and the radial displacement of the specimen's lateral surface as functions of time. For static tests on the small specimens, the data are more complete. The applied lateral pressure and the radial displacement of the rock specimen's lateral surface are recorded as functions of the applied vertical pressure. The crown-invert and springline diameters are measured after each increment in the vertical pressure to yield a curve of tunnel closure as a function of applied vertical pressure. This is in contrast to the single point (residual tunnel closure versus peak vertical pressure) obtained in the dynamic test.

For many cases, however, even more comprehensive data are required. Testing larger tunnels and tunnel reinforcing structures permits more detailed tunnel deformation data to be obtained. For example, the tunnel is large enough to accommodate several closure transducers so

that a record of tunnel closure as a function of time can be obtained at several angular orientations. Still more detailed deformation of the tunnel reinforcing structure can be studied by placing strain gages at several locations. For the 2-inch (50-mm) diameter structures placed in the tunnels of the 12-inch (0.3-m) diameter rock specimens, strain gages are commercially available that permit the measurement of strain over an area small enough to be useful. If the area covered by the strain gage is large compared to the gradients in strain, as would be the case in the smaller specimens, the output of the strain gage will not give useful information.

Testing of the 12-inch (0.3-m) diameter rock specimen also permits the insertion of gages in the rock itself to determine the stress and flow fields around the tunnel. At this larger scale, for example, it may be possible to place small ytterbium stress gages at several positions in the rock specimen to determine the character of the stress field around the tunnel. Passive grids can also be introduced to observe the geometry of the flow field.

An advantage of 12-inch-diameter specimens over larger diameter specimens is that they can be sectioned more easily after testing. Post-test sectioning of the specimen is important because by studying the cross section of the structure and surrounding rock we can investigate mechanisms that contribute to structural failure.

1.3 OVERALL MACHINE CAPABILITIES

The testing machine can be used to perform both static and dynamic tests. In the static tests, the vertical and lateral confining pressures are applied hydraulically with two separately controlled air-driven pumps. In the dynamic tests, the vertical and lateral confining pressures are applied by separate explosive gas sources. Peak pressures are controlled by the size of the explosive charges used. By selecting explosive charges of suitable size, any desired combination of peak vertical pressure and peak lateral confining pressure can be obtained.

Since the vertical and lateral pressures can be controlled separately, the testing machine can be used to apply various triaxial loadings. Figure 1.2 shows several standard load paths that can be followed by the testing machine. The load path designated isotropic has the lateral pressure (P_H) and the vertical pressure (P_V) increasing at the same rate. The loading on the specimen is hydrostatic; however, since this load pathcan be followed in both static and dynamic tests, this type of loading will be called isotropic to allow consistent nomenclature. This load path is significant because it gives a symmetric pressure around the tunnel, as occurs in end-on loading of a deep-based structure.

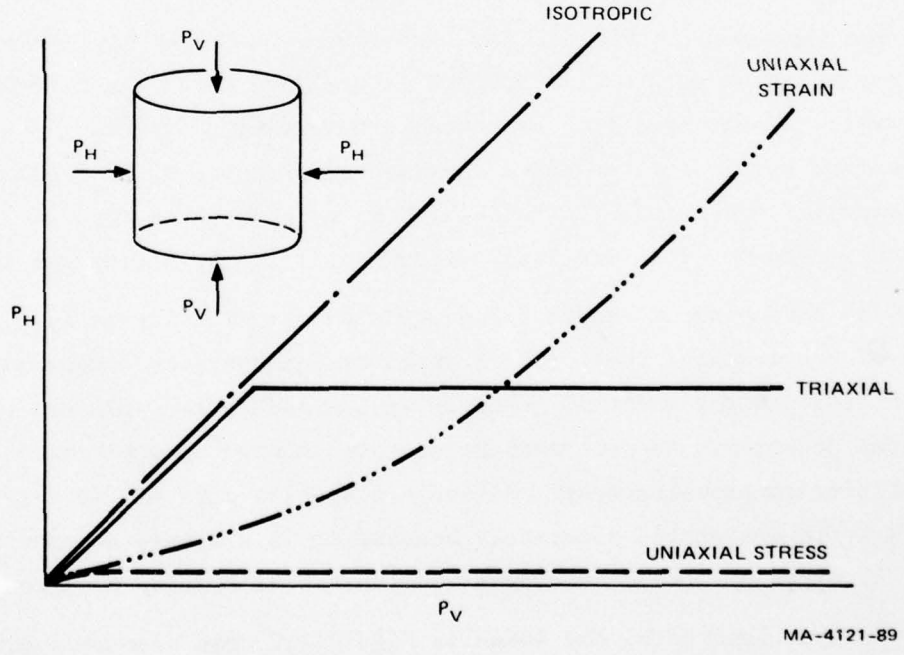

FIGURE 1.2 SCHEMATIC SHOWING SEVERAL STANDARD LOAD PATHS

The load path designated uniaxial strain in Figure 1.1 follows a trajectory in the P_H - P_V plane such that the strain in the specimen far from the tunnel is entirely in the vertical direction, i.e., the lateral pressure, P_H, is just large enough so that the specimen does not expand radially under the applied vertical pressure. This type of loading is important because it simulates side-on loading of a deep-based structure. In the static tests, this path can be followed exactly since pumping rates for the vertical and lateral pumps can be changed independently during the test. In the dynamic tests, however, this path can be followed only approximately, since the shapes of the pressure pulses determine the trajectory of the load path in the P_H - P_V plane. However, loading states near the peak lateral and vertical pressures, where most deformation takes place, can be made to fall on the uniaxial strain line.

The load path in Figure 1.2 designated triaxial is isotropic in the beginning of the test, i.e., the lateral pressure, P_H, is equal to the vertical pressure, P_V, (hydrostatic compression phase). Then, during the second portion of the test, the lateral pressure is held constant and the vertical pressure is increased (shear phase). This type of test is commonly used to determine the failure properties of geological materials.

The load path in Figure 1.2 designated uniaxial stress is a special case of the traixial load path in which the hydrostatic compression phase is omitted and the vertical pressure is applied to the specimen with no lateral pressure. In rock mechanics, this is more commonly called an unconfined compression test. Although a special case of the triaxial test, it is designated separately because it is a simple, common test that is often performed on conventional material testing machines.

Another load path, not shown in Figure 1.2, can also be applied to the specimen with the larger-scale testing machine. Initially, the specimen is subjected to a relatively small static loading. Then the

specimen is loaded dynamically. The dynamic loading may follow an isotropic, uniaxial strain, or some other more general triaxial trajectory in the $P_H - P_V$ plane. This load path is important because it simulates the overburden loading of a deep-based structure and a subsequent weapon loading.

The testing machine was designed so that the maximum vertical pressure that can be applied to the specimen in static tests is 2 kbar (0.2 GPa). This limit is obtained from simple strength and force balance calculations presented in Appendix A. In dynamic tests, the maximum vertical pressure that can be applied is about 1 kbar (0.1 GPa). The dynamic limit is based on calculations of machine stresses and fatigue limits also presented in Appendix A. The maximum lateral pressure that can be applied in either test is 1.5 kbar (0.15 GPa). The maximum static pressures that simulate overburden stresses are about 0.2 kbar (0.02 GPa).

1.4 REPORT ORGANIZATION

The report is presented in two volumes. The remainder of this first volume describes the design and operation of the larger-scale testing machine. Chapter 2 deals with the machine design and operation for dynamic testing, including discussions of specimen preparation and testing machine assembly. Chapter 3 deals with machine design and operation for static testing. Part of this chapter describes the remote-operation control system that is used for static testing. Two appendixes conclude the first volume. Appendix A describes the determination of the maximum vertical pressures that can be applied in the dynamic tests, discusses explosive requirements of the testing machine, and presents an estimate of the maximum static pressures. Appendix B is a table of the testing machine parts.

The second volume discusses the results of a theoretical and laboratory study of scale model deep-based structures. In this study both closed-form and numerical solutions are compared with experimental measurements of tunnel closure in 4-inch (0.1-m) diameter laboratory specimens of SRI RMG 2C2, a tuff simulant.

2. MACHINE DESIGN AND OPERATION FOR DYNAMIC TESTING

2.1 OVERVIEW

The larger-scale testing machine can be used to perform both static and dynamic tests. For dynamic testing, the machine can be stacked in either of two ways. In the dynamic triaxial configuration, the lateral and vertical pressures are applied separately. A cross section of the testing machine in this configuration is shown in Figure 2.1. There are charge chambers at the top and bottom of the machine to provide the vertical and lateral loading, respectively. The specimen is located approximately midway between the two charge chambers. The explosive gases from the top charge chamber load the top of the specimen directly to provide the vertical loading. The explosive gases from the bottom charge chamber pressurize the oil across the Bellofram, and the oil transfers the load to the lateral surface of the specimen. The pressure in the oil surrounding the specimen is measured by three pressure gages, at stations 3, 4, and 5. The pressure in the gas above the specimen is measured by two pressure gages, at stations 1 and 2. The pressure in the oil under the specimen, which reacts the gas pressure above the specimen, is measured by one pressure gage, at station 6. The figure also shows one of the two tunnel access ports that permit high-speed photography and instrumentation access during the test. The hydraulic nuts at the bottom of the machine are used to compress the machine before a test. Their operation is discussed in greater detail later in this chapter.

The second dynamic configuration, the isotropic configuration, is shown in Figure 2.2. In this configuration, only the charge chamber at the top of the machine is used and the specimen is completely surrounded by oil. The oil is loaded by the explosive gases across a Bellofram under the charge chamber. The pressure in the oil surrounding the top and lateral surfaces of the specimen is measured by pressure gages at stations 3, 4, and 5. The pressure in the oil under the specimen is measured by the pressure gage at station 6.

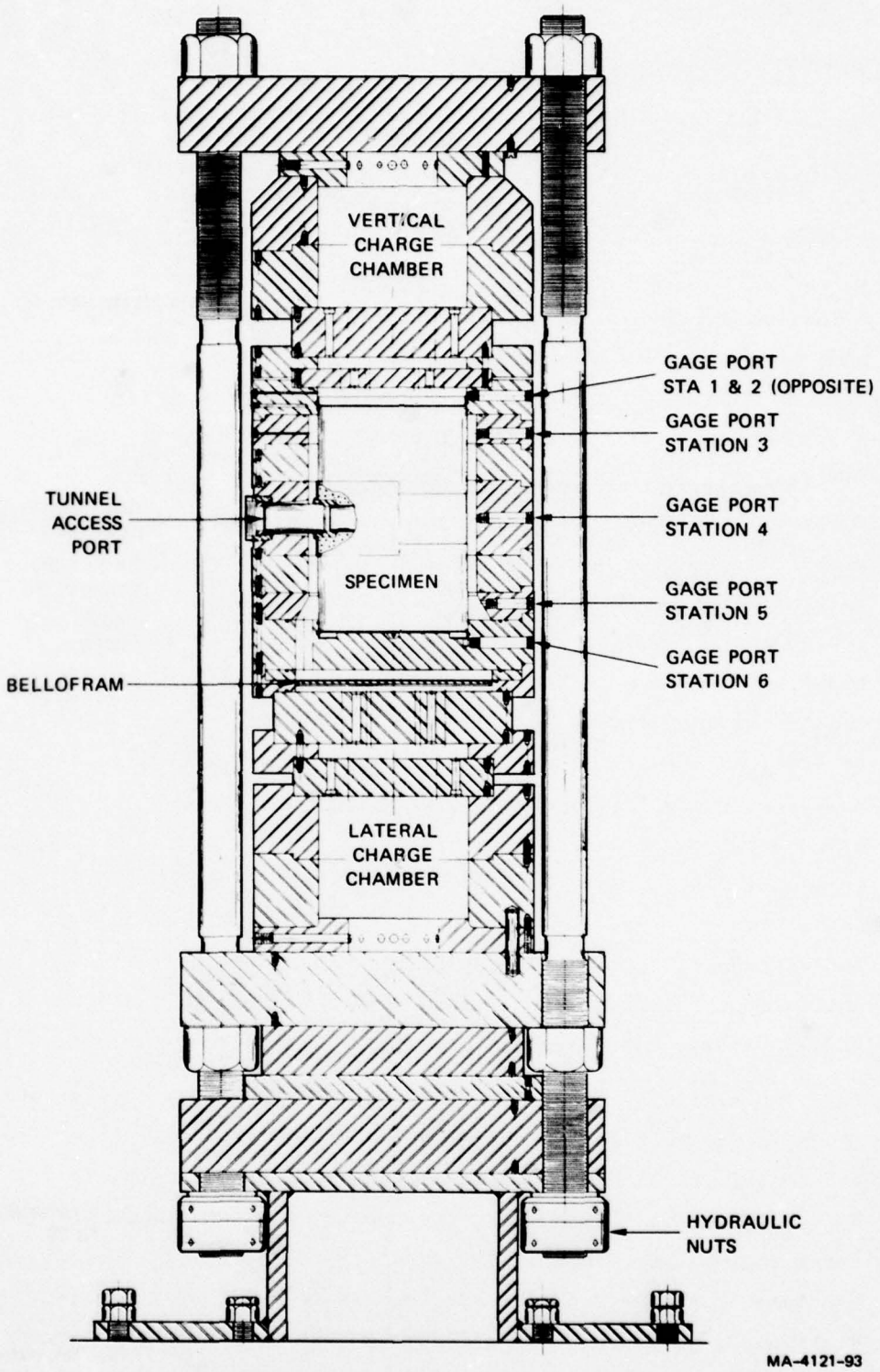

FIGURE 2.1 CROSS SECTION OF THE TESTING MACHINE IN THE DYNAMIC TRIAXIAL CONFIGURATION

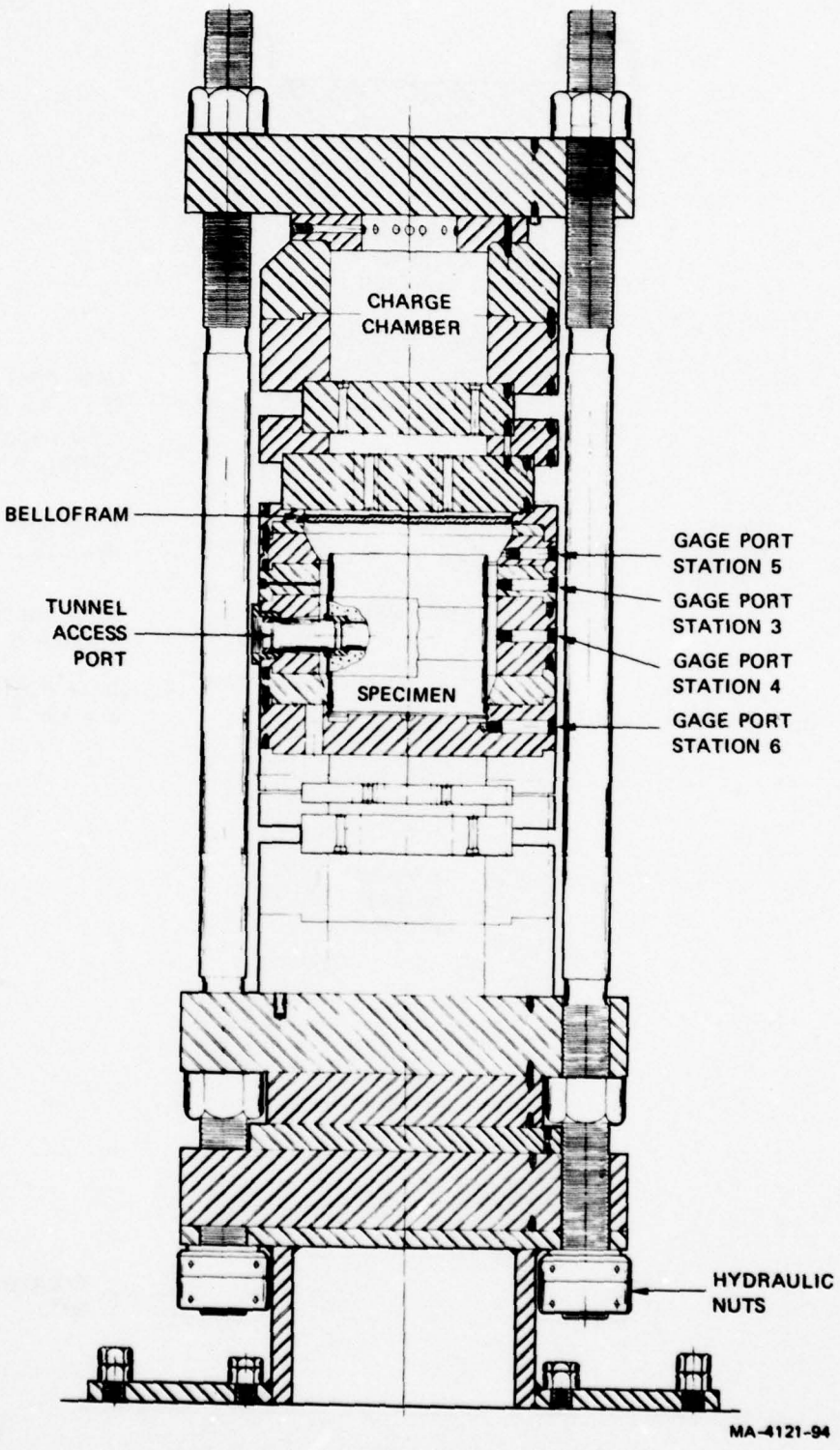

FIGURE 2.2 CROSS SECTION OF THE TESTING MACHINE IN THE DYNAMIC ISOTROPIC CONFIGURATION

2.2 SPECIMEN ASSEMBLY

The specimen is a right circular cylinder 12 inches (0.3 m) in diameter and 12 to 18 inches (0.3 to 0.45 m) tall. Figure 2.3 shows a 12-inch (0.3-m) tall specimen and a typical model tunnel reinforcing structure. The rock tunnel in this specimen is 2 inches (50 mm) in diameter. The centerline of the tunnel is along a specimen diameter at the midheight of the rock.

The initial procedure in specimen assembly is rock preparation, which is carried out in three steps: drilling the tunnel, moisturizing the rock, and taking pretest rock measurements. The tunnel is drilled with a diamond coring tool. In some early tests on a tuff simulant, the tunnel was cast into the specimen at Waterways Experiment Station. However, the residual stresses caused the specimen to crack around the tunnel. Results from preliminary tests indicated that these cracks grossly influenced the rock deformation. Therefore, the tunnels are drilled in both rock and rock simulant samples.

After the tunnel has been drilled, the moisture content of the rock is adjusted so that the desired level of saturation is obtained. Typically, the specimen is to be tested in the fully saturated state since most geological environments suitable for deep basing are nearly 100% saturated.

When the desired saturation level has been reached, the rock is measured and then stored in a suitable environment. Fully saturated rocks, for example, are completely submerged in water at atmospheric pressure. The diameter of the rock is measured at 30° (0.52 rad) intervals at the top, bottom, and midheight. The height of the rock is also measured at its center, and at its circumference in line with the tunnel axis and 90° (1.57 rad) from the tunnel axis. These dimensions are recorded and compared with those taken after the rock is tested.

The second step of specimen assembly is to install the model tunnel reinforcing structure. A typical model structure, shown in Figure 2.3, is a thin cylindrical shell with circumferential stiffeners. Direct-contact structures such as this are grouted into the tunnel. Backpacked

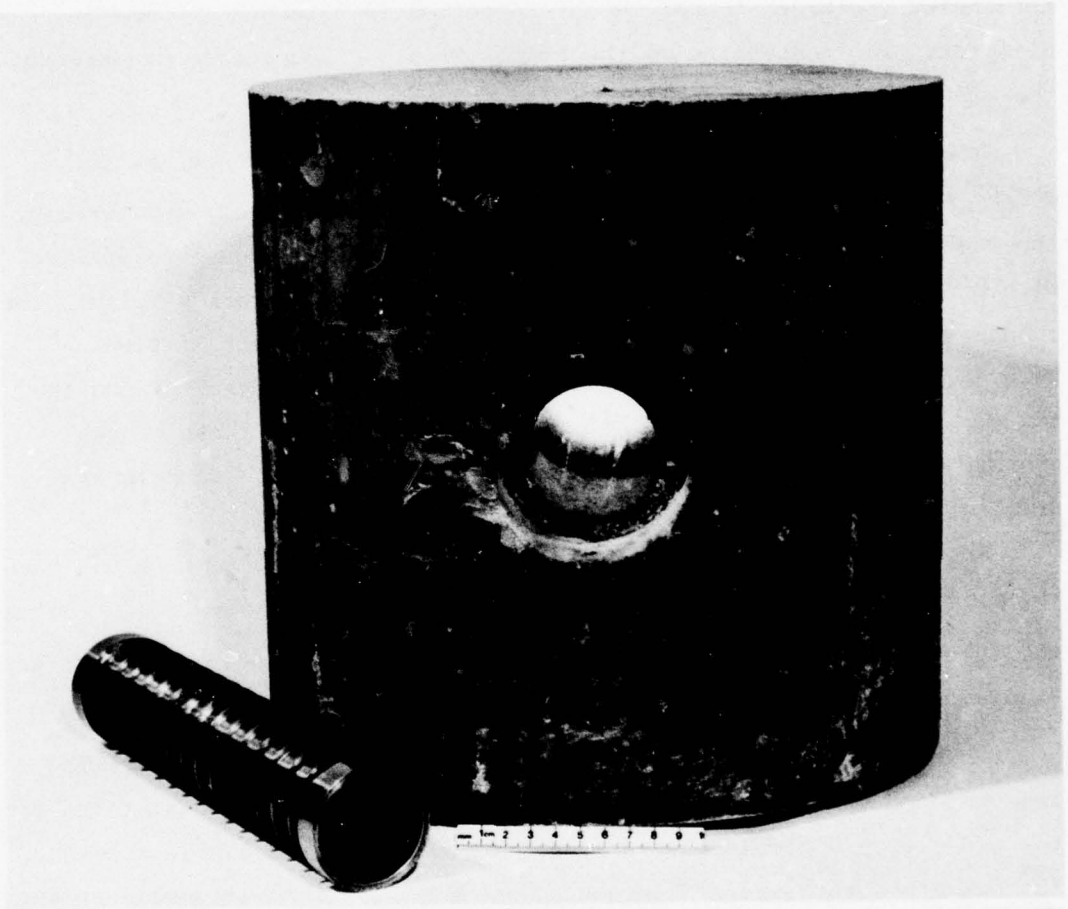

MP-4121-101

FIGURE 2.3 TWELVE-INCH DIAMETER SPECIMEN OF TUFF SIMULANT AND A TYPICAL TUNNEL REINFORCING STRUCTURE

structures (with a crushable backpacking material between the liner and rock opening) are simply pressed into the tunnel. The tolerance between backpacking and rock opening is taken up with a small amount of backpacking crush. With the structures in place, the end fitting assemblies are grouted into the counterbores in the rock at each end of the tunnel. Figure 2.4 shows an end fitting assembly and the adaptor assembly that is used to connect the tunnel with the ports in the machine. The cross section drawing in Figure 2.5 shows how these two assemblies connect the tunnel to the ports in the testing machine. The end fitting slips over the end of the tunnel reinforcing structure. In an undrained test, this fit is sealed with an O-ring. A stiffening ring is placed inside the end of the tunnel structure so that the structure will not deform locally and break the O-ring seal. Later, when the specimen is placed in the testing machine, the tunnel entry tube slips into the end fitting and butts against the reinforcing structure. This joint is also sealed with an O-ring. The tunnel entry tube extends from the end fitting in the rock to the entry portal in the test machine. The joint between the tunnel entry tube and the entry portal is sealed with an O-ring. The tunnel retaining ring is threaded into the entry portal until in contacts the tunnel entry tube. The end fitting assembly is generally stiffer than the rock, but experimental results show that, nevertheless, tunnel deformation is surprisingly uniform along its length.

After the tunnel reinforcing structure is emplaced, each end of the rock specimen is seated into a 4-inch (0.1-m) deep, 12-inch (0.3-m) diameter copper can. Figure 2.6 shows one copper can in place on the rock specimen and the other copper can before assembly. The walls of the copper cans are 25 mils (0.64 mm) thick and do not contribute appreciably to the strength of the rock. The Wilson seal, a rubber membrane used to seal the specimen around the end fitting at the end of the tunnel, is also shown.

Because of the difficulty in fabricating both the rock and the copper can to size so that the rock just slips into the copper can, the rock is purposely made undersize by about 60 mils (1.5 mm). To fill the resulting

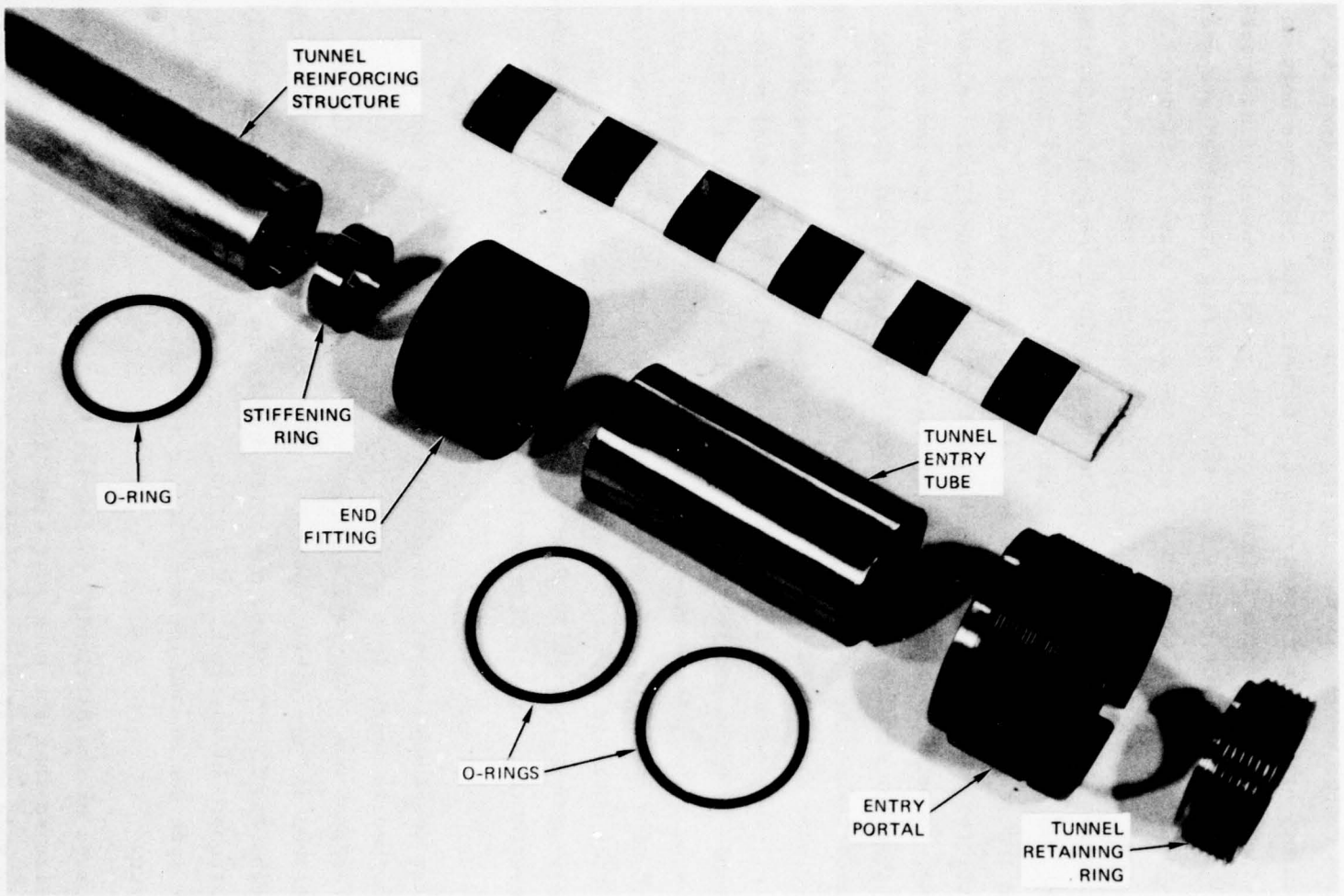

FIGURE 2.4 COMPONENTS OF THE END FITTING AND TUNNEL ADAPTOR ASSEMBLIES (TYPICAL AT BOTH ENDS)

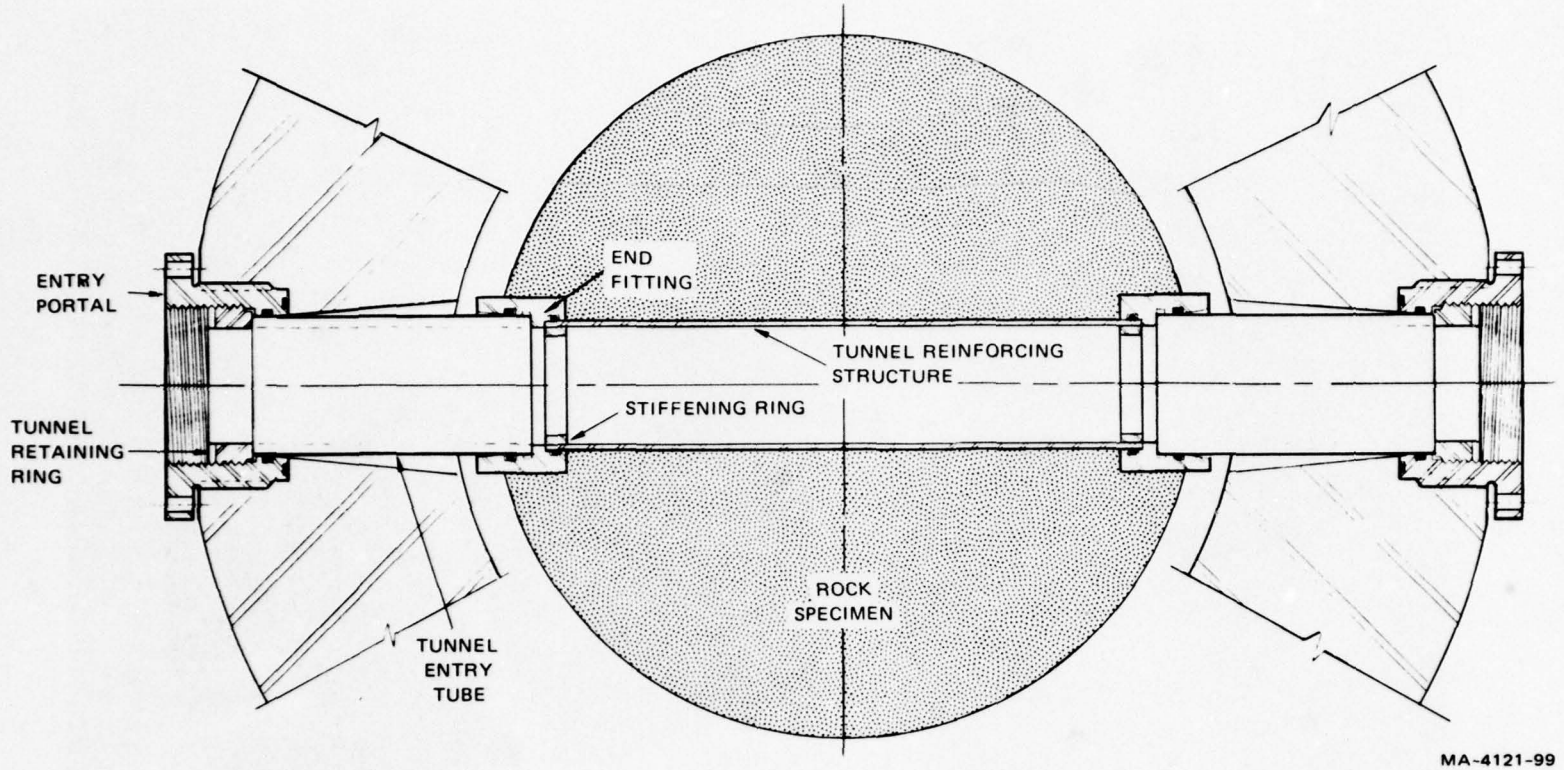

FIGURE 2.5 CROSS SECTION SHOWING HOW THE END FITTING AND TUNNEL ADAPTOR ASSEMBLIES CONNECT THE TUNNEL IN THE ROCK TO THE PORTS IN THE TESTING MACHINE

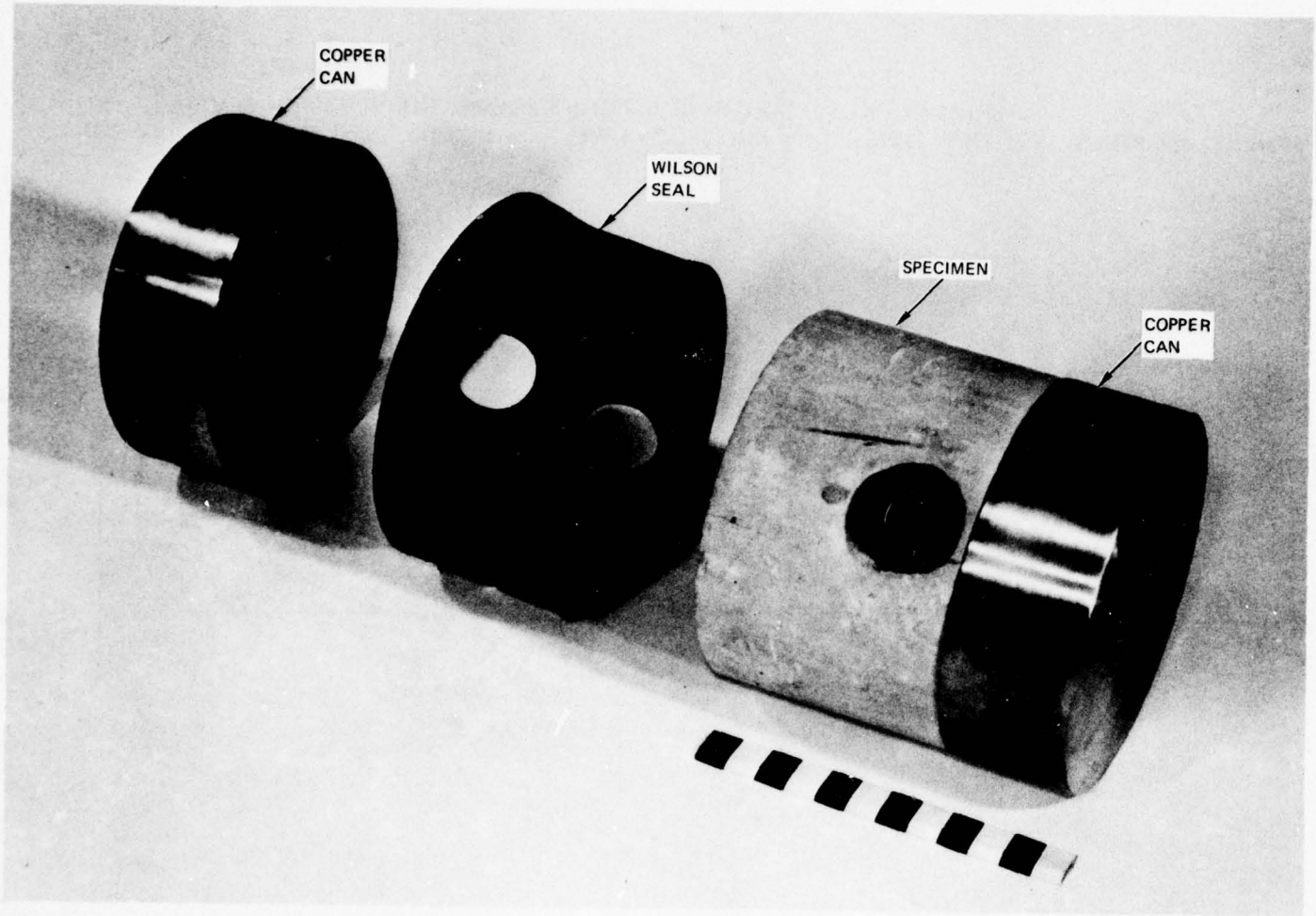

MP-4121-103

FIGURE 2.6 ROCK SPECIMEN WITH COPPER CANS AND WILSON SEAL

gap, a thin grout slurry is poured into the annulus between the rock and the wall of the copper can. The composition of the grout is such that it expands as it cures, holding the rock firmly in the copper can.

Figure 2.7 shows both copper cans on the rock specimen and the Wilson seal in place. Also shown are two copper cups, 12 inches (0.3 m) in diameter and 1 inch (25 mm) deep, which along with the O-rings comprise the seal between the vertical and lateral loading fluids in the testing machine. The copper cup and O-ring above the specimen separate the explosive gases that apply the vertical load above the specimen from the oil that applies the lateral load. Similarly, the copper cup and O-ring below the specimen separate the oil under the specimen that reacts the vertical loading from the oil that applies the lateral load to the specimen.

Description of one step in the specimen assembly has been postponed until now so that the general features of rock preparation and specimen assembly could be presented succinctly. This step was introduced after the first few tests because large oscillations were observed in the oil pressure under the specimen.* Analysis of these oscillations suggested that the specimen was accelerated downward by the gas pressure above it and impacted the pool of oil below. The specimen rebounded after the impact and was again accelerated downward by the gas pressure. This impact and rebound sequence gradually damped out near the peak of the pressure pulse. The analysis showed that an initial gap of only a few mils was sufficient for this process to be initiated. One source of this gap could be a small amount of air trapped in the pool of oil under the specimen. This will be discussed in greater detail in the following section. Another source of the gap could be deviations from flatness of the bottom of the copper can that seals the specimen and the copper cup that seals the pool of oil under the specimen. Because the specimen rests on this copper cup, if either the copper can or the copper cup is not exactly flat, the specimen will not be properly seated and a gap will exist.

---

*A detailed description, example pressure pulses, and the cure to eliminate these oscillations are given in Appendix C of Volume II.

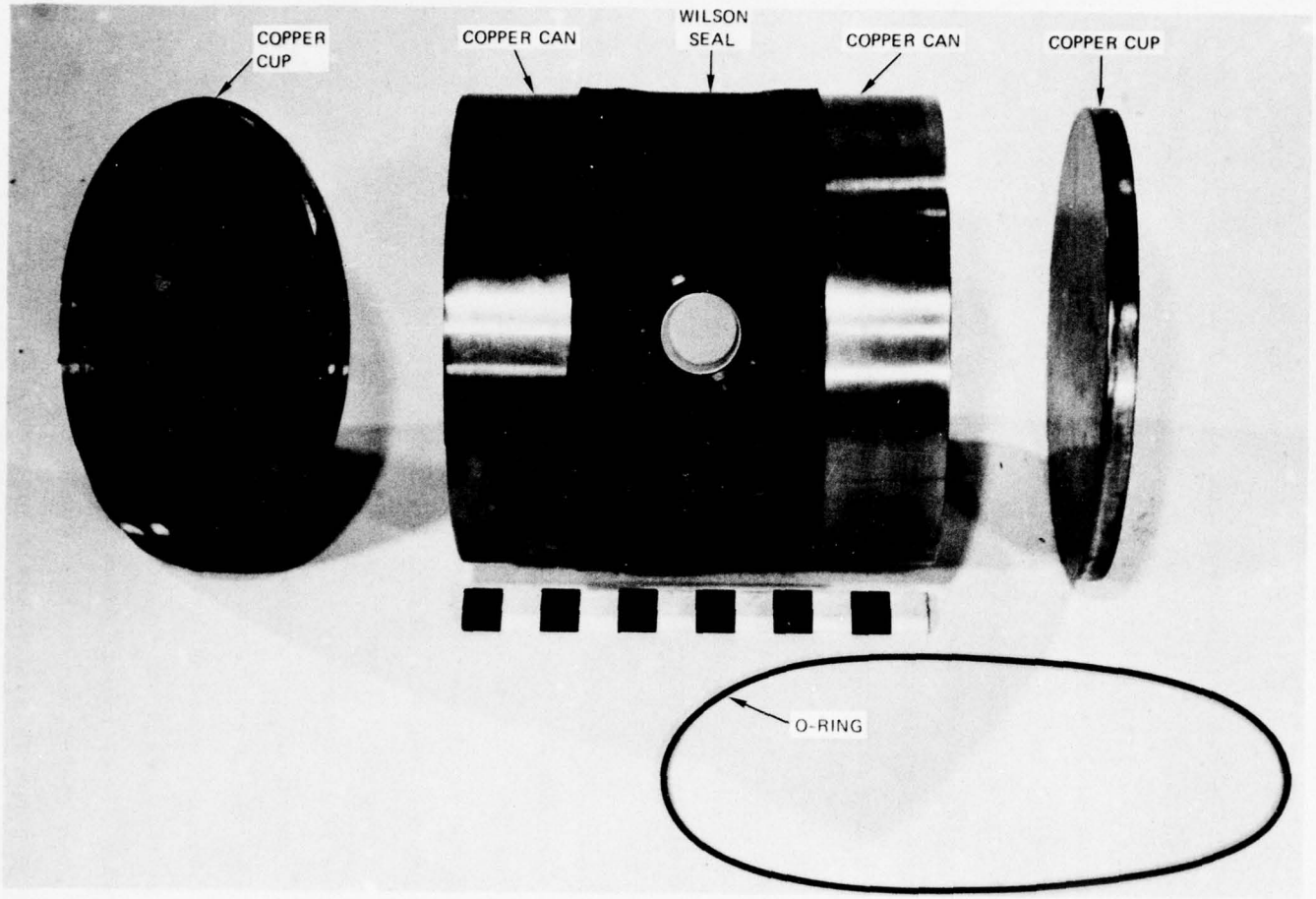

FIGURE 2.7 SEALED ROCK SPECIMEN WITH COPPER CUPS AND O-RINGS USED TO SEPARATE VERTICAL AND LATERAL LOADING FLUIDS

Whatever the source of the gap, it could not be eliminated entirely. To soften the impact and to facilitate the damping of the impact-rebound sequence, 0.3-inch (7.5-mm) diameter lead shot are placed in the copper can under the specimen. The shot are fairly compliant and soften the impact of the specimen on the pool of oil. The impact-rebound sequence then damps out very quickly because the energy is dissipated during the plastic deformation of the lead shot. Figure 2.8 shows the lead shot, a copper can, a wire mesh to hold the shot uniformly separated in place, and a thin steel plate that is placed between the lead shot and the bottom of the specimen. Figures 2.9 and 2.10 show the preparation of the bottom copper can with the lead shot. The wire mesh is placed in the bottom of the can and the lead shot are distributed uniformly in the mesh. The amount of shot is half that which can be put in the bottom of the can using the most dense packing possible without the mesh. After the lead shot are in place, a thin, 30-mil (0.75-mm) thick steel plate is placed on top of the assembly and is sealed around its circumference to the side of the copper can with a silicone rubber compound. The steel plate is used so that the specimen does not sit directly on the lead shot, eliminating problems associated with point contacts. The silicone-rubber seal is necessary so that water does not drain from the specimen, reducing its level of saturation. The silicone rubber compound cures quickly, and the rock is then placed in the copper can and assembly of the specimen continues as described before.

2.3 MACHINE ASSEMBLY FOR DYNAMIC TESTING

The machine is assembled using an electric 2-ton hoist to lift each part from its storage cart, over the tops of the studs, and onto the stack. Stacking the test machine takes about 20 hours and requires two technicians.

Before discussing the actual assembly of the testing machine, the foundation supporting the test machine will be described briefly. At the SRI remote test site, an area 8 feet (2.4 m) square was excavated to a depth of 3 feet (0.9 m) through an existing concrete pad. Reinforcing steel, shown in place in Figure 2.11, was lowered into the pit before the concrete was poured. The long bolts, which are welded to the reinforcing steel, anchor the testing machine in the concrete pad with the

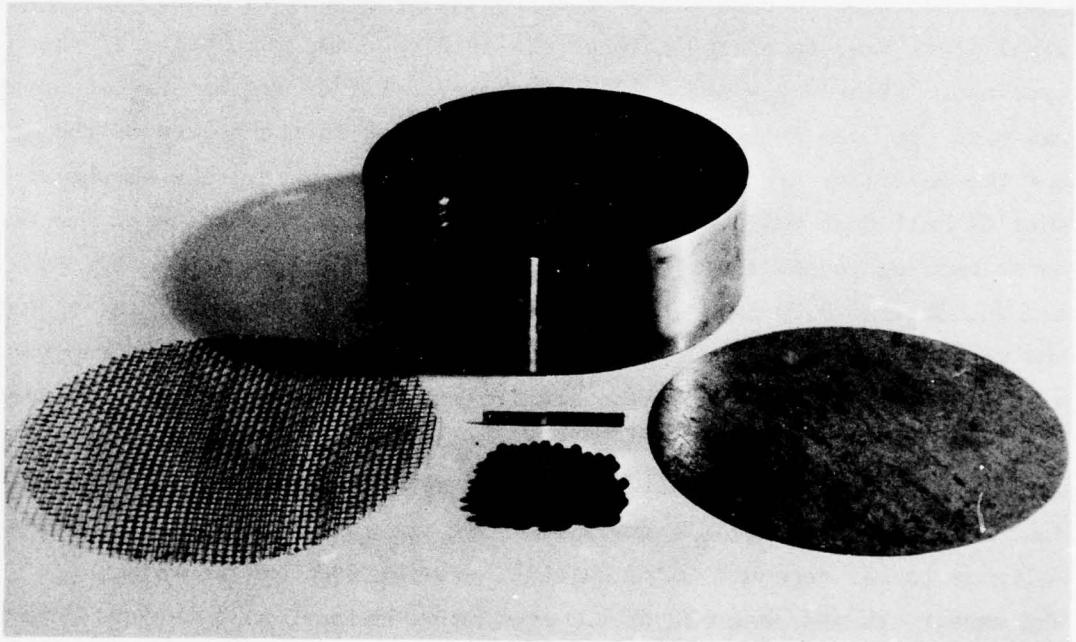

MP-4121-105

FIGURE 2.8 WIRE MESH, LEAD SHOT, AND STEEL PLATE THAT ARE PLACED IN THE BOTTOM COPPER CAN TO CUSHION LOADING IMPACT

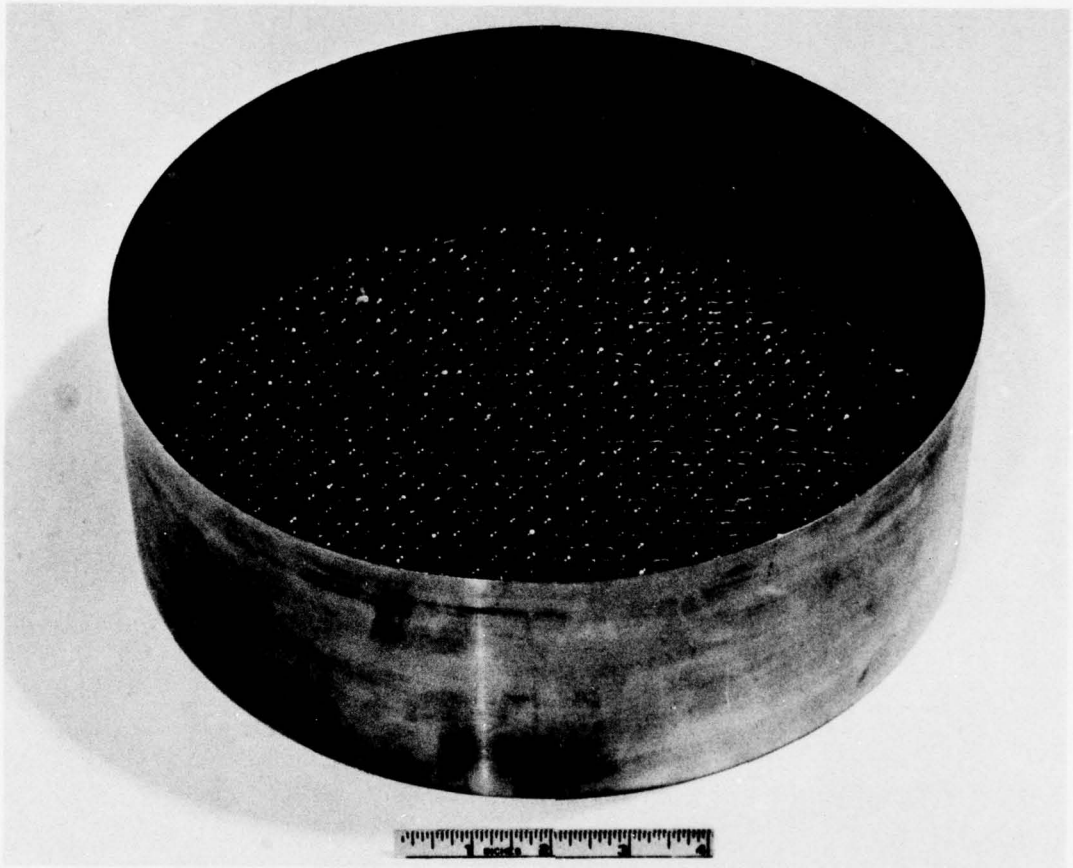

MP-4121-106

FIGURE 2.9 WIRE MESH AND LEAD SHOT IN PLACE IN THE BOTTOM COPPER CAN

MP-4121-107

FIGURE 2.10 STEEL PLATE IN PLACE OVER THE LEAD SHOT, AND THE ASSEMBLY BEING SEALED WITH A SILICONE-RUBBER COMPOUND

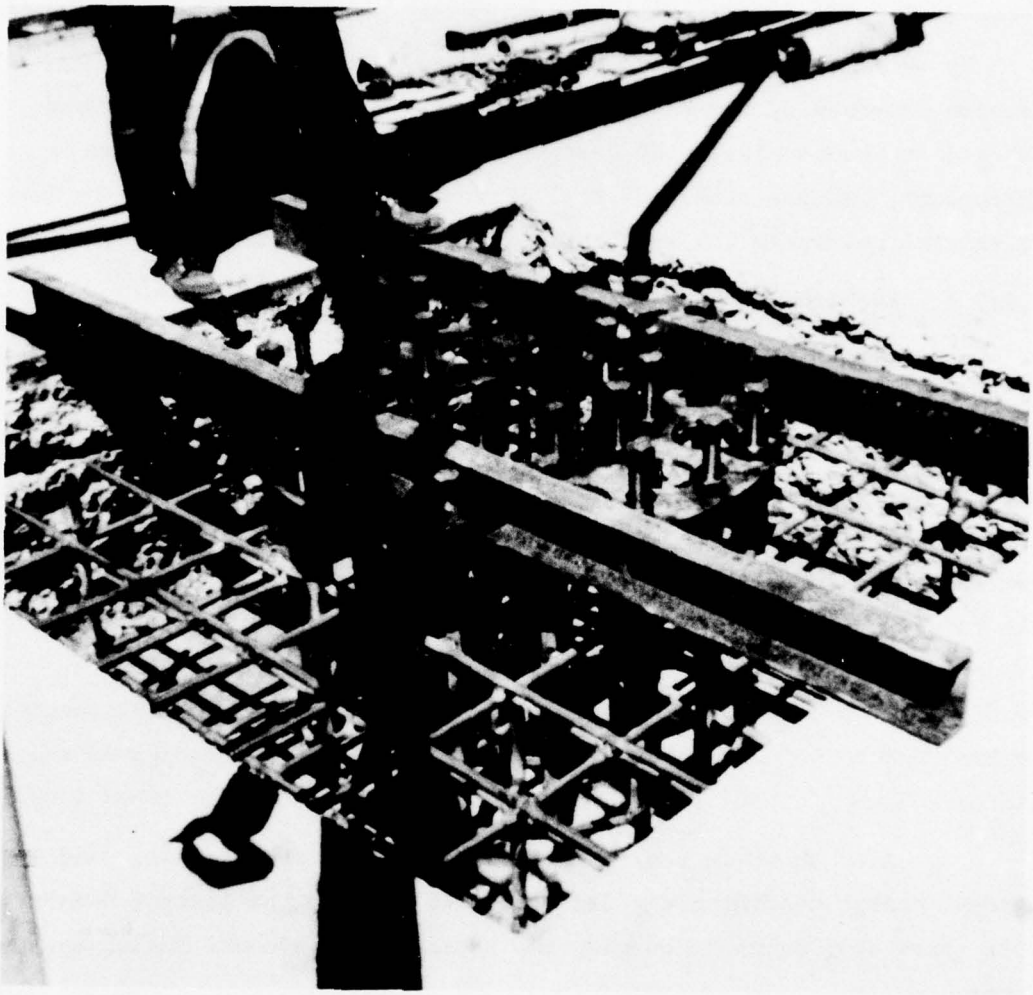

MP-4121-108

FIGURE 2.11 REINFORCING STEEL PLACED IN THE CONCRETE PAD UNDER THE TESTING MACHINE

thin ring shown. A short cylinder was welded to the inner diameter of this ring, and a circular plate was welded to the top of this cylinder to form a spool-like structure, the assembly mounting pad, part 37.* This structure supports the testing machine as well as anchoring it in the concrete pad.

In the remainder of this section, we will describe the testing machine components, their functions, and the order in which they are stacked in the machine. The description of each part will include a photograph, and the status of the testing machine stack will be reviewed at several points in the stacking sequence.

2.3.1 Machine Assembly for Triaxial Testing

Figure 2.12 shows the state of the testing machine stack between shots. A number of parts are already in place. The spool end plate, (part 16), the upper and lower backup nut spacer plates (parts 18 and 19), and the bottom end plate (part 14), are stacked on the assembly mounting pad. The diameters of these plates vary to accommodate the studs (part 33), the hydraulic nuts (part 101), and the mechanical backup nuts (part 100). The studs, hydraulic nuts and mechanical backup nuts are initially in place as shown. These parts, in conjunction with the upper mechanical nuts (part 100), form the reaction frame and are used to preload the testing machine and to hold it together during a test. The preloading sequence is discussed later, after stacking of the machine has been described completely.

Also shown in their places in the stack are the upper and lower lateral charge chamber rings (parts 10 and 11) and the lateral chamber vent ring (part 56), which is between the bottom end plate and the charge chamber rings.

The lateral charge chamber rings and the lateral chamber vent ring can be cleaned adequately of the corrosive explosive residue without being removed from the stack. However, occasionally these three parts are lifted from the machine and cleaned more thoroughly.

---

*The part numbers given in the text may be used to locate the part in the cross section of the testing machine stack shown in the foldout of Figure B.1, Appendix B. Also, further information regarding part names, part numbers, etc., is given in Appendix B at the end of the report.

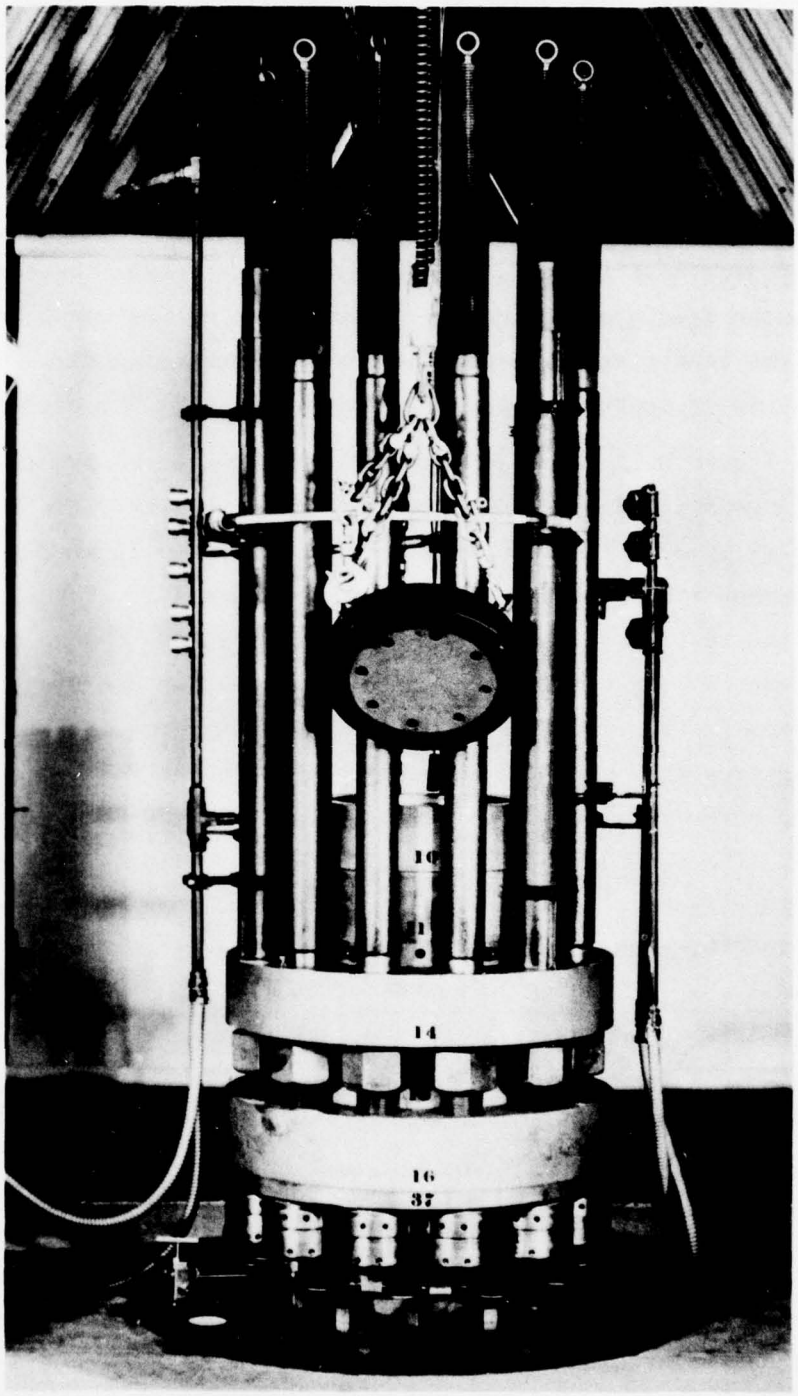

MP-4121-109

FIGURE 2.12 TESTING MACHINE STACK CONDITION BETWEEN SHOTS
No further unstacking is needed to install new charges and specimen

The lateral chamber vent ring, shown in Figure 2.13, allows the explosive gases to escape to the atmosphere through twelve 11/16-inch (17.5-mm) diameter holes. A number of these holes can be constricted or blocked completely to vary the rate at which the gas escapes. The primary effect of changing the total area of the holes in the vent ring is to change the length of the pressure pulse, i.e., reducing the total area increases the length of the pulse. Also, reducing the total area of the holes in the vent ring increases the peak pressure slightly. However, the peak pressure is controlled primarily by the size of the explosive charge.

Figure 2.14 shows an internal view of the two lateral charge chamber rings stacked on the lateral chamber vent ring. The charge chamber is 12 inches (0.3 m) in diameter and 9-3/4 inches (0.25 m) deep. With the charge chamber rings in place, as shown in Figure 2.12, the first step in stacking the testing machine is to place an explosive charge in the lateral charge chamber. The explosive used is a low-density mixture of PETN and microspheres in the ratio 9:1 by weight. Microspheres are tiny inert plastic spheres that slow the detonation rate in the PETN and therefore reduce the detonation pressure from over 200 kbar (20 GPa) to about 7 kbar (0.7 GPa). The PETN/microsphere mixture is loaded into a cylindrical paper canister whose aspect ratio is roughly unity. The charge has a 36-inch (0.91-m) long Primacord lead. (The Primacord leads for both the lateral and vertical charges are 36 inches (0.91 m) long and are connected to a common detonator to ensure simultaneous detonation of both charges.) The charge is placed in the charge chamber, and the Primacord lead is threaded through one of the open holes in the vent ring. The charge is centered in the charge chamber with Styrofoam spacers.

After the charge has been placed in the lateral charge chamber, the lateral chamber orifice plate (part 28, Figure 2.15) is lifted onto the stack. The plate is 16 inches (0.4 m) in diameter and 3 inches (75 mm) thick and has eight 5/8-inch (15-mm) holes equally spaced on a 10-inch (0.25-m) diameter. By reducing the area of these holes, the rate at which the explosive gases load the specimen, and hence the rise time of the

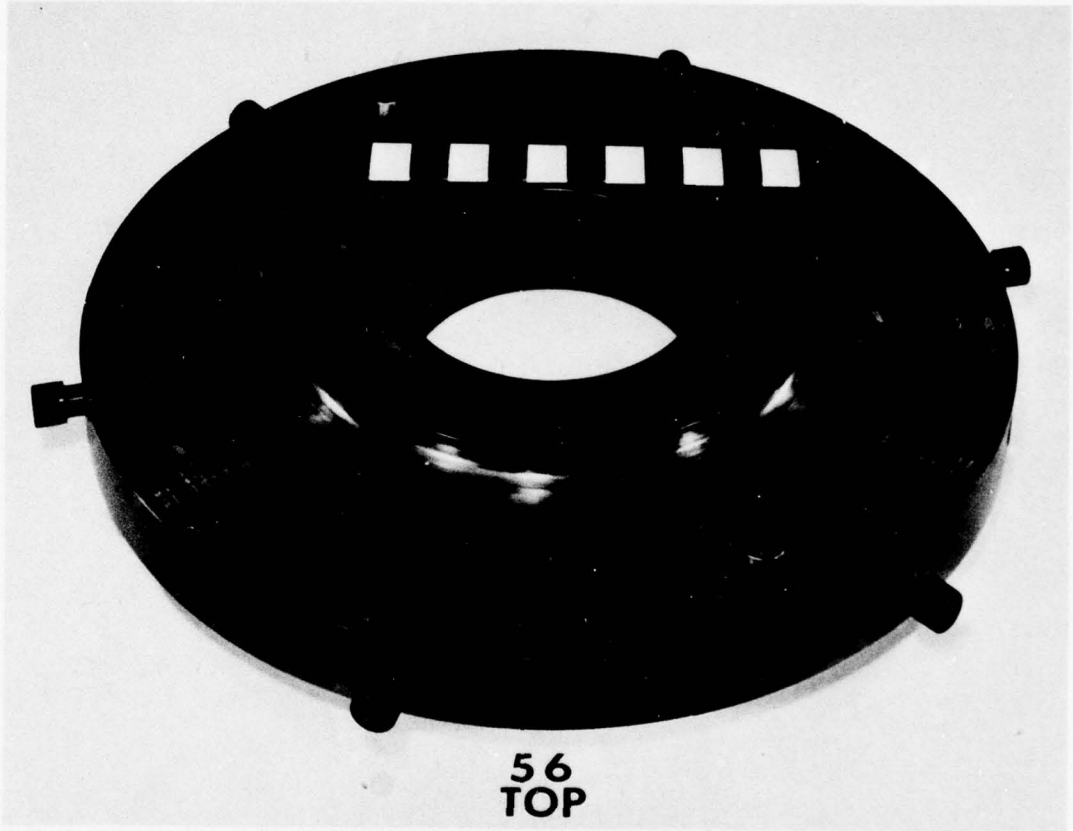

MP-4121-110

FIGURE 2.13 LATERAL CHAMBER VENT RING, PART NUMBER 56. SIX OF THE 12 VENT HOLES ARE PLUGGED TO LENGTHEN DURATION OF THE LATERAL PRESSURE PULSE

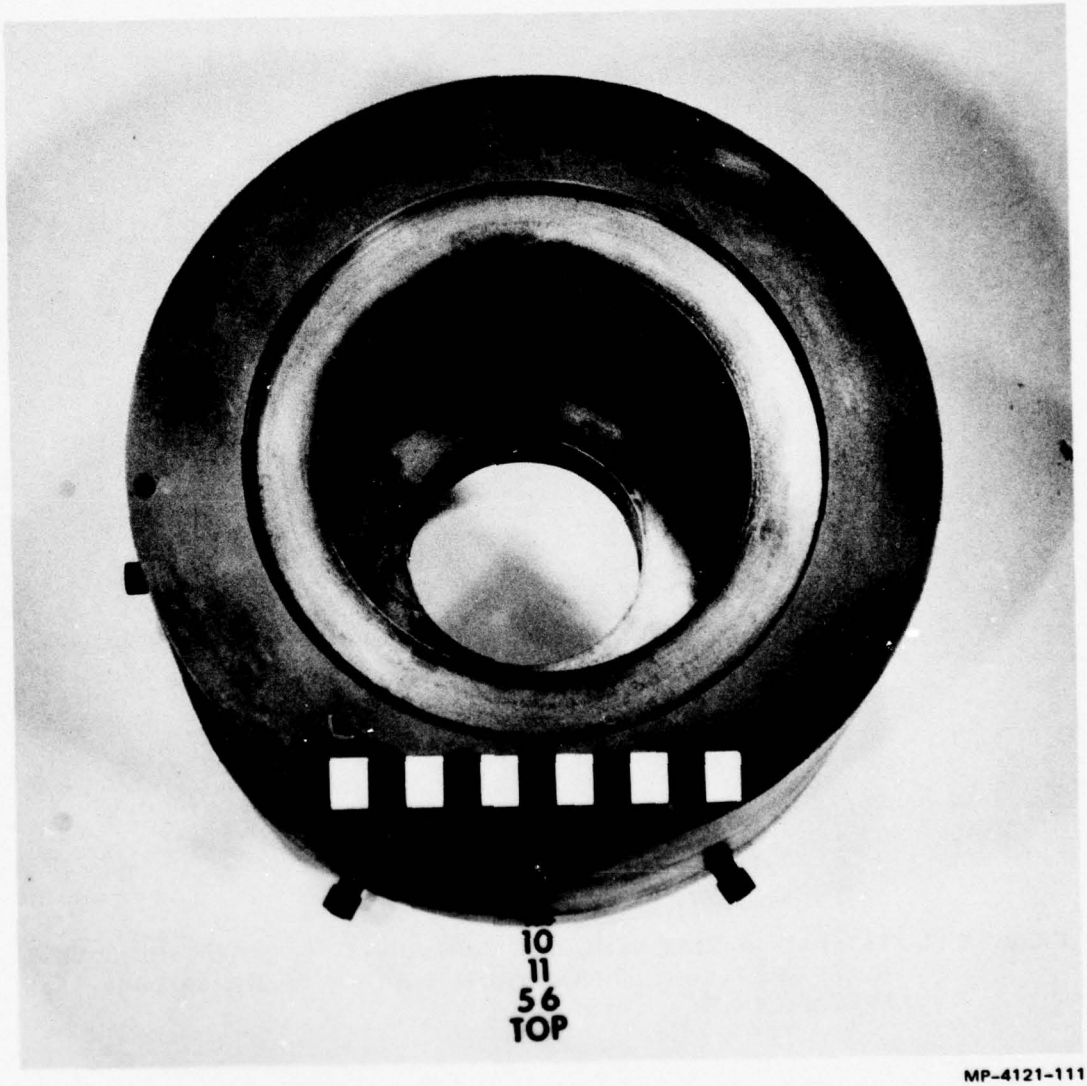

MP-4121-111

FIGURE 2.14 INTERNAL VIEW OF LATERAL LOADING CHARGE CHAMBER, MADE UP OF CHAMBER RINGS (10 AND 11) AND VENT RING (56)

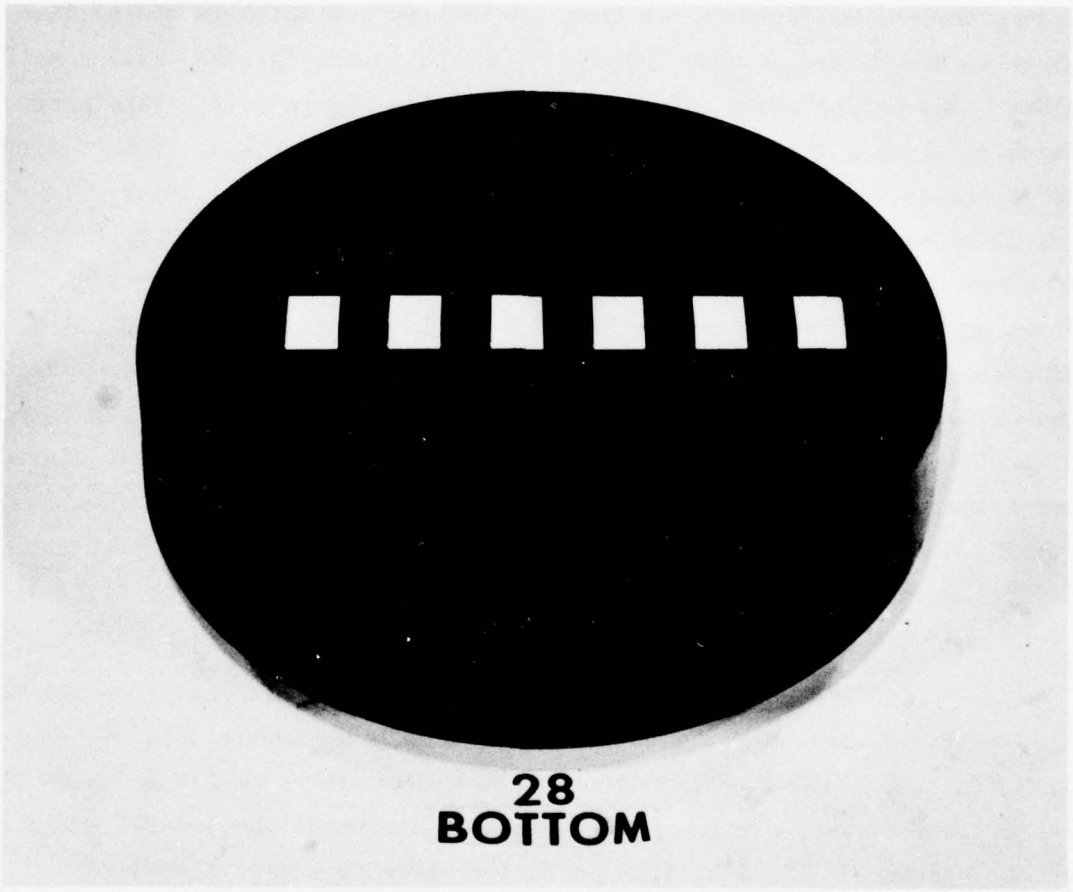

MP-4121-112

FIGURE 2.15 LATERAL CHAMBER ORIFICE PLATE, PART NUMBER 28

pressure pulse, can be reduced. Constricting these holes decreases the peak pressure slightly, but as mentioned before, peak pressure is determined mainly by the amount of explosive charge.

The next part stacked onto the machine is the lateral mixing chamber ring (part 9). This ring, shown in Figure 2.16, provides a small volume for the explosive gases that jet through the holes in the orifice plate to mix before passing through the holes in the lateral chamber baffle plate. The baffle plate (part 30), is shown in Figure 2.17. This part, which is stacked in the machine on top of the lateral mixing chamber ring, is 19 inches (0.48 m) in diameter and 4-1/4 inches (0.11 m) thick. It has 16 holes on two circles: the outer eight holes are on a 9-inch (0.23-m) diameter and have 3/4-inch (19-mm) diameters; the inner eight holes are on a 6-inch (0.15-m) diameter and have 11/16-inch (17.5-mm) diameters. All 16 holes lie inside the diameter on which the holes through the orifice plate are located. Therefore, the explosive gases cannot jet directly through aligned holes in the orifice plate and the baffle plate, but rather must mix in the chamber between the two plates. If direct jetting were permitted, the aluminum plate that protects the rubber Bellofram would be unable to withstand the locally high temperatures and pressures of the jets, and the Bellofram would be ruptured.

Figure 2.18 shows the Bellofram, the Bellofram protector plate, the Bellofram ring, and the Bellofram clamping ring (parts 109, 59, 34, and 35), respectively. The Bellofram is a thin rubber membrane across which the explosive gases pressurize the oil that surrounds the lateral surface of the specimen. The Bellofram protector plate is a thin A16061-T6 circular plate, 15-1/2 inches (0.39 m) in diameter and 3/8 inches (9.5 mm) thick. This plate is cemented to the side of the Bellofram that faces the explosive gases and prevents the hot explosive gases from rupturing the Bellofram. Typically, neither the Bellofram nor the Bellofram protector plate is damaged during a test, and the Bellofram protector plate is reused. The Bellofram itself, however, is not reused because the deleterious effect of the oil on rubber may cause failure in subsequent tests.

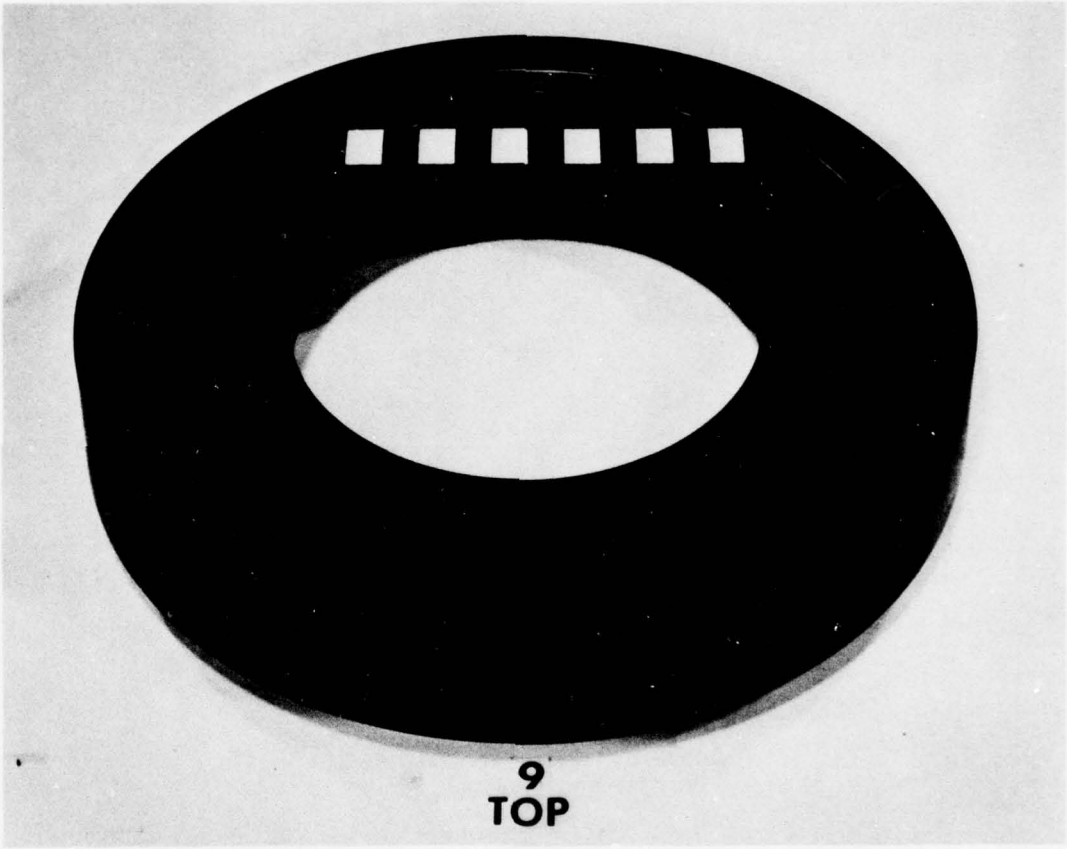

MP-4121-113

FIGURE 2.16 LATERAL MIXING CHAMBER RING, PART NUMBER 9

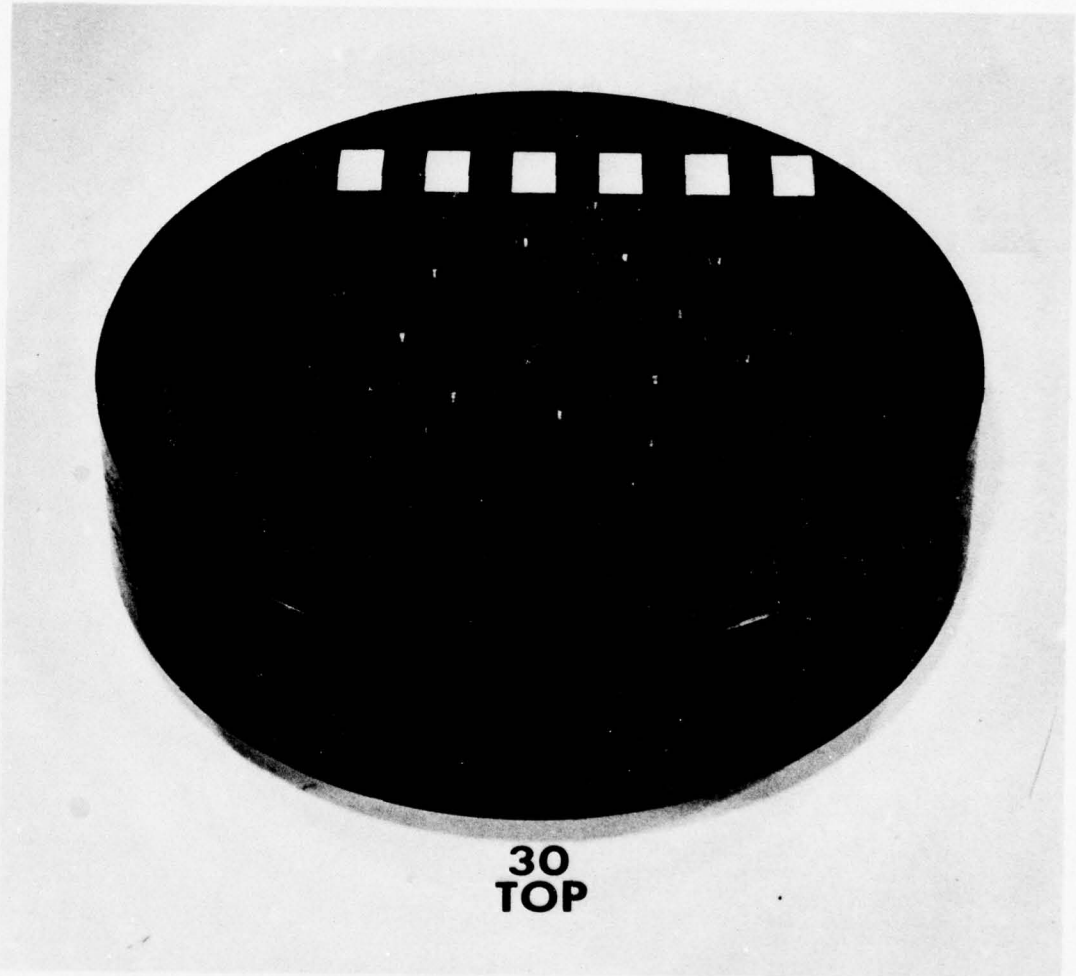

MP-4121-114

FIGURE 2.17 LATERAL CHAMBER BAFFLE PLATE, PART NUMBER 30

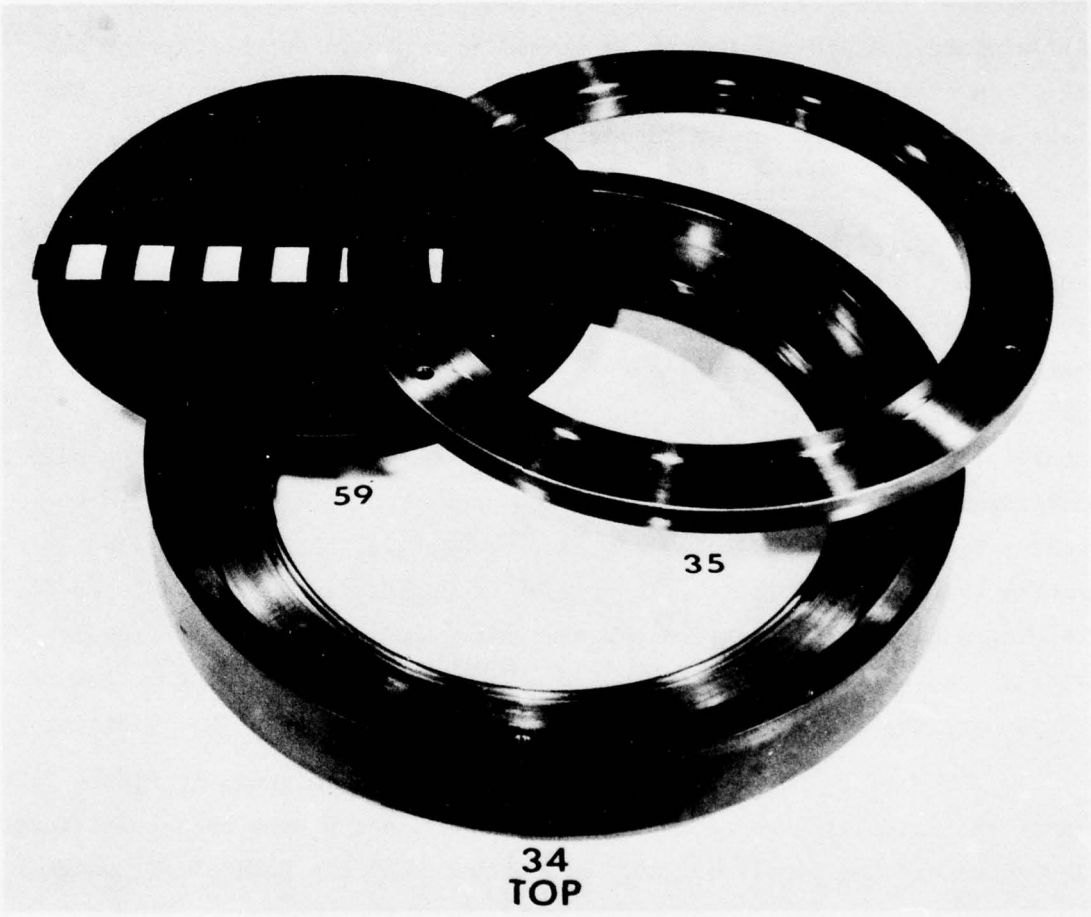

MP-4121-115

FIGURE 2.18 BELLOFRAM, BELLOFRAM PROTECTOR PLATE, BELLOFRAM RING AND BELLOFRAM CLAMPING RING, PARTS 109, 59, 34, AND 35, RESPECTIVELY

The Bellofram has a lip around its circumference, which fits into a matching groove in the Bellofram ring and is held in place by the Bellofram clamping ring. When these parts are assembled and lifted into the machine, a 17-1/4-inch (0.44-m) O-ring is placed in an O-ring groove on the face of the Bellofram ring that mates with the lateral chamber baffle plate. A similar O-ring is placed in a groove on the face of the Bellofram clamping ring that mates with the specimen receiver plate, the plate above the Bellofram and Bellofram rings.

The specimen receiver plate (part 20), is shown in Figure 2.19. This plate supports the specimen in the test machine. The twelve 1-3/8-inch (35-mm) diameter holes through the plate permit transmission of the pressure from the pool of oil below the receiver plate into the chamber surrounding the specimen. A problem arose with this system because of oscillations in the oil pressure surrounding the specimen; details regarding this problem and its solution are presented in Appendix C of Volume II of this report, which gives results of similar tests in the smaller machine. This problem was also present in the smaller-scale machine which, because of the lower cost of performing tests, was used for the diagnostic and calibration tests required to resolve the difficulty. Briefly, the solution is to introduce a large amount of damping in the oil by reducing the area of the holes through the specimen receiver plate.

The plate, with this change incorporated, is shown in Figure 2.20. Six of the 12 holes have been blocked and the other 6 have been constricted. Also shown are the copper cup and O-ring that seal the pool of oil under the specimen from the oil in the chamber around the specimen. (These are the same cup and O-ring shown with the rock specimen in Figure 2.7.)

In the previous section, where the specimen assembly was described, the problem of oscillations in the oil pressure under the rock was outlined. The oscillations result from the specimen's being accelerated through a short distance by the gas pressure above the specimen and then impacting the pool of oil under the specimen. Part of the reason that the specimen can be accelerated through this short distance is that some air is trapped with the oil under the specimen. The scheme devised for removing the

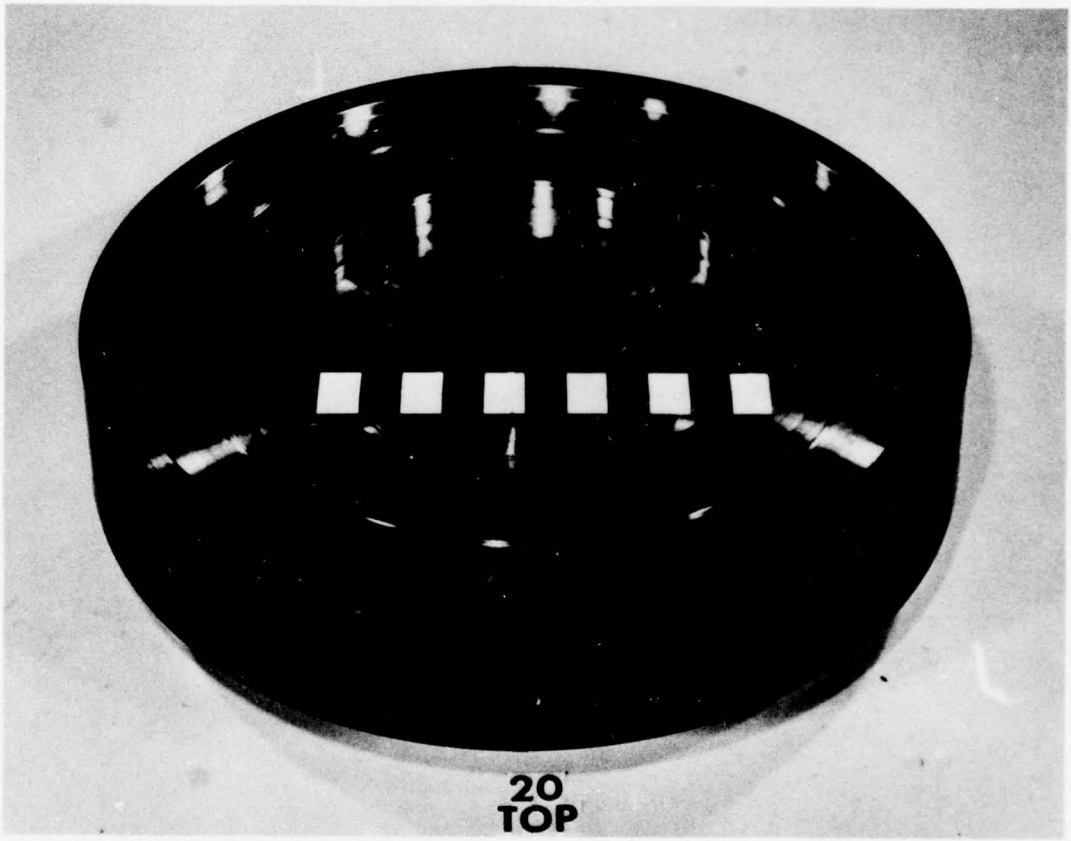

MP-4121-116

FIGURE 2.19 SPECIMEN RECEIVER PLATE, PART NUMBER 20

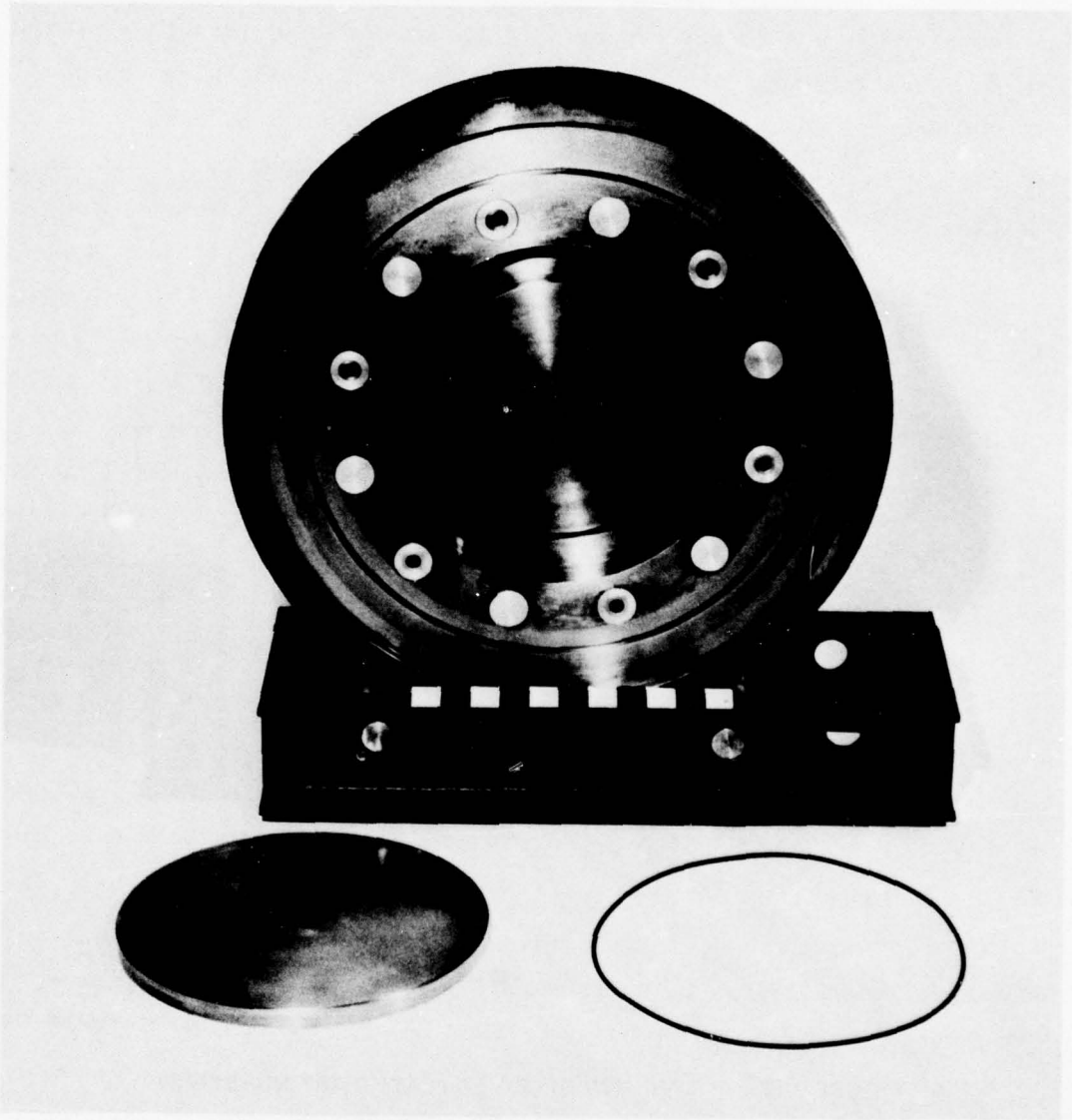

MP-4121-117

FIGURE 2.20 SPECIMEN RECEIVER PLATE WITH SIX HOLES BLOCKED AND REMAINING SIX CONSTRICTED TO DAMP OUT OSCILLATIONS IN THE LATERAL PRESSURE

The copper cup and O-ring (foreground) fit into the recess shown to form an oil-filled reaction chamber under the rock

trapped air is shown in Figures 2.20, 2.21, and 2.22. The specimen receiver plate is placed in a holder with the gage port at the top as shown in Figure 2.20. The copper cup and O-ring are inserted into the plate to form the chamber for the oil. Figure 2.21 shows the oil being poured into the chamber through the gage port. Heat lamps are directed onto the plate and the entire assembly is heated. The copper cup is flexed and the level of the oil rises and falls in the gage port. The motion of the oil helps to float bubbles of trapped air to the top of the chamber and out the gage port. Heating the oil also helps to remove the trapped air. Since the viscosity of the oil decreases with temperature, the air bubbles meet with less resistance while floating to the top of the chamber. Also, the heat expands the trapped air much more than the oil, so that the buoyant force pushing the bubbles up increases. When no more bubbles can be made to float out through the gage port, the pressure gage is inserted. This seals the chamber, and the specimen receiver plate is hoisted onto the stack.

Figure 2.23 shows the status of the machine at this point in the stacking sequence. The explosive charge has been placed in the lateral charge chamber, the orifice and baffle plates have been hoisted onto the machine, the Bellofram assembly has been stacked above the baffle plate, the specimen receiver plate has been filled with oil and placed onto the machine, and one pressure gage is in place.

The next machine part to be stacked is the lateral chamber reducer ring (part 21), shown in Figure 2.24. This is the first of three rings that form the lateral chamber around the specimen. The lateral chamber reducer ring reduces the diameter of the lateral chamber from 15-3/4 inches (0.4 m), which encompasses the holes through the specimen receiver plate, to 13-1/2 inches (0.34 m), 1-1/2 inches (38.1 mm) larger than the specimen diameter. The interface between the specimen receiver plate and the lateral chamber reducer ring is sealed with a face-seal O-ring, as are all the interfaces between rings that make up the lateral chamber. The lateral chamber reducer ring has a single gage port, in which a gage is inserted to measure the lateral pressure applied to the specimen near the bottom of the lateral chamber.

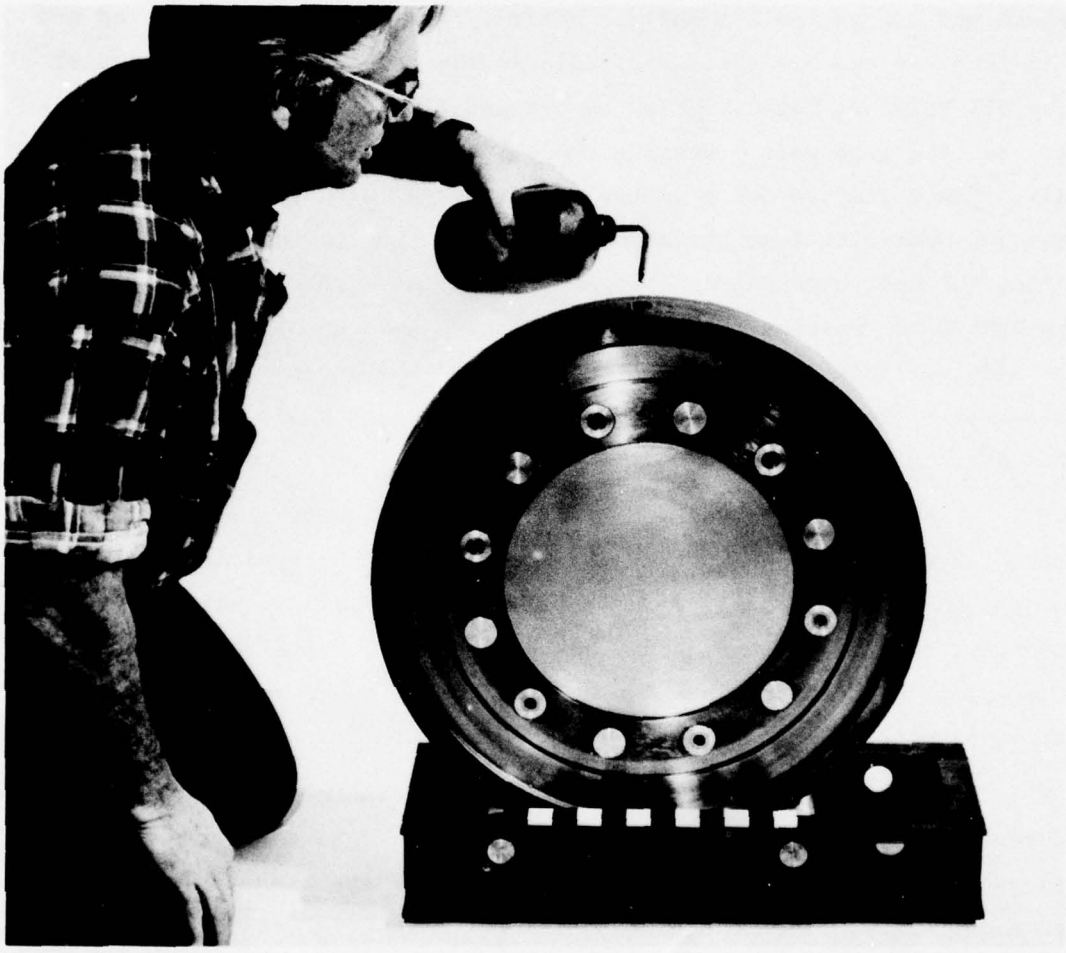

MP-4121-118

FIGURE 2.21 OIL BEING POURED THROUGH A GAGE PORT INTO THE REACTION CHAMBER

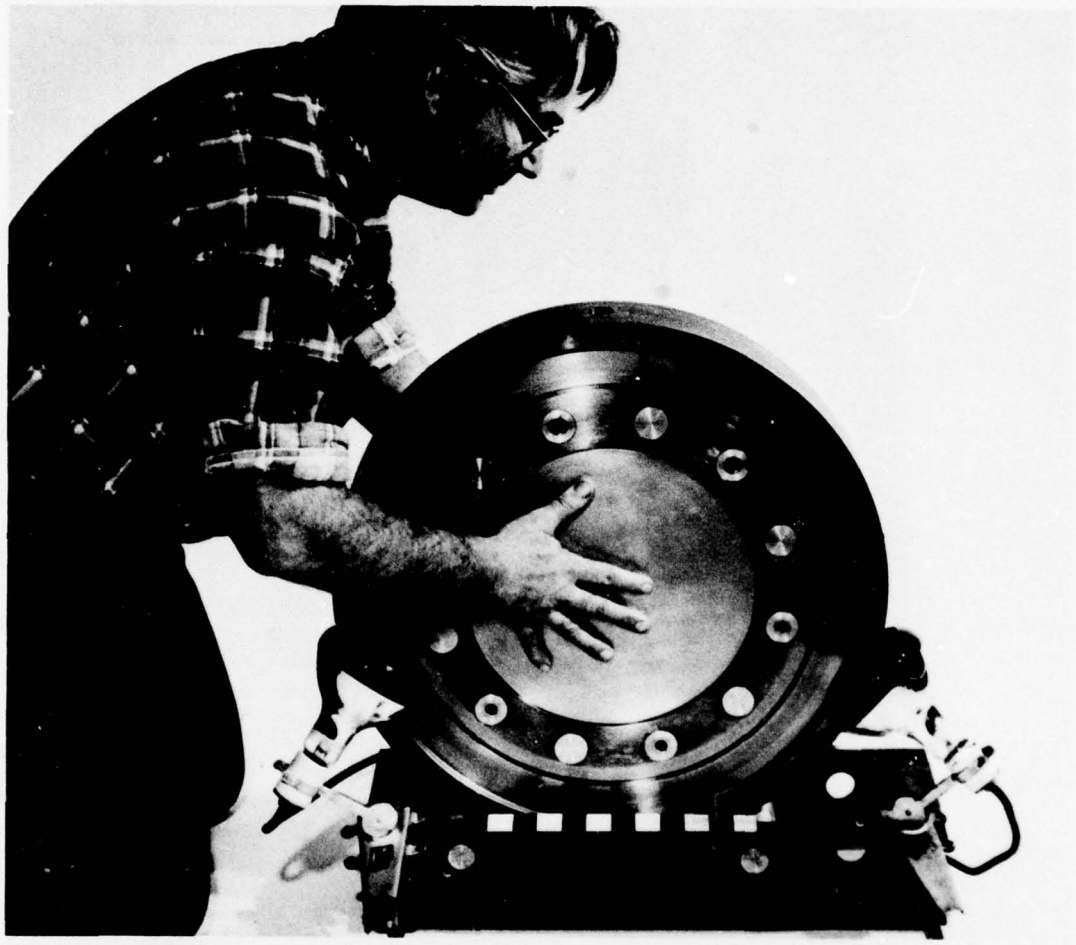

MP-4121-119

FIGURE 2.22 COPPER CUP BEING FLEXED TO HELP REMOVE TRAPPED AIR FROM REACTION CHAMBER

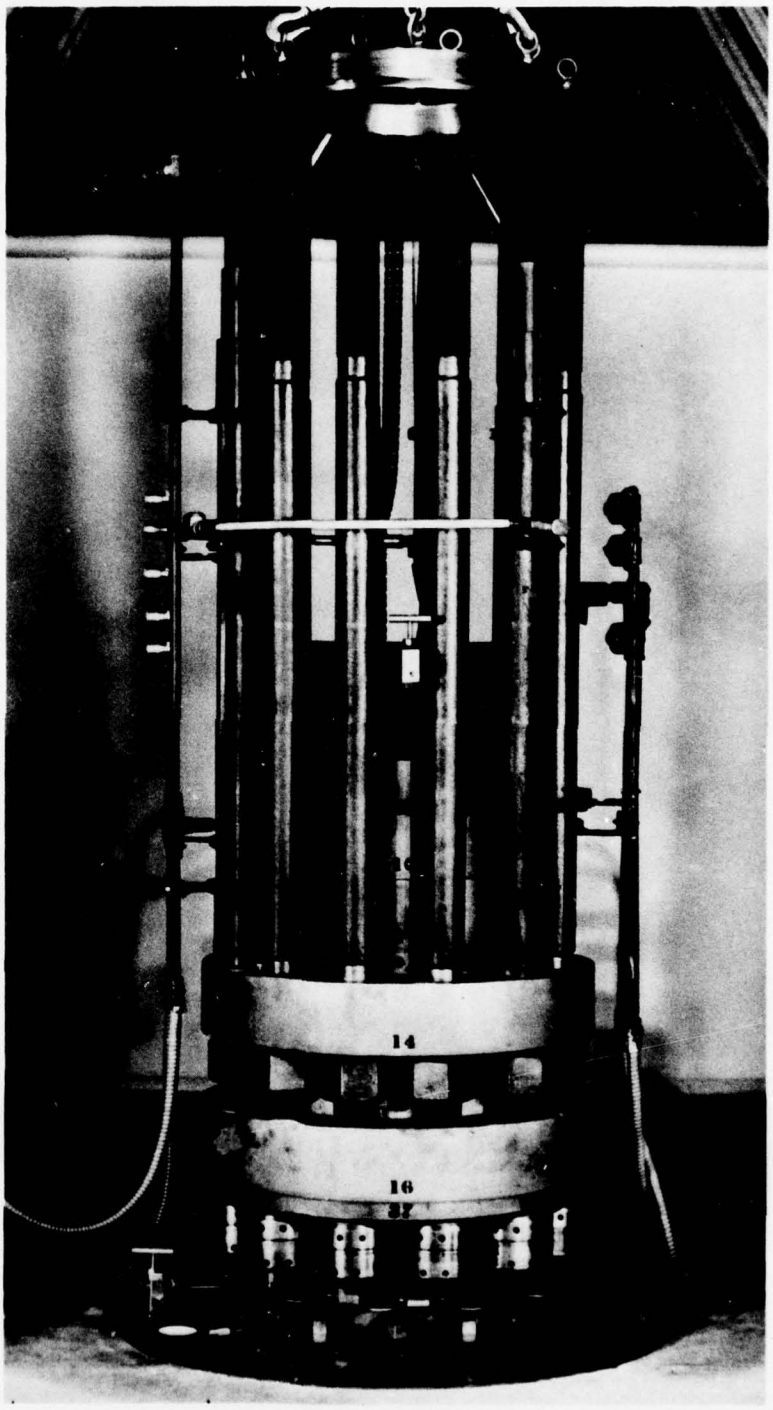

MP-4121-120

FIGURE 2.23 TESTING MACHINE STACK AFTER SPECIMEN RECEIVER PLATE IS IN PLACE

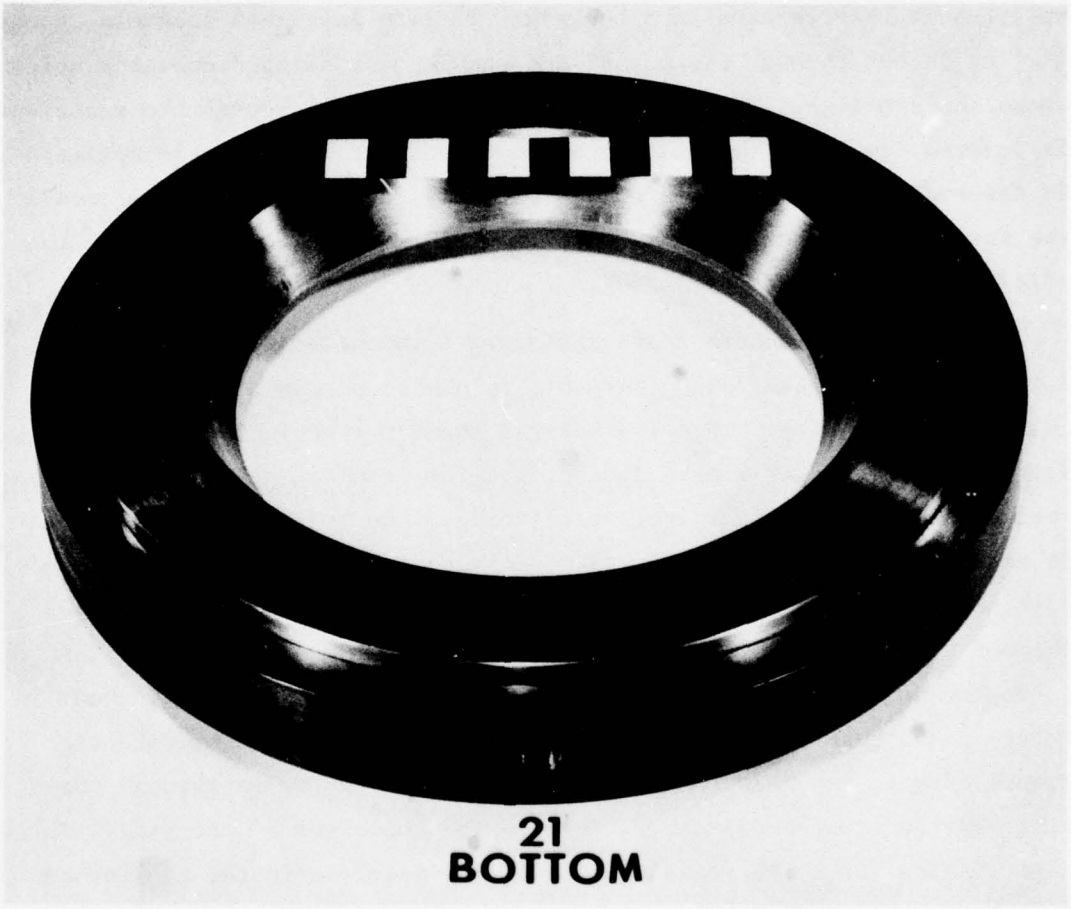

MP-4121-121

FIGURE 2.24 LATERAL CHAMBER REDUCER RING, PART NUMBER 21

At this point in the stacking sequence, a pressure gage is put into the gage port and oil is poured into the holes in the specimen receiver plate. Oil is added until it fills the space above the Bellofram, rises through the holes and is about one inch deep above the copper cup on which the specimen sits. Next, the specimen is hoisted into the testing machine. Figure 2.25 shows an aluminum dummy being lifted with an eye-bolt that threads into the top. To lift an actual specimen, however, a sling is put through the tunnel and each end is slipped over the hoist above the specimen. The specimen is lifted over the top of the studs and is lowered down into the oil above the copper cup. Before the specimen is lowered completely, it is rocked slightly to remove air trapped under the specimen. The specimen is then lowered onto the copper cup and the sling is removed from the tunnel.

If specimens that are 18 inches (0.45 m) high are tested, the lateral chamber spacer ring (part 8), is placed on top of the lateral chamber reducer ring. Then the lateral chamber tunnel ring (part 13), is stacked on the spacer ring. Another lateral chamber spacer ring is then stacked on the lateral chamber tunnel ring. The stacking sequence that is described here, however, is for specimens that are 12 inches (0.3 m) high, and the two spacer rings are omitted. In this case, the lateral chamber tunnel ring is stacked into the machine immediately after the lateral chamber reducer ring. The lateral chamber tunnel ring, shown in Figure 2.26, has two diametrically opposed holes that accommodate the tunnel adaptor assembly from the specimen. The two holes through the ring have 10° (0.17-rad) tapers through the thickness of the ring. These tapers allow for slight misalignment of the specimen in the machine and for movement of the tunnel during the test. There is a gage port in this ring 90° (1.57 rad) from the diameter defined by the two tunnel ports. The pressure gage that is put in this port is used to measure the lateral pressure applied to the specimen at midheight. At this time, the tunnel adaptors are put in place and the entire assembly is secured by tightening the tunnel retaining rings as described in the previous section. After the rock is secured in the machine, the leads from the four strain gages mounted on the specimen copper cans to measure lateral strain are soldered into the signal conditioning circuit.

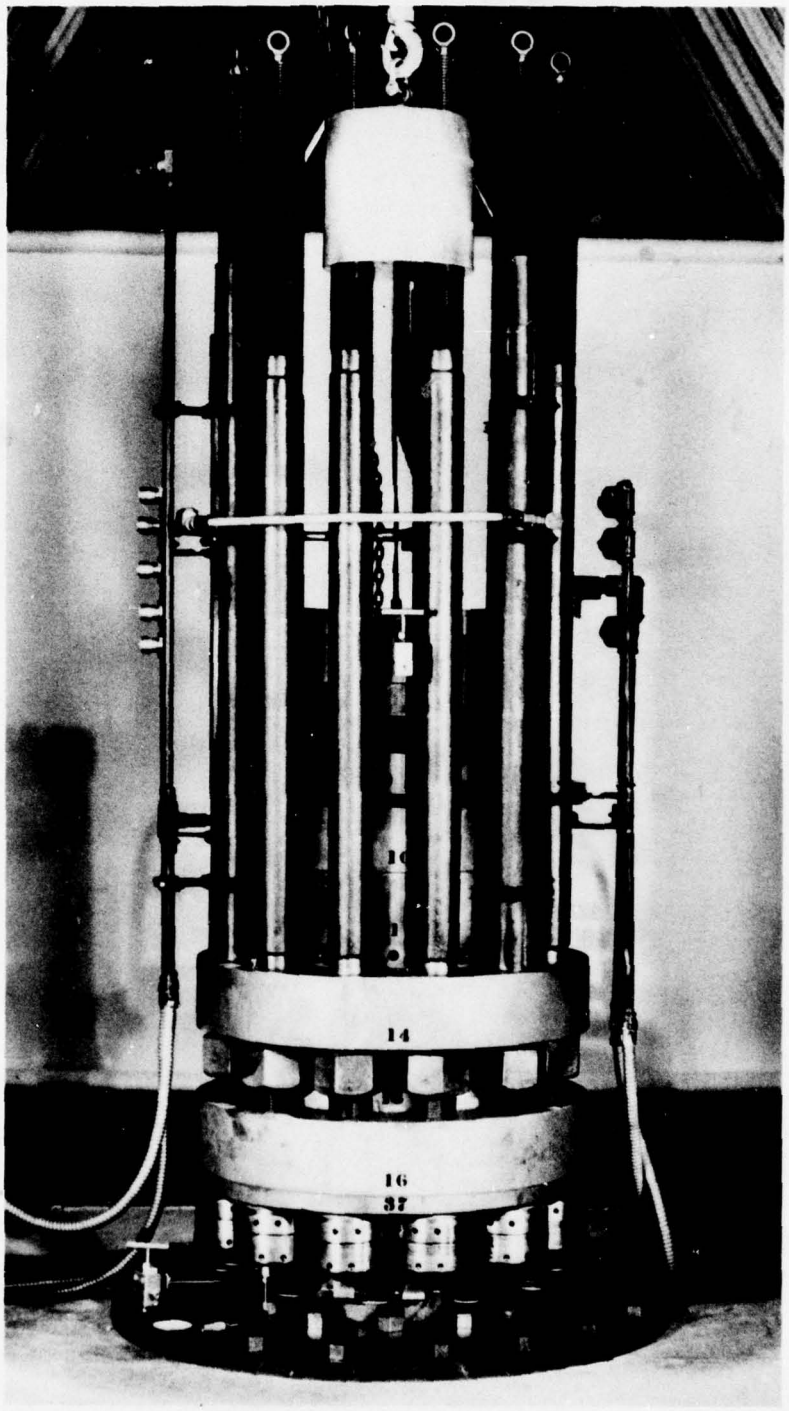

MP-4121-122

FIGURE 2.25 ALUMINUM DUMMY SPECIMEN BEING HOISTED INTO THE TESTING MACHINE

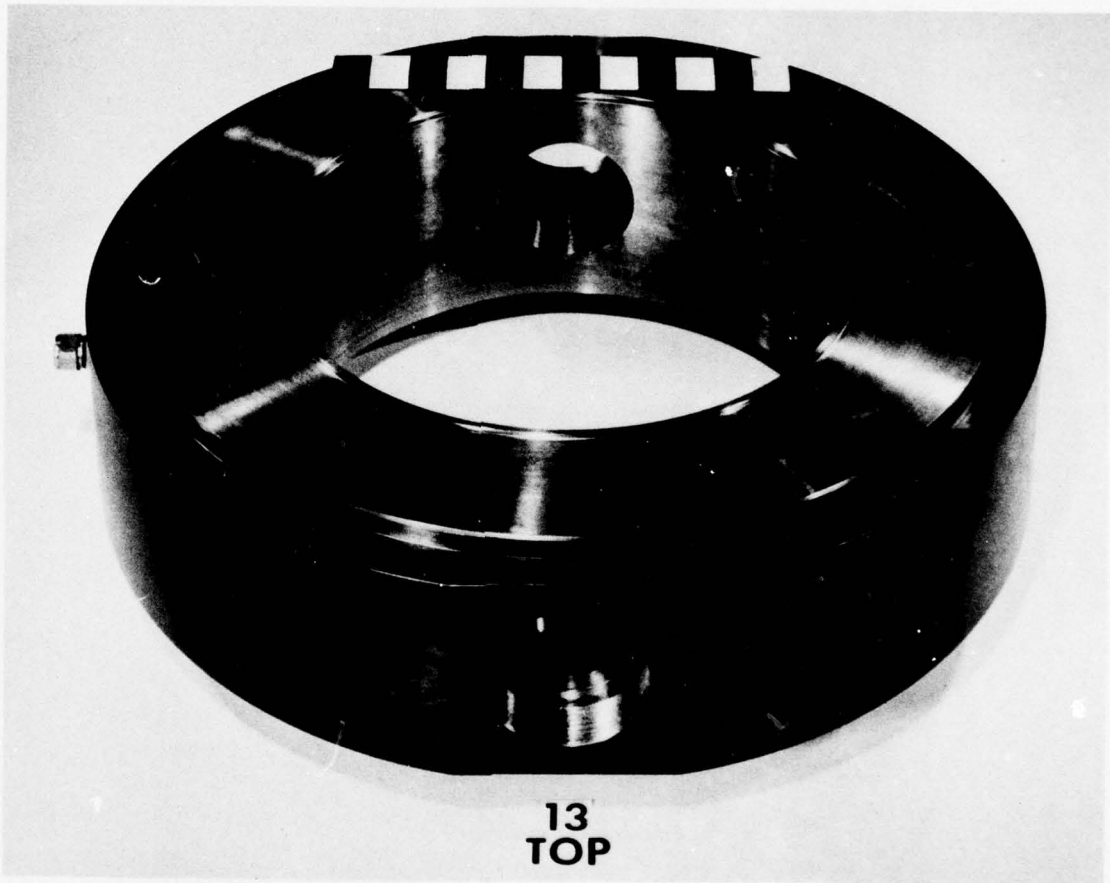

MP-4121-123

FIGURE 2.26 LATERAL CHAMBER TUNNEL RING, PART NUMBER 13

The next part to be stacked into the machine is the lateral chamber top ring (part 25), shown in Figure 2.27. There is a gage port in this ring to measure the lateral pressure near the top of the specimen. In summary, we see that each of the three rings that comprise the lateral chamber has a single gage port. These are used to verify that the confining pressures at the bottom, midheight, and top of the specimen are identical. With the pressure pulse rise times that are imposed, the pressure records obtained from gages in each gage port are indeed identical, as will be shown later. It is, however, possible to apply loadings with very short rise times so that the pressures recorded at the three gage locations are not identical because of wave propagation effects in the oil. These effects, which were observed by the three gages in early developmental tests, served to guide our understanding of machine operation and led to modifications that gave uniform, smooth pulses.

After installing pressure gages into the gage ports in the lateral chamber tunnel ring and the lateral chamber top ring, more oil is added to the lateral chamber until it just covers the top of the specimen.

The next ring to be stacked is the specimen vertical/lateral sealing ring (part 12). This ring is shown in Figure 2.28 along with the copper cup and O-ring that seal the gases that apply the vertical loading above the specimen from the oil that applies the lateral loading on the side of the specimen. (Again, these are the same as shown earlier in Figure 2.7.) This ring has six standpipes that are used to finish filling the lateral chamber with oil and to purge any air trapped in the lateral chamber. Each standpipe is connected to a 1/16-inch (1.6-mm) diameter hole in the lower face of the specimen vertical/lateral sealing ring through a high-pressure valve. One of the 1/16-inch (1.6-mm) diameter holes is shown in Figure 2.29. To completely fill the lateral chamber, four of the six valves are closed. Oil is pumped into the lateral chamber through one of the open valves and air escapes through the other. When the chamber is full, oil flows out the escape valve. Oil flow through this valve is permitted for a few minutes to allow trapped air to escape. Then, the escape valve is closed and an adjacent one is opened and oil is

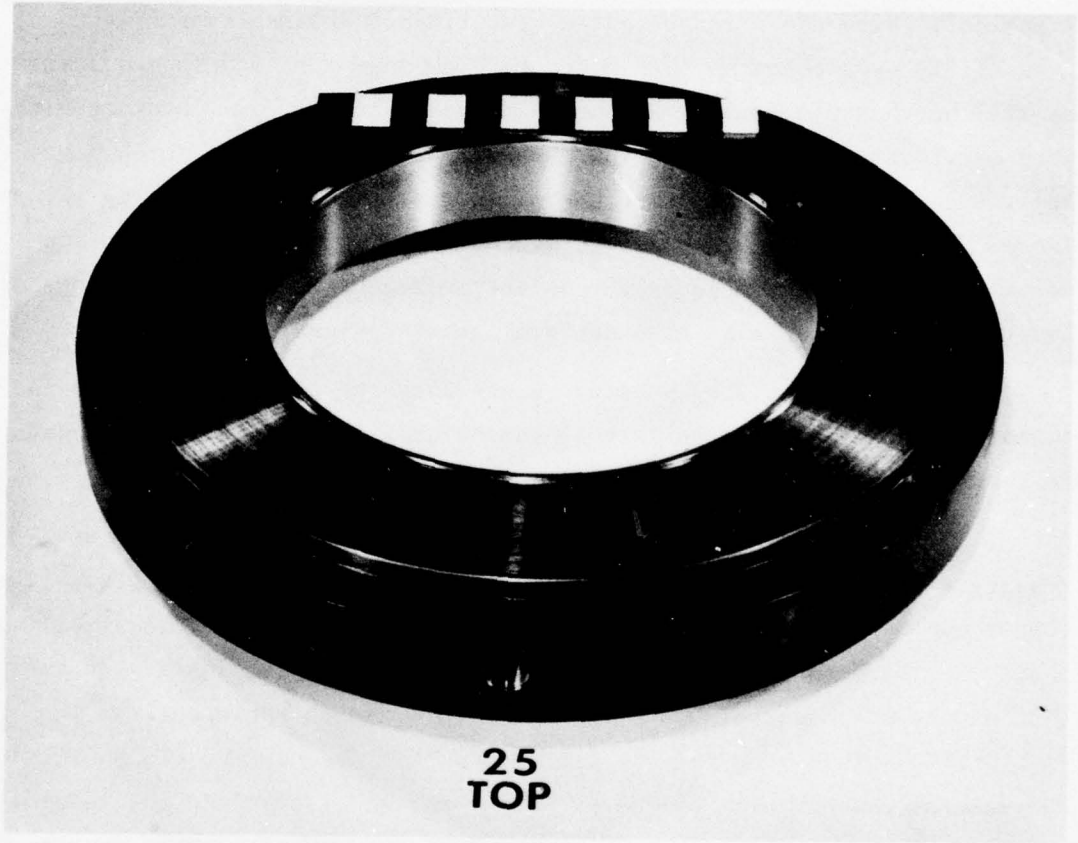

MP-4121-124

FIGURE 2.27 LATERAL CHAMBER TOP RING, PART NUMBER 25

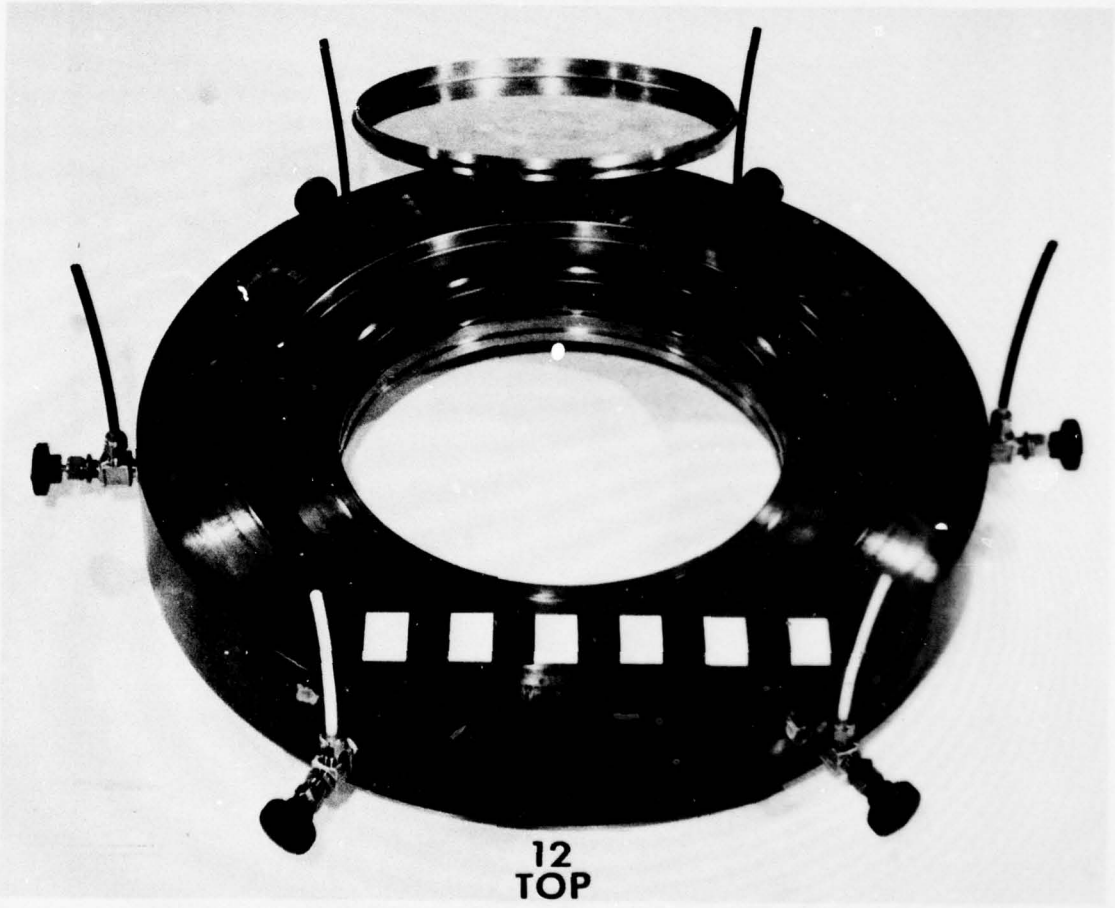

MP-4121-125

FIGURE 2.28 SPECIMEN VERTICAL/LATERAL SEALING RING, PART NUMBER 12

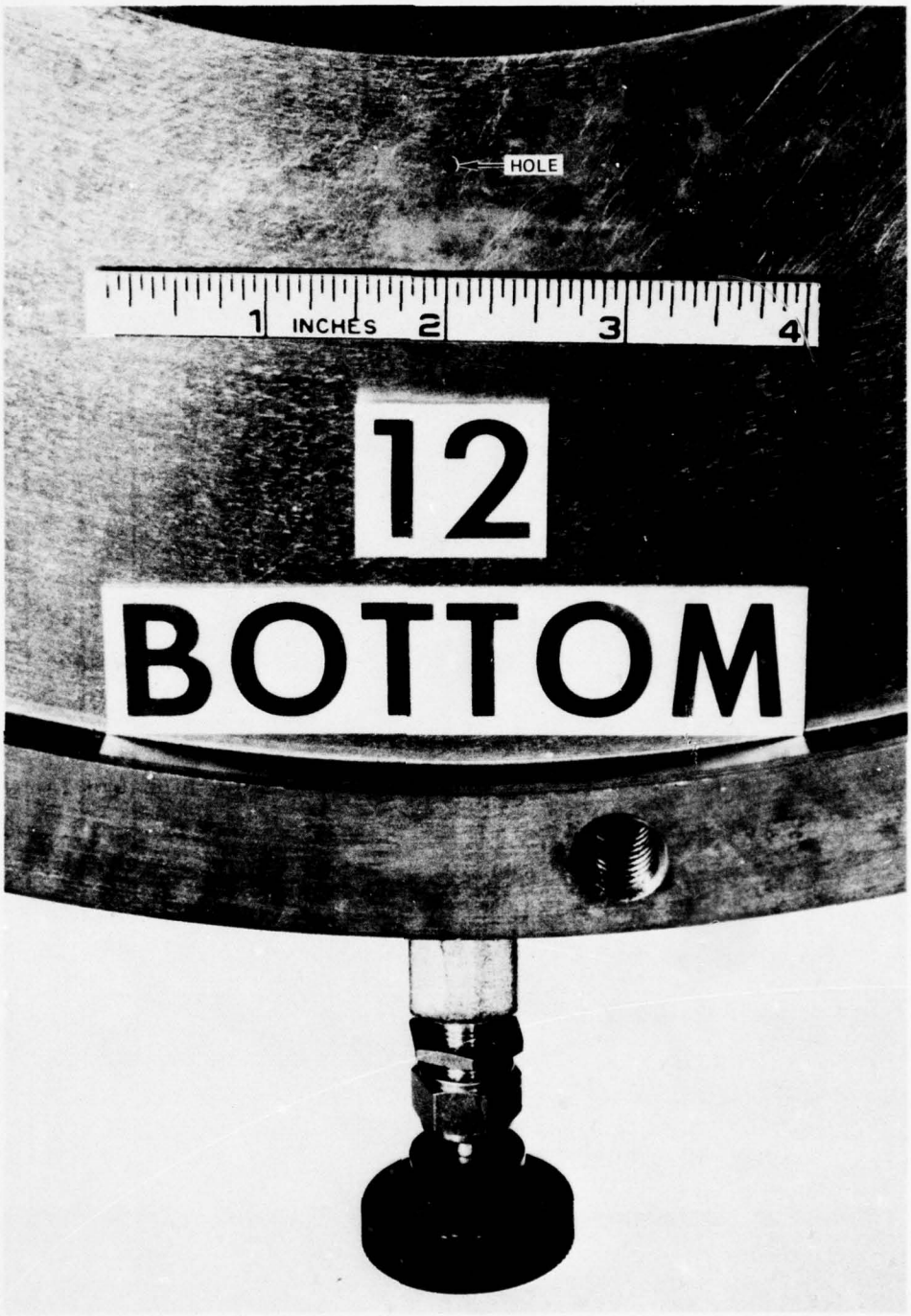

MP-4121-126

FIGURE 2.29 1/16-INCH DIAMETER HOLE IN LOWER FACE OF SPECIMEN VERTICAL/ LATERAL SEALING RING USED TO COMPLETE FILLING LATERAL CHAMBER AND TO PURGE TRAPPED AIR

allowed to flow out for a few minutes. Each valve is opened in turn and oil is allowed to flow out, releasing any trapped air. After each valve has been opened and closed, all six valves are opened and the standpipes are filled with oil. The valves remain open until just before the shot is fired so that any remaining air can escape.

The specimen vertical/lateral sealing ring has two diametrically opposed gage ports. Pressure gages are put into these ports after the ring has been stacked into the machine. These two redundant gages measure the pressure in the explosive gases that apply the vertical pressure loading to the top of the specimen.

It is important in these tests that the rise times and peaks of the vertical and lateral pressure pulses coincide. Although the general magnitudes of the rise times are set by changing the area of the holes through the orifice plates, it is impractical to match the rise times precisely with this technique. To fine-tune the timing of the vertical pulse to that of the lateral pulse, a small amount of inert, claylike material (Duxseal) is placed in the copper cup above the specimen, reducing the volume that the explosive gases must fill and consequently shortening the rise time. This material is added to the copper cup before the specimen vertical/lateral sealing ring-copper cup assembly is hoisted onto the stack.

Next, the vertical chamber baffle plate (part 29), is lowered onto the stack. This plate, shown in Figure 2.30, has the same hole pattern as the lateral chamber baffle plate but is 16 inches (0.41 m) in diameter and 2-1/8 inches (54 mm) thick. It serves the same purpose as the lateral chamber baffle plate, namely, to prevent the explosive gases from jetting directly onto the loading surface, which in this case is the top of the rock.

Figure 2.31 shows the status of the testing machine stack at this point. Since the last photograph of the testing machine status in Figure 2.23, the specimen has been loaded into the machine and the three lateral chamber rings have been stacked around the specimen. The leads

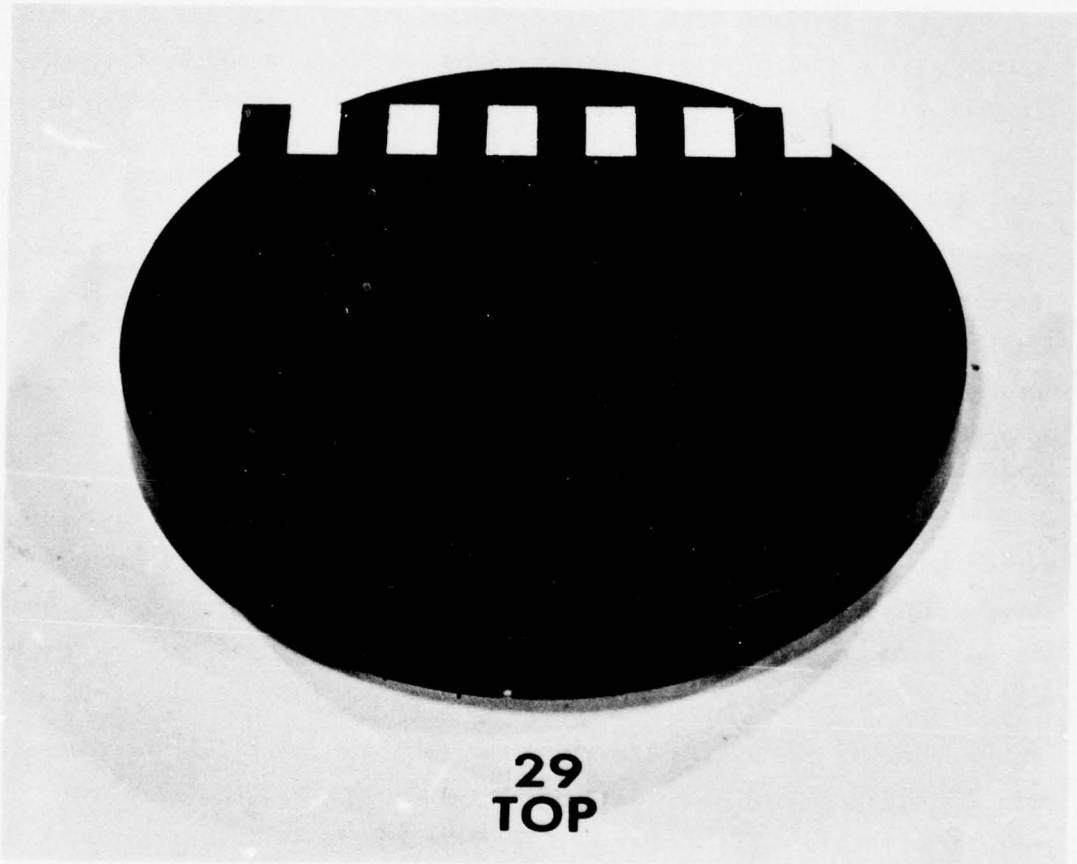

MP-4121-127

FIGURE 2.30 VERTICAL CHAMBER BAFFLE PLATE, PART NUMBER 29

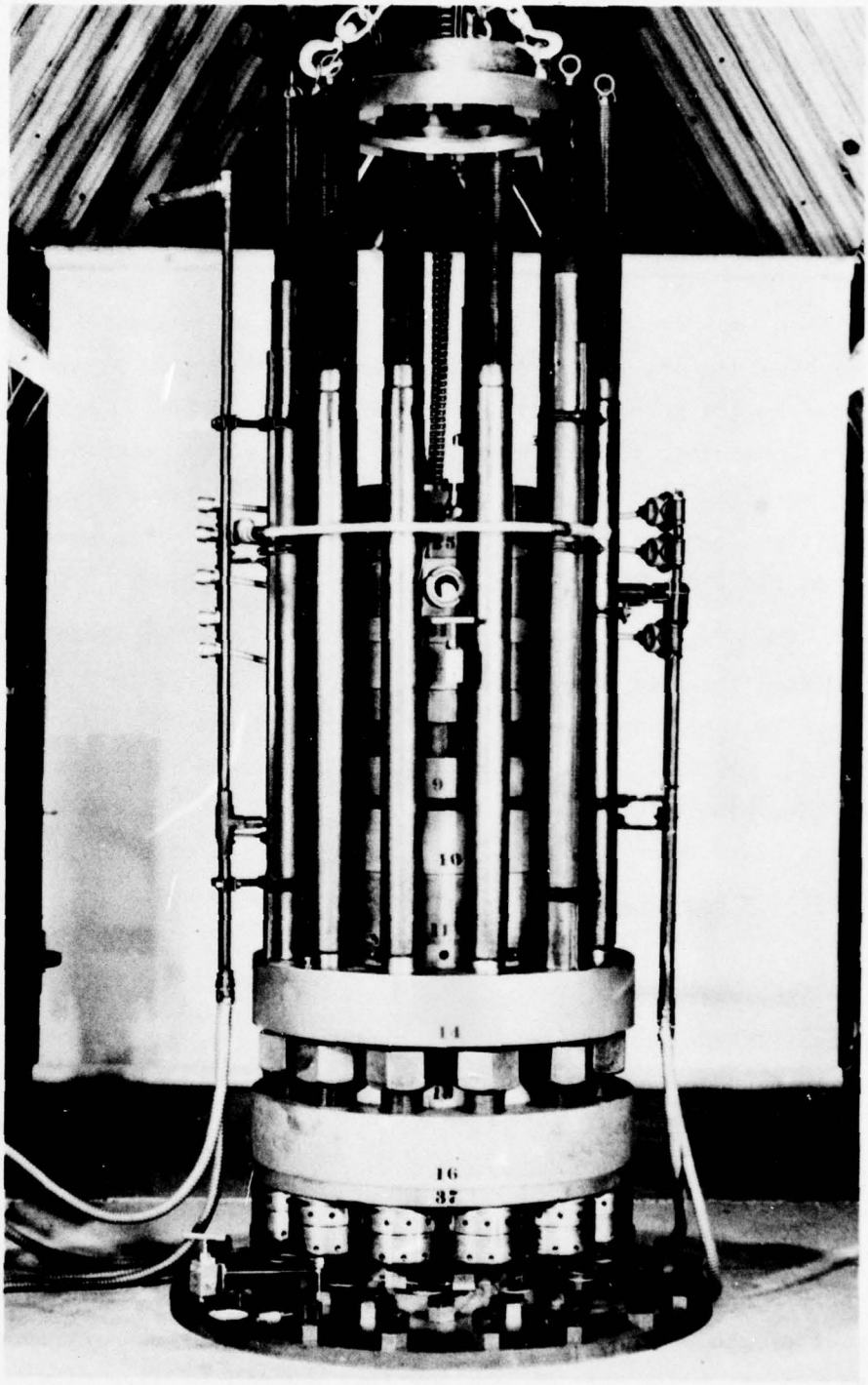

MP-4121-128

FIGURE 2.31 TESTING MACHINE STACK AFTER VERTICAL CHAMBER BAFFLE PLATE IS IN PLACE

to the four specimen lateral strain gages have been soldered into the power supply/amplifier circuits. Then the tunnel adaptors, which connect the tunnel in the specimen to the ports in the lateral chamber tunnel ring were put in place, followed by the three pressure gages used to measure the pressure in the oil around the specimen. The lateral chamber has been filled with oil and the specimen vertical/lateral sealing ring has been hoisted onto the stack. The last two pressure gages, which measure the explosive gas pressure above the specimen, have been placed in the gage ports in the specimen vertical/lateral sealing ring. Also, a small amount of inert material has been placed in the copper cup above the specimen to adjust the rise time of the vertical pressure pulse, if necessary; and, finally, the vertical chamber baffle plate has been stacked on the specimen vertical/lateral sealing ring.

The next two parts to be placed on the machine stack are shown being hoisted together over the top of the studs in Figure 2.31. The lower part is the vertical mixing chamber ring (part 7), which is shown in Figure 2.32. This ring has the same function as its lateral chamber counterpart, namely, to provide a volume between the orifice plate and the baffle plate where the explosive gases that jet through the holes in the orifice plate mix before flowing through the holes in the baffle plate.

The second part shown being hoisted into the machine in Figure 2.31 is the vertical chamber orifice plate (part 31). The closeup view of this plate in Figure 2.33 shows the same hole pattern as that in the lateral chamber orifice plate. The hole patterns in the orifice plate and the baffle plate, both lateral and vertical, are such that the explosive gases cannot jet directly through both plates. Just as the rise time of the lateral pressure pulse can be lengthened by reducing the area of the holes through the lateral chamber orifice plate, the rise time of the vertical pressure pulse can be lengthened by reducing the area of the holes through the vertical chamber orifice plate.

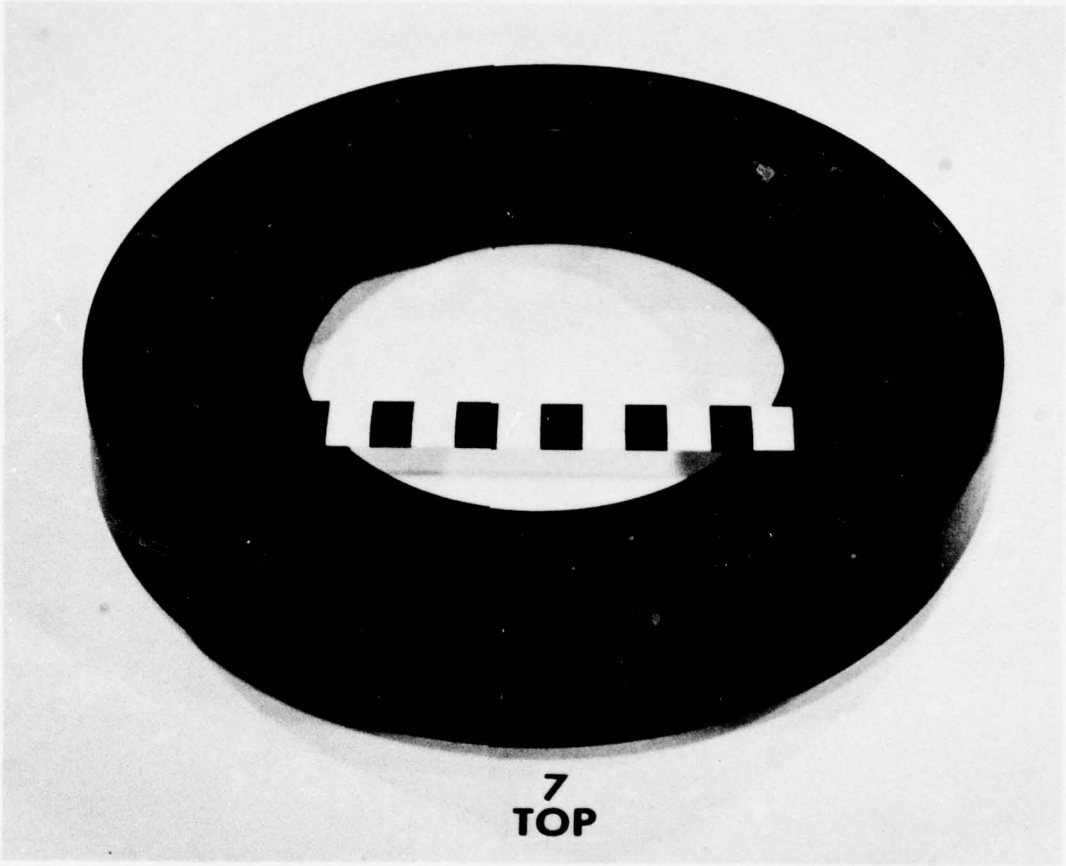

MP-4121-129

FIGURE 2.32 VERTICAL MIXING CHAMBER RING, PART NUMBER 7

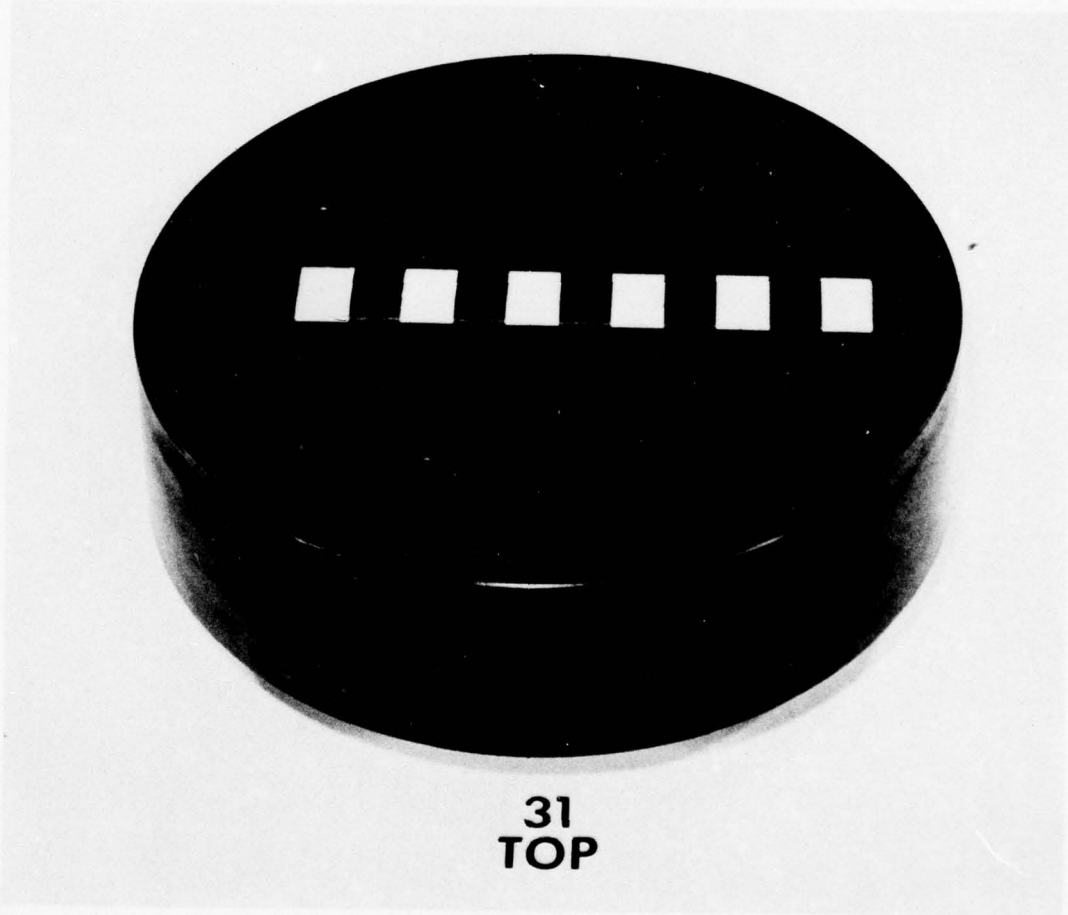

MP-4121-130

FIGURE 2.33 VERTICAL CHAMBER ORIFICE PLATE, PART NUMBER 31

Figure 2.34 shows the lower vertical charge chamber ring (part 6), which is lifted into the stack and mated with the vertical chamber orifice plate. This is followed by the upper vertical charge chamber ring (part 5), shown in Figure 2.35. The vertical charge chamber is the same size as the lateral charge chamber: 12 inches (0.3 m) in diameter and 9-3/4 inches (0.25 m) deep.

The vertical chamber vent ring (part 57), is stacked on top of the upper vertical charge chamber ring. This vent ring, shown in Figure 2.36, is similar to the lateral chamber vent ring discussed previously. By reducing the area of the 12 holes that allow the explosive gases to escape from the chamber, the duration of the vertical pressure pulse can be increased.

The last of the machine parts to be hoisted onto the stack is the top end plate (part 15). Figure 2.37 shows this plate and the triangular shield that protects two strain gages mounted at the center of its upper surface. The output of these strain gages is used to determine the stress in the plate during a test. The top end plate has twelve 3-5/8-inch (92-mm) diameter holes, which must be fitted over the 12 studs. The plate must be aligned carefully so that the studs are not twisted. Figure 2.38 shows the top end plate being lowered over the studs onto the stack.

Figure 2.39 shows the completely assembled machine. The 12 nuts above the top end plate are tightened by hand and mallet because there is not enough clearance between the nuts to use a wrench. Hydraulic nuts are used to tension the studs. Pressure is supplied to the hydraulic nuts by a pumping system mounted on a cart, shown next to the testing machine in Figure 3.5 (page 105). Because the pressures in the hydraulic nuts reach 30 ksi (0.21 GPa), shields are bolted into place around the bottom of the test machine. These shields are shown in Figure 2.39, offset from their functional positions so that the hydraulic nuts can be seen.

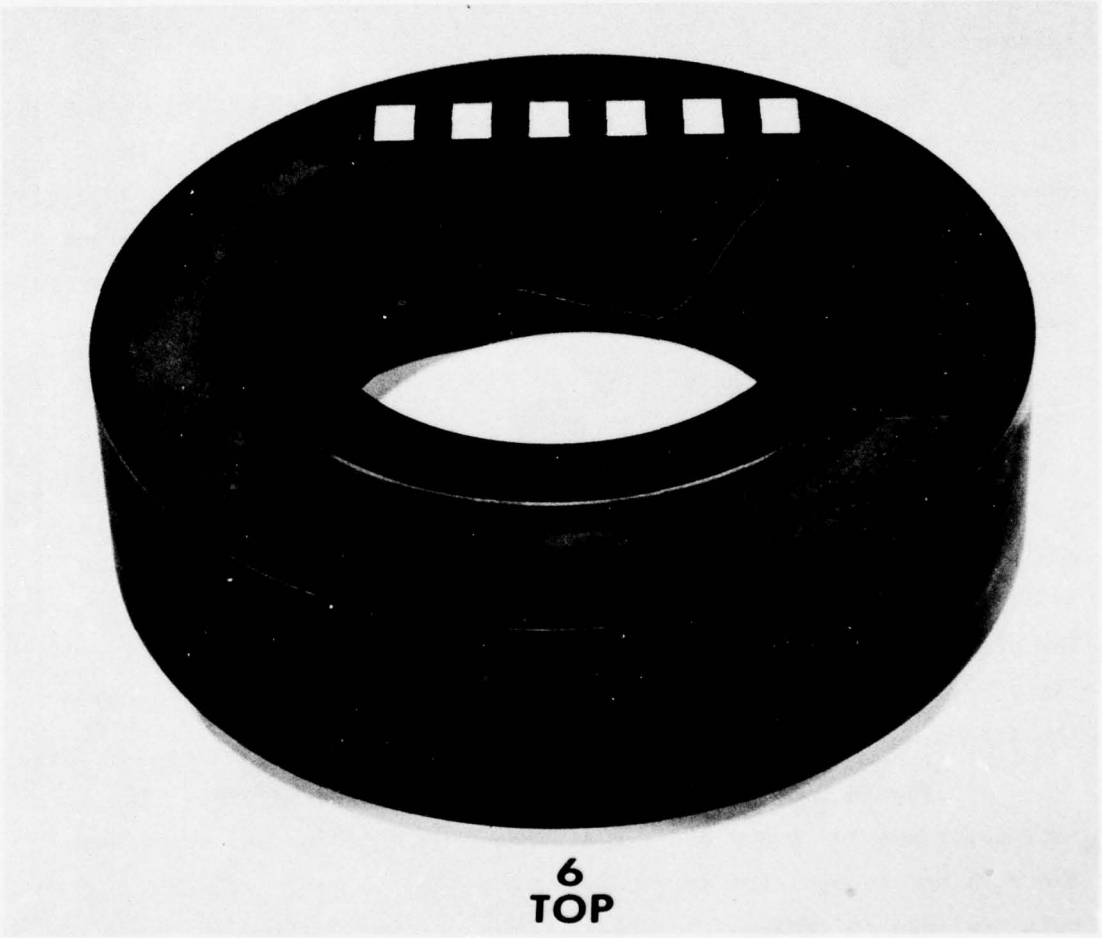

MP-4121-131

FIGURE 2.34 LOWER VERTICAL CHARGE CHAMBER RING, PART NUMBER 6

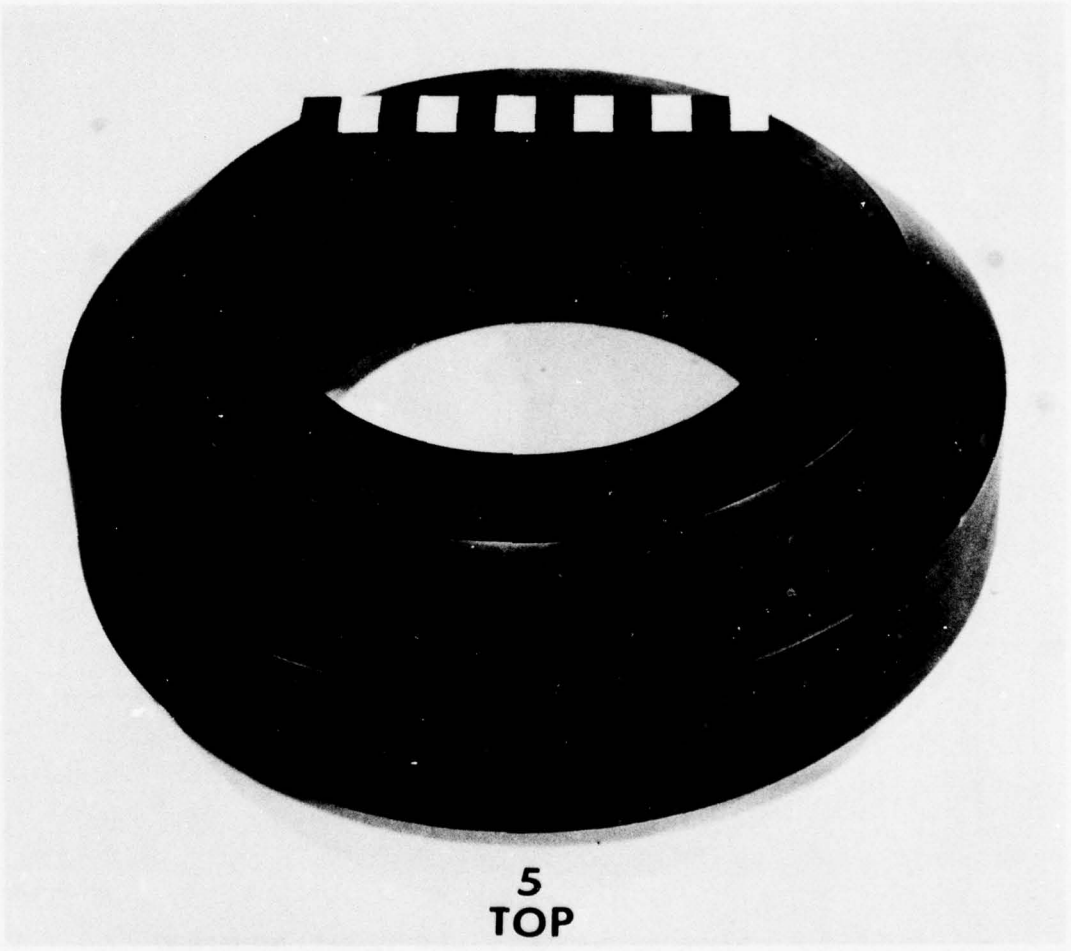

MP-4121-132

FIGURE 2.35 UPPER VERTICAL CHARGE CHAMBER RING, PART NUMBER 5

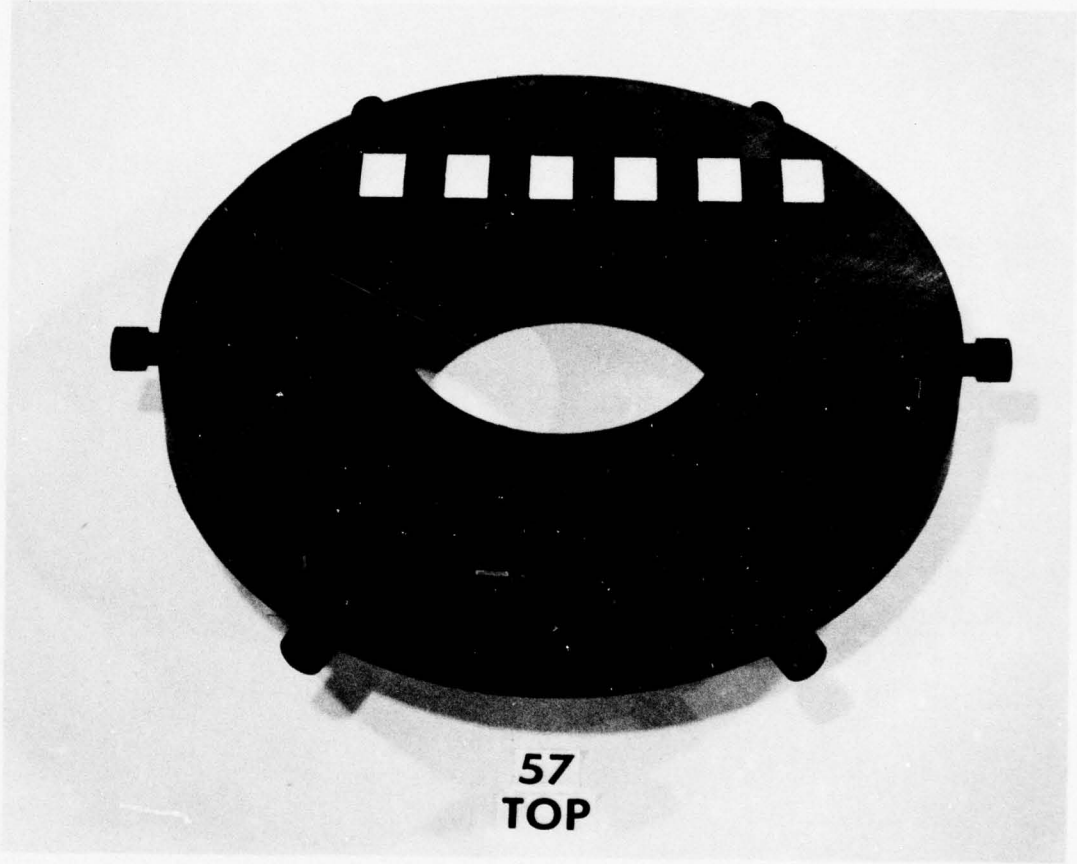

MP-4121-133

FIGURE 2.36 VERTICAL CHAMBER VENT RING, PART NUMBER 57
Six of the 12 vent holes are plugged to lengthen duration of the vertical pressure pulse

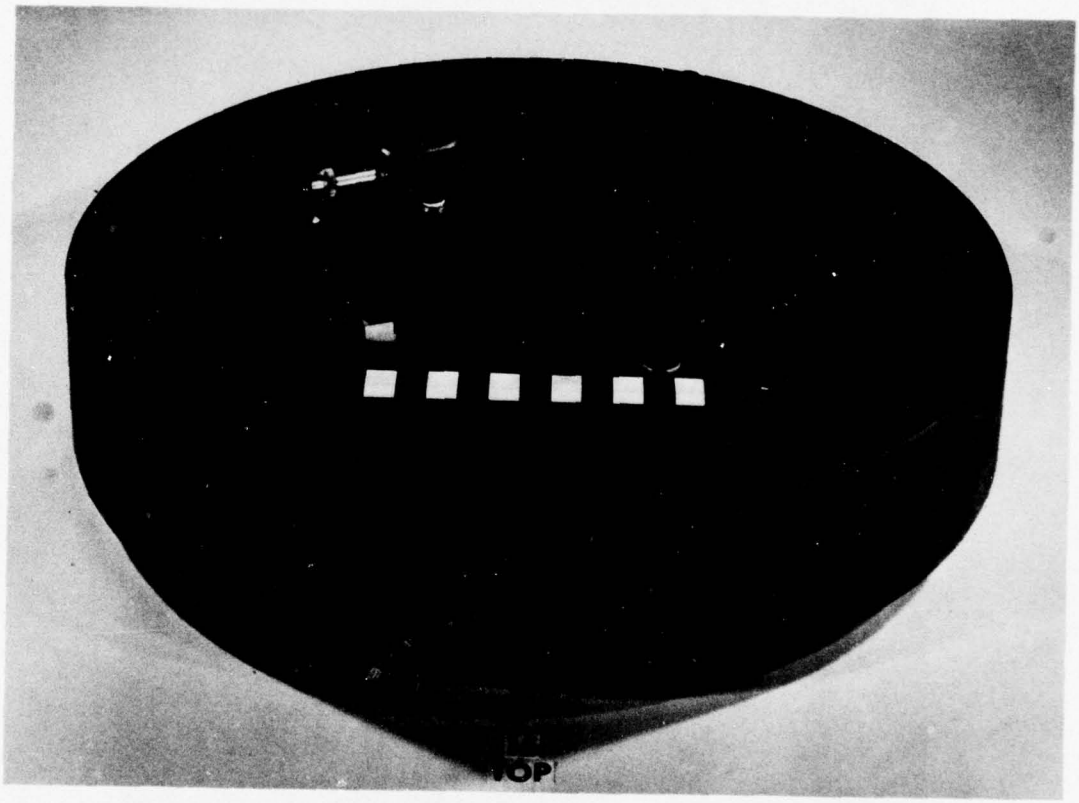

MP-4121-134

FIGURE 2.37 TOP END PLATE, PART NUMBER 15, SHOWING TRIANGULAR SHIELD THAT PROTECTS STRAIN GAGES USED TO MEASURE STRAIN DURING TEST

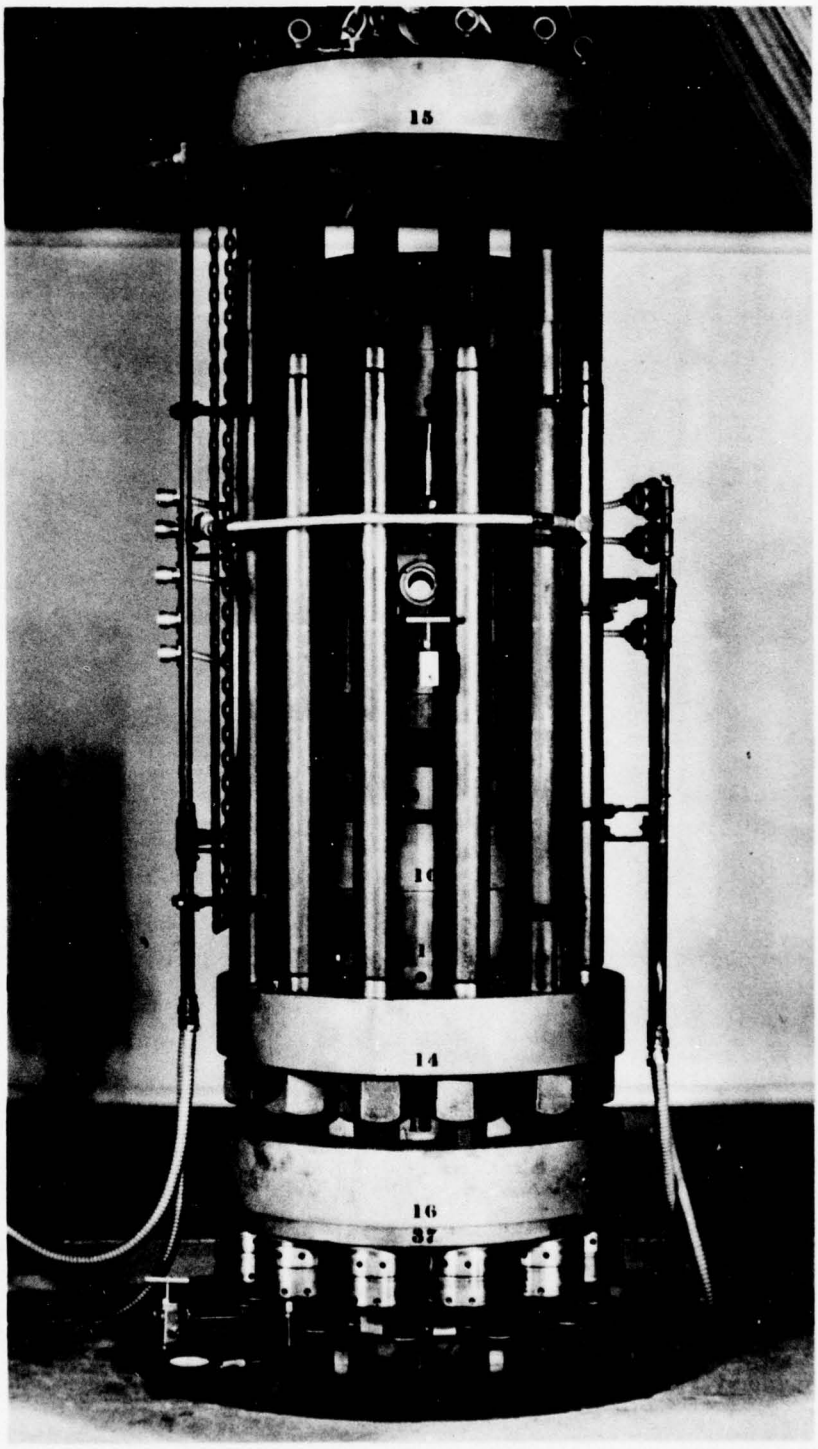

MP-4121-135

FIGURE 2.38 TOP END PLATE BEING LOWERED OVER STUDS

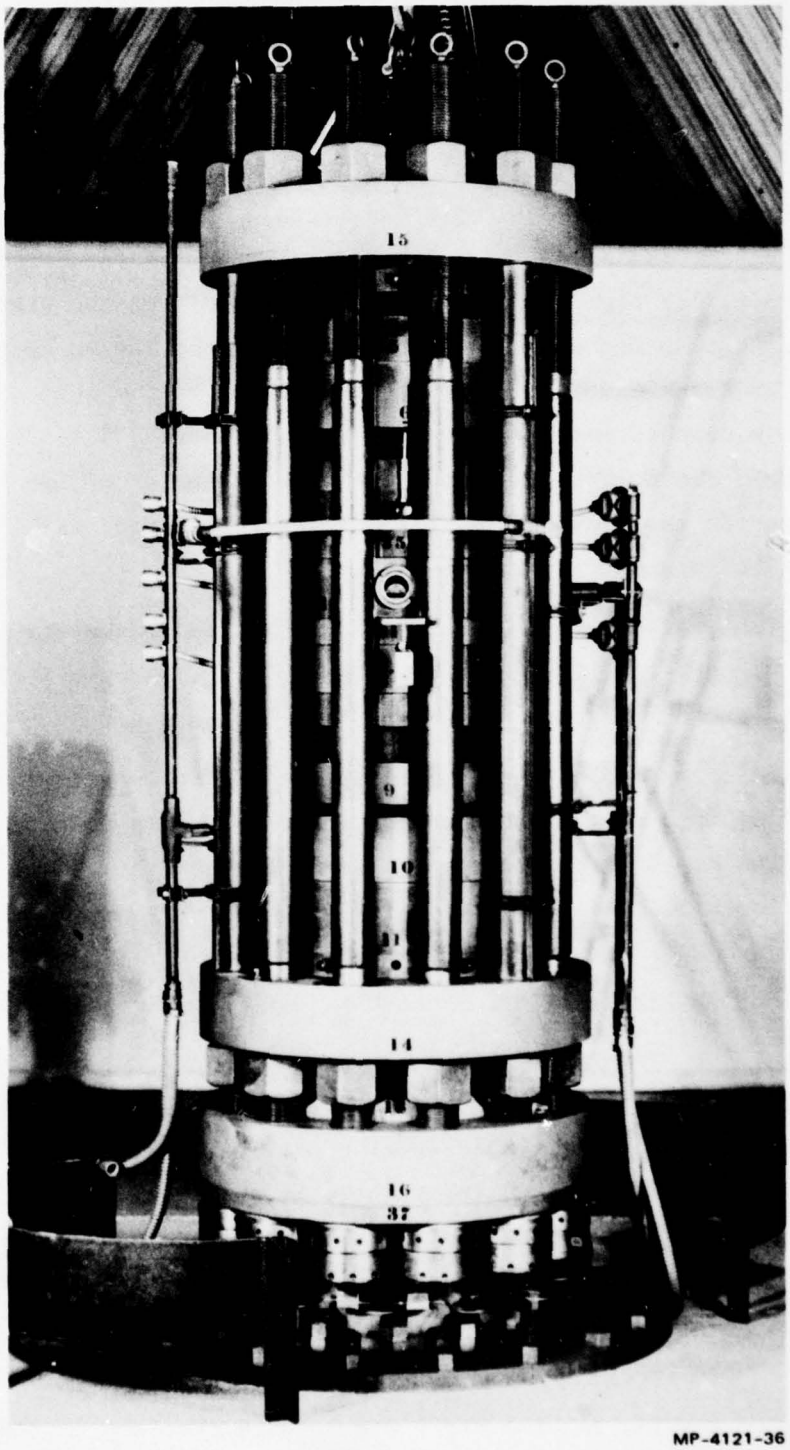

MP-4121-36

FIGURE 2.39 TESTING MACHINE COMPLETELY ASSEMBLED, WITH HYDRAULIC NUT SHIELDS SET BACK TO REVEAL HYDRAULIC NUTS

Figure 2.40 shows a close-up of the hydraulic nuts. As pressure is applied to the hydraulic nuts, they tension the studs. When the pressure in the hydraulic nuts is 30 ksi (0.21 GPa), the tensile stress in the studs is approximately 45 ksi (0.31 GPa), measured by strain gages at a stress-relieved diameter near the threads. Mechanical backup nuts, below the bottom end plate (part 14) at the bottom of the functional machine stack, are tightened against plate 14 and then the pressure in the hydraulic nuts is released so that they are not loaded by the test firing. The transfer of load from the hydraulic to the mechanical nuts results in a drop in tensile stress in the studs from 45 to 36 ksi (0.31 to 0.25 GPa), about 20%. The stress-relieved diameter of the 12 studs is 3.20 inches (81 mm), so that the total force holding the machine together is 3.4 million pounds (15 million newtons).

The instrumentation cables are hooked up to the six pressure gages and are shielded from the escaping explosive gases by 1/2-inch (12.7-mm) diameter flex conduit as shown in Figure 2.41.

Before proceeding to a description of the instrumentation and the firing of the test, differences in the stacking sequence between the dynamic triaxial configuration, just described, and the dynamic isotropic configuration will be discussed.

2.3.2 Machine Assembly for Isotropic Testing

In the isotropic loading tests, the lateral confining pressure is equal to the vertical loading pressure, and only one explosive charge is necessary to provide a single loading pulse. Only the vertical charge chamber at the top of the testing machine is used, so that the machine need only be unstacked to the level of the specimen receiver plate. This saves considerable time stacking and unstacking the test machine during a series of tests. The changes that accompany these major alterations will be discussed as the stacking sequence is described.

The testing machine stack starts with the lateral charge chamber and vent rings in place. No explosive charge is put into the lateral charge chamber. The lateral chamber orifice plate is stacked

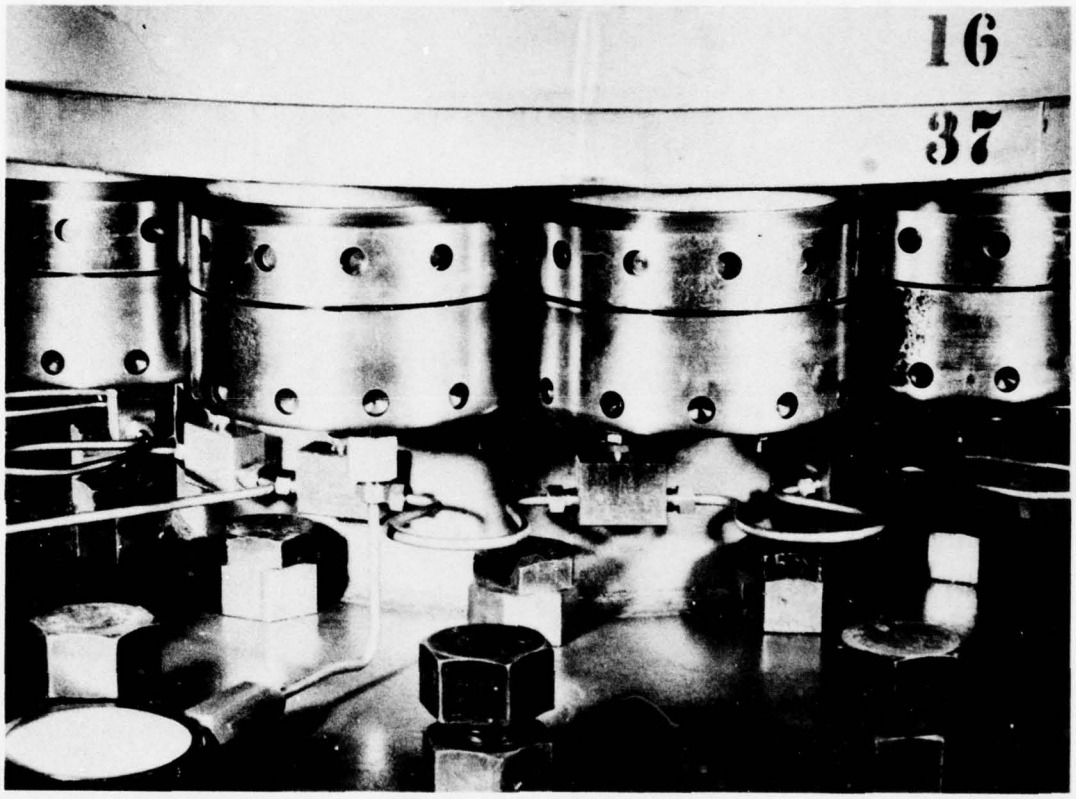

MP-4121-137

FIGURE 2.40 CLOSE-UP VIEW OF THE HYDRAULIC NUTS THAT ARE USED TO TENSION THE STUDS

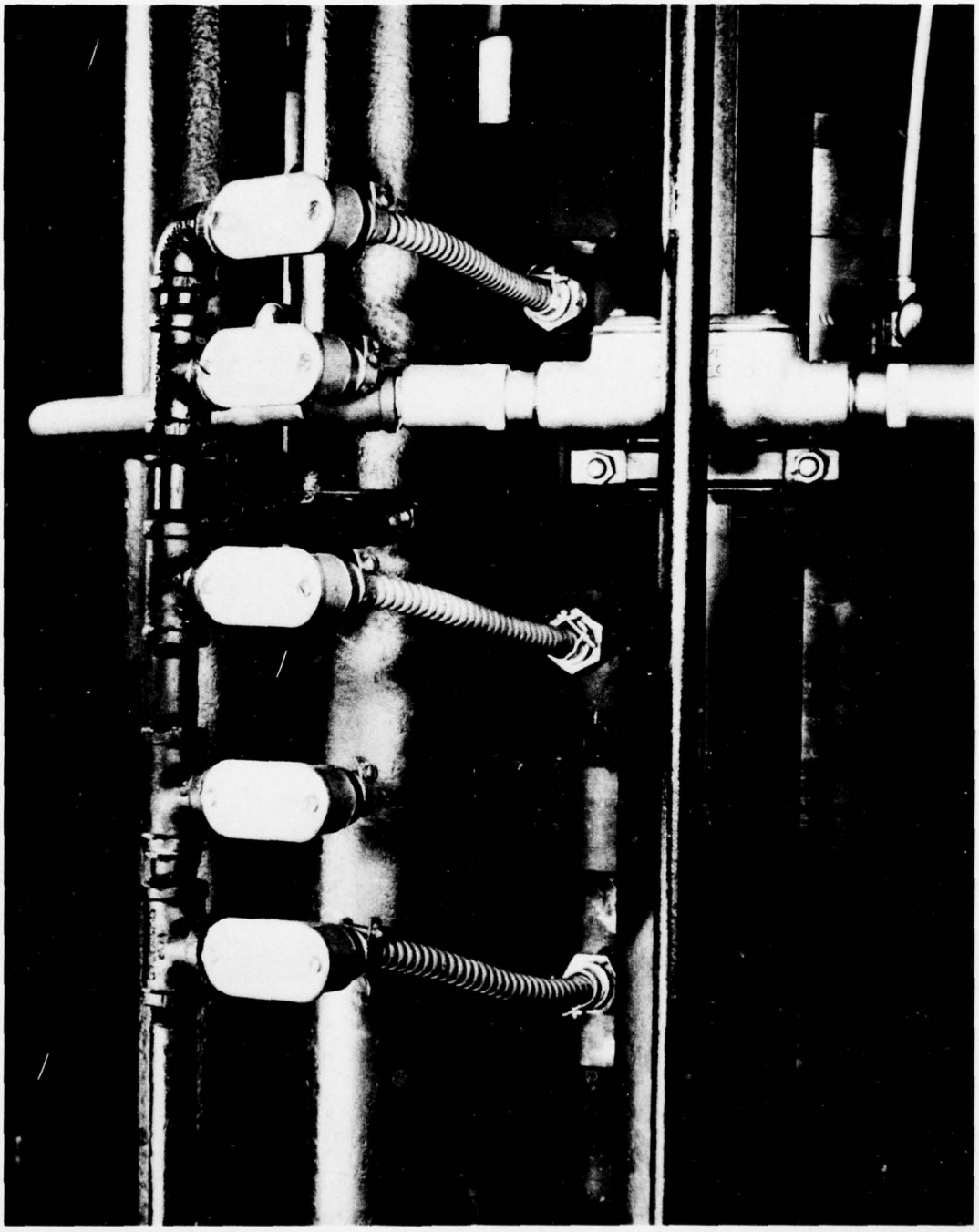

MP-4121-138

FIGURE 2.41 PIPE AND FLEX CONDUIT THAT PROTECTS INSTRUMENTATION CABLES FROM ESCAPING EXPLOSIVE GASES

on top of the charge chamber as in the triaxial configuration. Next, however, the vertical mixing chamber ring and the vertical chamber baffle plate are stacked instead of their lateral counterparts. The lateral chamber baffle plate and lateral mixing chamber ring are needed later to allow the Bellofram to be placed above the specimen rather than below as in the triaxial configuration.

The next part to be stacked is the specimen vertical/lateral sealing ring. In the isotropic configuration, this ring serves as a spacer ring and no pressure gages are put into the two gage ports. The specimen receiver plate is stacked on top of the specimen vertical/lateral sealing ring. The oil chamber under the specimen is not sealed with a copper cup and O-ring since the oil pressure under the rock is the same as that around the rock. A pressure gage is inserted into the gage port in the specimen receiver plate.

The next part to be stacked is the lateral chamber adaptor close-off ring (part 23). This ring, shown in Figure 2.42, blocks the 12 holes through the specimen receiver plate and seals the bottom of the lateral chamber. The interface between the specimen receiver plate and the lateral chamber close-off ring is sealed by two O-rings. The interfaces between all the rings that comprise the lateral chamber have single O-ring seals, just as in the triaxial configuration.

At this point, oil is poured into the lateral chamber until it reaches a depth of a few inches. Then the specimen is hoisted into the machine. Before the specimen is seated in the bottom of the lateral chamber, it is slowly rocked to release any air trapped under it.

Next, the lateral chamber tunnel ring is lowered onto the stack and the tunnel adaptor assembly is put in place. Then the lateral chamber and lateral chamber reducer rings are stacked onto the machine. The lateral chamber reducer ring opens the lateral chamber to the same diameter as the Bellofram, and the Bellofram assembly is the next component stacked on the machine.

MP-4121-139

FIGURE 2.42 LATERAL CHAMBER ADAPTOR CLOSE-OFF RING, PART NUMBER 23

However, before the Bellofram assembly is stacked on top of the lateral chamber reducer ring, pressure gages are put into the gage ports of the lateral chamber tunnel, lateral chamber, and lateral chamber reducer rings. Then the lateral chamber is filled with oil to cover the specimen.

After the Bellofram assembly has been put in place, the lateral chamber baffle plate is hoisted onto the stack. The lateral chamber baffle plate is used here rather than the vertical chamber baffle plate because its larger diameter is compatible with that of the Bellofram and the Bellofram ring. Similarly, the lateral mixing chamber ring is used instead of the vertical mixing chamber ring because its diameter is compatible with that of the lateral chamber baffle plate. After the lateral mixing chamber ring, the vertical chamber orifice plate is lifted onto the machine. This is followed by the two vertical charge chamber rings. The explosive charge is placed in the charge chamber, and the vertical chamber vent ring is lowered onto the stack.

The top end plate is hoisted into place just as in the triaxial configuration, and the nuts are placed on the studs and hand tightened against the plate. Pressure is applied to the hydraulic nuts to tension the studs. The backup nuts are tightened, and the pressure is relieved in the hydraulic nuts.

When the Bellofram assembly was put in place at the top of the lateral chamber, the Bellofram was permitted to sag under the weight of the Bellofram protector plate. This sagging allowed the Bellofram and Bellofram protector plate to be floated on the oil in the lateral chamber. Since the Bellofram was in contact with the oil in the lateral chamber, no air was trapped below the Bellofram. However, the sagging increased the gap between the baffle plate and the Bellofram and therefore the volume that must be filled by the expanding gases was increased. This means that larger explosive charges are required to achieve the same pressures and that the rise time of the pressure pulse is lengthened. To remedy this situation, more oil is pumped into the lateral chamber

through a port in the lateral chamber ring. This extra oil pushes the Bellofram up until the protector plate contacts the baffle plate. The pumping continues until the pressure in the oil is a few psi.

The stacking sequences for the two dynamic testing machine configurations have been described and at this point the shot is ready to be fired. However, before discussing the firing and recording procedures, the instrumentation will be described.

2.4 INSTRUMENTATION

2.4.1 Pressure

The pressure applied to the specimen is measured by six pressure gages in the triaxial configuration and by four pressure gages in the isotropic configuration. Figure 2.43 shows the locations of the six pressure gages in the triaxial configuration. Stations 1 and 2 are diametrically opposed, and the gages there are used to measure the pressure in the explosive gases above the specimen. The pressure gage at station 6 is used to measure the pressure in the oil under the specimen. The three gages at these stations provide independent measurements of the vertical pressure applied to the specimen. The three gages at stations 3, 4, and 5 are used to measure the pressure in the oil in the lateral chamber near the top, midheight, and bottom of the specimen. These three gages provide independent measurements of the lateral pressure applied to the specimen. To be assured that the specimen is being loaded uniformly, it is essential that the pressure records obtained from the gages at stations 1, 2, and 6 be identical and that those obtained from the gages at stations 3, 4, and 5 be identical also.

The locations of the four pressure gages in the isotropic configuration are shown in Figure 2.44. The stations are numbered so that the gage port in a particular ring is assigned the same station number in both the triaxial and isotropic configurations. The four gages at these stations provide independent measurements of the pressure applied to the specimen. As in the triaxial configuration, the pressure records obtained from the four gages must be identical to ensure uniform loading on the specimen.

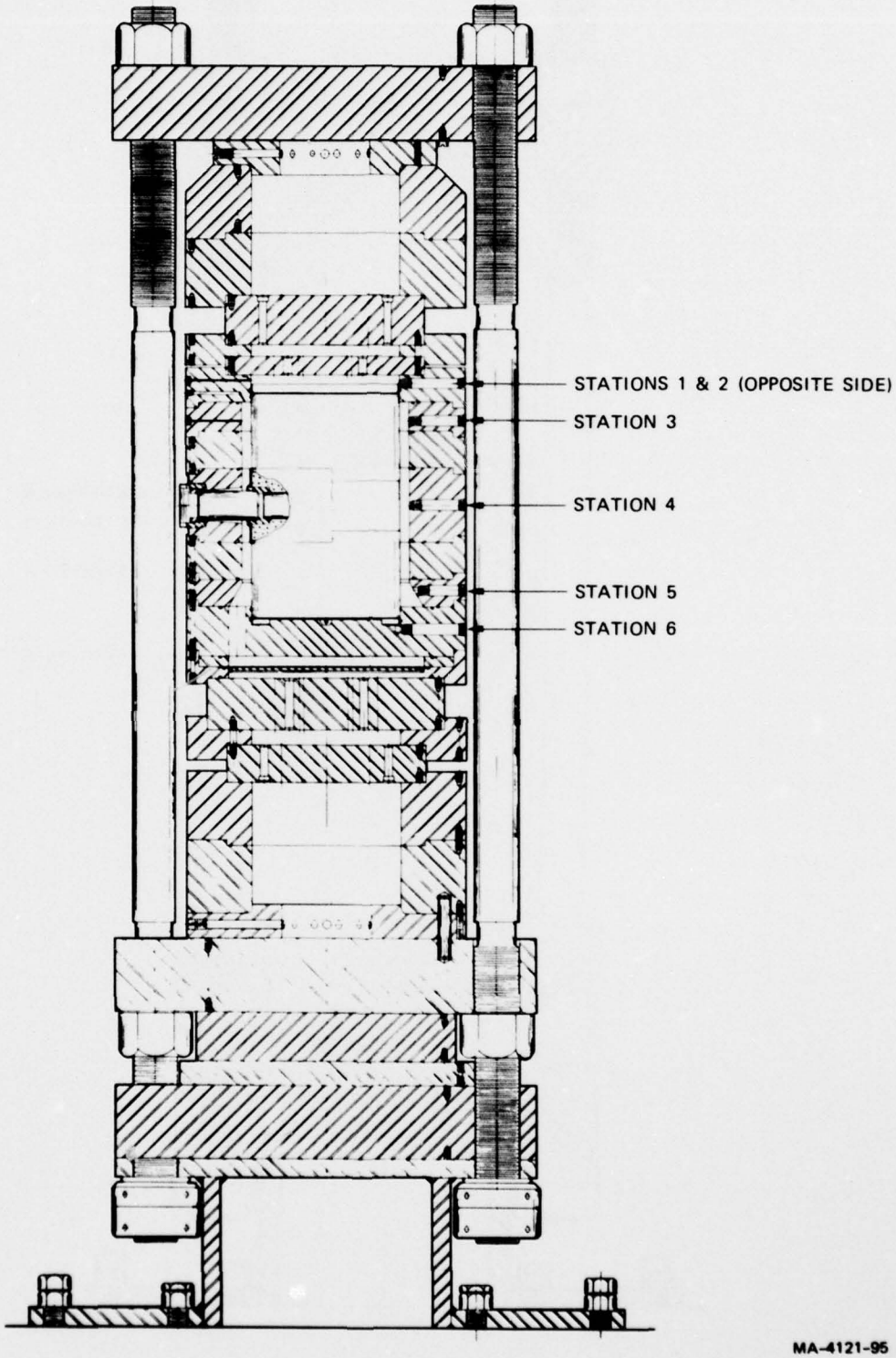

FIGURE 2.43 LOCATION OF THE SIX PRESSURE GAGE STATIONS IN THE DYNAMIC TRIAXIAL CONFIGURATION

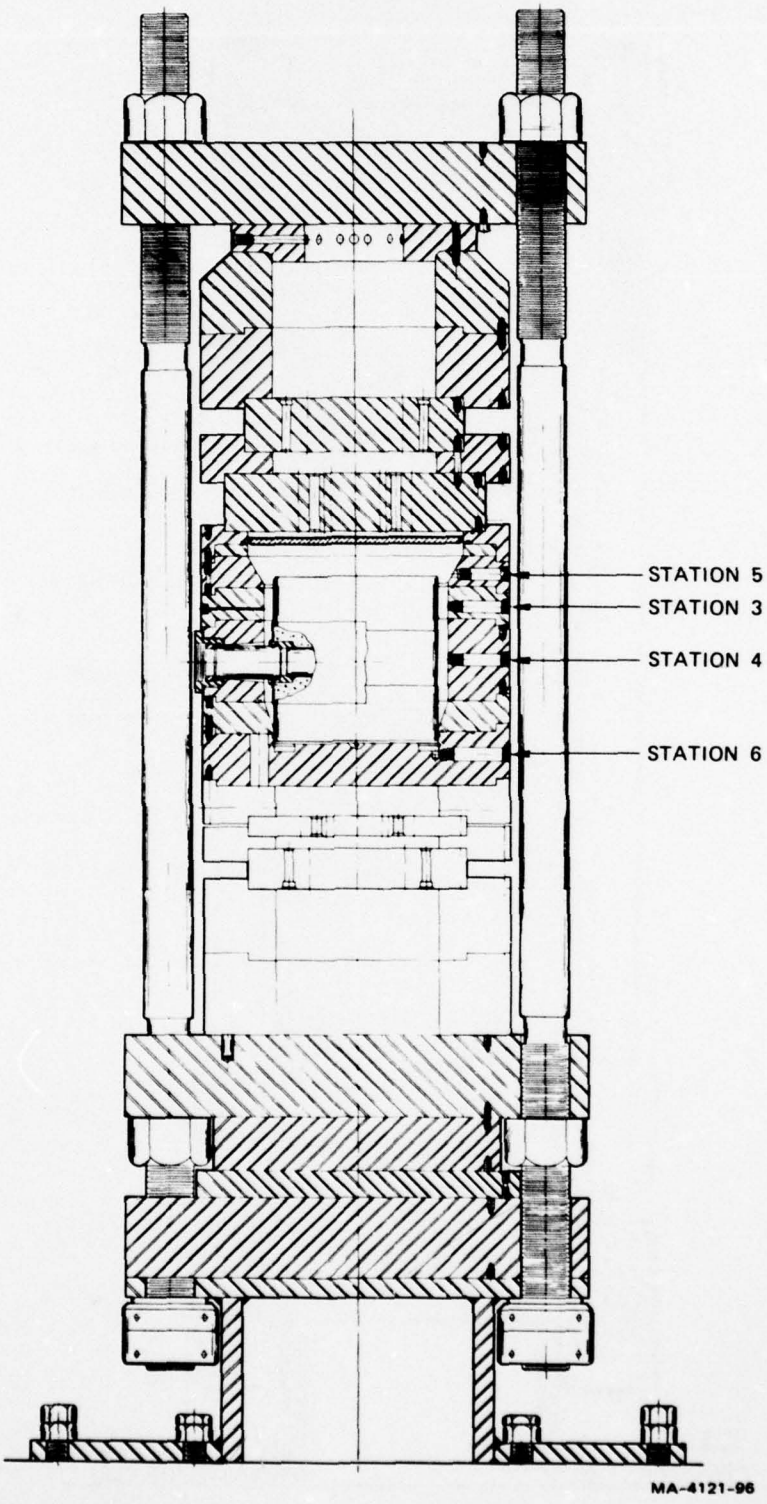

FIGURE 2.44 LOCATION OF THE FOUR PRESSURE GAGE STATIONS IN THE DYNAMIC ISOTROPIC CONFIGURATION

A photograph of one of the pressure gages is shown in Figure 2.45. The gages (model 119A, supplied by PCB Piezotronics, Inc.) have a pressure range of 0-80 ksi (0-0.55 GPa) with an overrange to 100 ksi (0.69 GPa). The gages are acceleration-compensated and have a resonant frequency of 500 kHz. The model 119A gages can be calibrated statically, and such a calibration is performed before and after each test to ensure that the gage characteristics have not changed.

2.4.2 Specimen Strain

For uniaxial-strain tests, we measure the radial displacement at the lateral surface of the specimen to monitor the accuracy with which the pressures applied to the specimen produce uniaxial compression of the specimen. To make this measurement, four strain gages are mounted on the copper cans that contain the rock. The gages are located on diameters perpendicular to the tunnel axis 2-1/2 inches (65 mm) above and below the midheight of the specimen.

These four strain gages measure the hoop strain in the thin copper cans. Since the copper cans deform to follow the rock, the strain ε_θ is related to the radial displacement u by the relation $\varepsilon_\theta = \frac{u}{r}$, where r is the radius of the specimen. A positive value for ε_θ indicates that the rock is expanding radially and that the lateral confining pressure is too low. Similarly, a negative value for ε_θ indicates that the rock is contracting radially and that the lateral confining pressure is too high.

2.4.3 Testing Machine Strain

There are 12 strain gages mounted on the testing machine to measure strain in the machine before and during the test. The output of the gages before the test is used to determine the magnitude of the preload that holds the machine together during the test. The output of the gages during the test is recorded and used to determine the peak dynamic stress in several of the machine parts and hence to estimate the capability and life of these machine parts. An estimate of the machine life based on the strain gage records is presented in Appendix A of this volume.

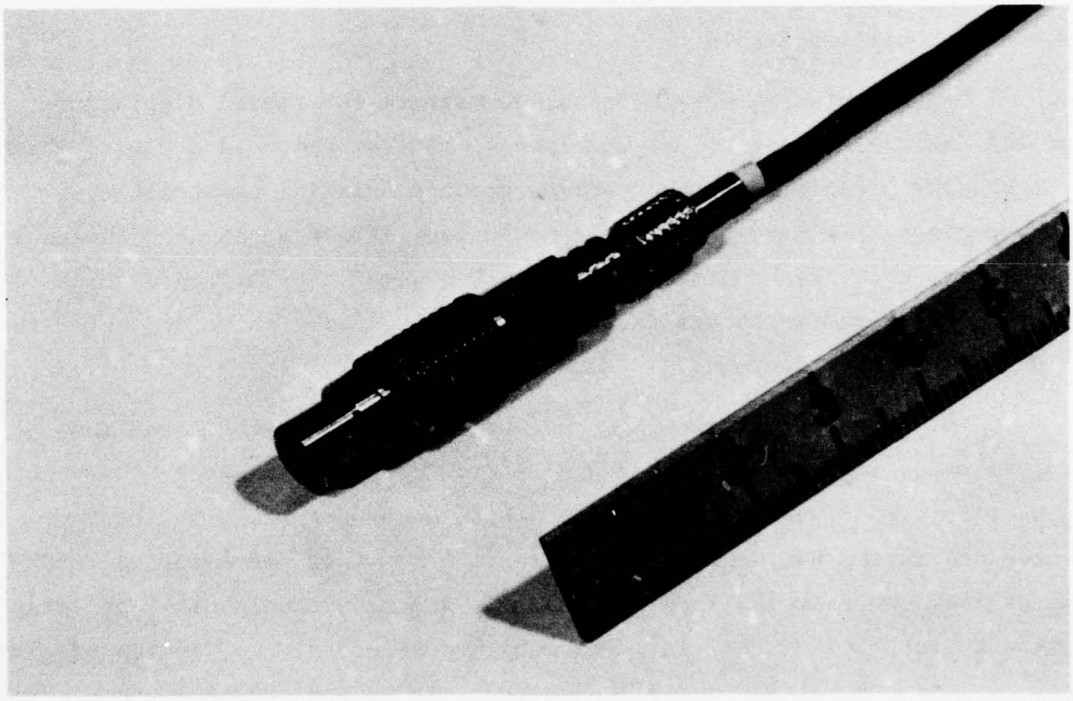

MP-4121-140

FIGURE 2.45 TYPICAL PRESSURE GAGE USED IN DYNAMIC TESTS

As described previously, two of the strain gages are mounted in the center of the upper surface of the top end plate. The remaining 10 gages are located on 3 of the 12 studs. The strain gages are mounted just inside the threaded ends of the studs, where the diameter of the stud is stress relieved to the root diameter of the threads. On two of these three studs, three gages are located 120° (2.09 rad) apart around the stud at the top end, and a fourth gage is at the other end. The third instrumented stud has a single gage at each end. Output from the two three-gage groups is used to determine stud bending because of inevitable imperfections in the nuts.

2.4.4 Tunnel Diameter

The diameter of the tunnel in the specimen is measured with a standard bore gage. The gage, shown in Figure 2.46, is a Mitutoyo series 511 bore gage with a range from 1.4 inches (35.6 mm) to 2.5 inches (63.5 mm). The dial indicator has gradations for every 0.005 inch (0.013 mm), so that for a nominally 2-inch (50-mm) diameter tunnel, closures can readily be determined to 0.05% accuracy. The scale on the dial gage is adjusted so that a zero reading corresponds to the diameter of the tunnel before the test. Therefore, after the test, the closure is read directly from the gage.

The deformation of the tunnel during a test can be recorded by high-speed photography. A Hycam camera, model 410004, having a maximum rate of 10,000 frames per second (fps) provides photographs of the closure at 0.1-millisecond intervals for the entire period of interest, approximately 30 milliseconds. To obtain data at shorter time intervals, the camera can record half or quarter frames, in which case the time interval drops to 0.05 or 0.025 milliseconds. However, since pressure pulse rise times are typically about 12 milliseconds, the full-frame 10,000-fps rate gives 120 pictures during tunnel deformation, which is more than adequate.

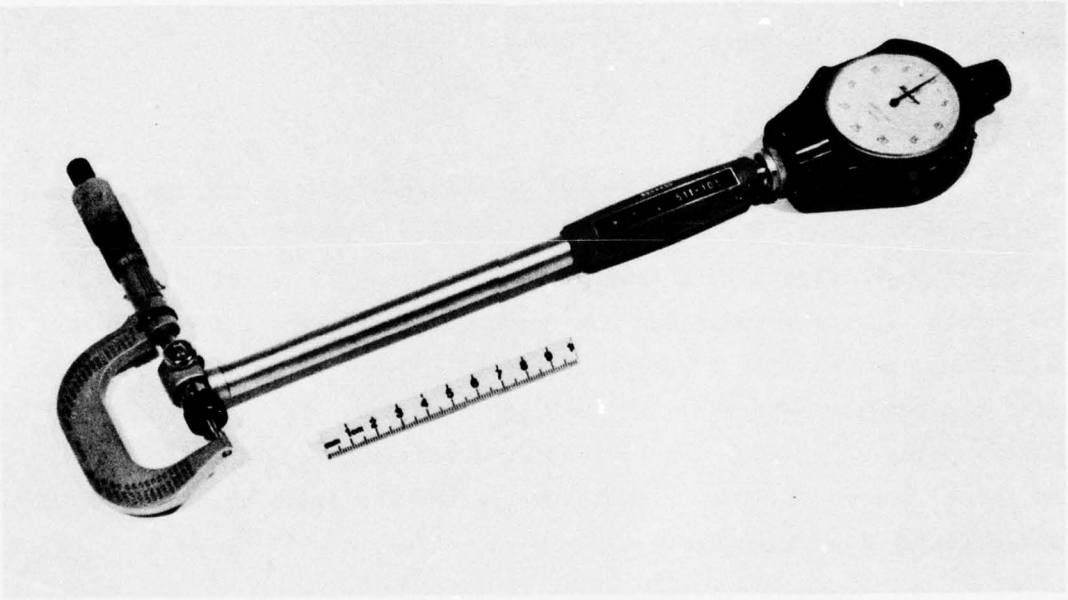

MP-4121-141

FIGURE 2.46 BORE GAGE USED TO MEASURE TUNNEL DIAMETER

2.4.5 Future Instrumentation

There are two areas in which instrumentation for the specimen can be developed. Short-range plans call for more comprehensive data collection in the tunnel, including active measurements of tunnel closure and liner strain. Longer-range plans include the measurement of the stress and flow fields in the rock.

2.4.6 Testing, Firing, and Recording Procedures

While the testing machine is being stacked and the instrumentation is being connected, the signal conditioning circuits are patched into the tape recorder and oscilloscopes and then calibrated. As each gage is tied into the system, it is checked to be sure that it is functioning. To check the pressure gages, the sensitivity of an oscilloscope is increased and the testing machine is tapped with a brass mallet near each gage. A sharp spike in the signal indicates that the gage is functioning properly. The strain gages, both on the specimen and on the testing machine, are checked by measuring the resistance of the strain gage circuit. A low resistance indicates a short circuit and a very high resistance indicates an open circuit. The latter is much more common than the former, and usually indicates that the gage has loosened and burned out and must be replaced.

Just before the shot is fired, the electronic detonator unit (EDU) and the detonator cable are checked out. The EDU supplies a power surge (from a 5-μF capacitor charged to 4.1 kV) through an exploding bridgewire, which in turn detonates the Primacord leads to the explosive charges. After the EDU and detonator cable have been checked out, all site personnel go under cover in the bunker and the explosive technician connects the exploding bridgewire to the detonator cable and brings the Primacrod leads into contact with the exploding bridgewire. Then the explosive technician goes under cover and the shot is fired. The testing machine can be watched throughout the test via closed-circuit television.

After the shot is fired, work begins on unstacking and cleaning the testing machine in preparation for the next shot. It is important that the machine be cleaned thoroughly within a day or so because the explosive residue is corrosive.

AD-A063 487 SRI INTERNATIONAL MENLO PARK CA F/G 13/13
THEORETICAL AND LABORATORY STUDY OF DEEP-BASED STRUCTURES. VOLU--ETC(U)
DEC 77 P E SENSENY, H E LINDBERG DNA001-75-C-0245
UNCLASSIFIED DNA-4425F-1 NL

2 OF 2
AD
063487

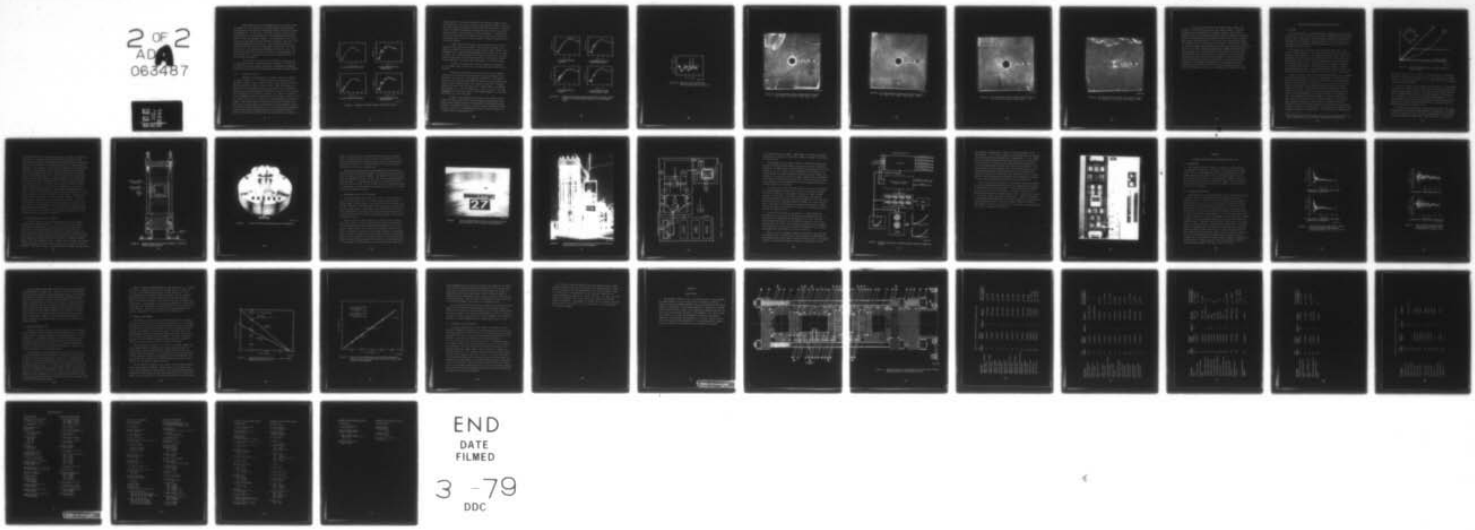

END
DATE
FILMED
3 -79
DDC

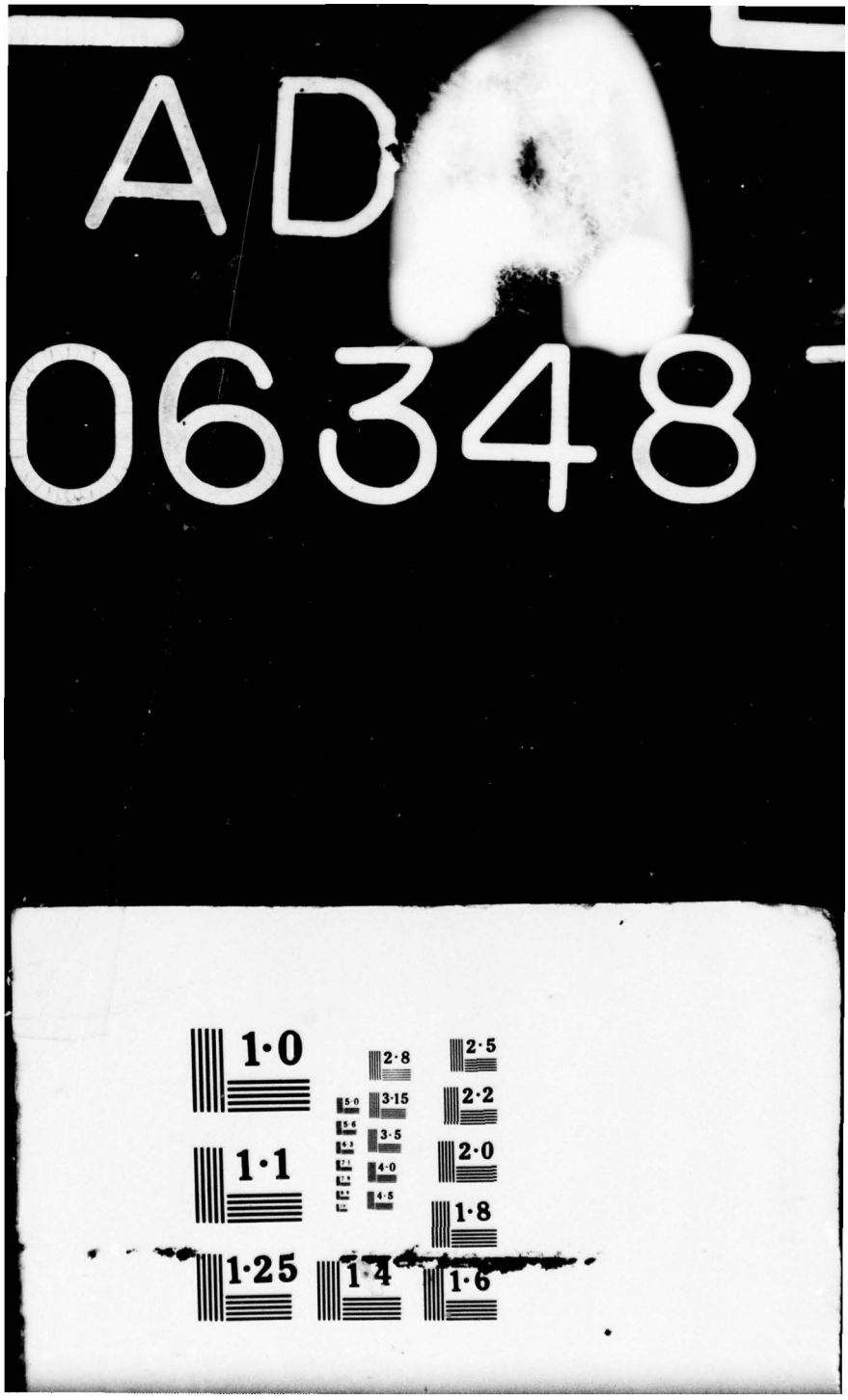
AD
06348
1·0
1·1
1·25
1·4
1·6
1·8
2·0
2·2
2·5
2·8
3·15
3·5
4·0
4·5
5·0

Data from all the active instrumentation are recorded on tape in analog form. The output from the pressure gages and the specimen strain gages are also fed into oscilloscopes and the traces are recorded photographically. In this way, if for some unforeseen reason the tape recorder does not function properly, the oscilloscope traces provide records of the most important channels. The photographs of the oscilloscope traces also permit the most significant results of the test to be evaluated immediately after the test. Data recorded on tape are retrieved at the test site using a light-beam oscillograph. This allows all the data to be studied in detail immediately after the test. The results of the test may influence the choice of certain parameters in the upcoming test, so having the data available immediately after the test is fired is essential.

After a series of tests has been completed, the data on tape are digitized, and then scaled and plotted by computer. With the data in digitized form, more complex data analysis is performed, including optimum filtering and plotting lateral pressure against vertical pressure

2.4.7 Example Test Results

Pressure records obtained in a uniaxial strain test, LDUX-10, are shown in Figure 2.47. The vertical pressure in the gas above the specimen is shown in Figure 2.47(a), and the vertical pressure in the oil under the specimen is shown in Figure 2.47(b). With the exception of a small blip at the beginning of the pressure pulse in the oil under the specimen, the two vertical pressure records are identical. This indicates that the loading of the specimen is uniform, i.e., there is no evidence of wave propagation effects along the axis of the specimen. Figures 2.47(c) and 2.47(d) show two of the records of the pressure pulse in the lateral chamber. That these pressure records are also identical indicates that the lateral pressure loading is uniform, with no wave propagation effects in the oil surrounding the specimen. There is an oscillation superimposed on the desired lateral confining pressure, but developments with the smaller testing machine indicate that this oscillation can be reduced or

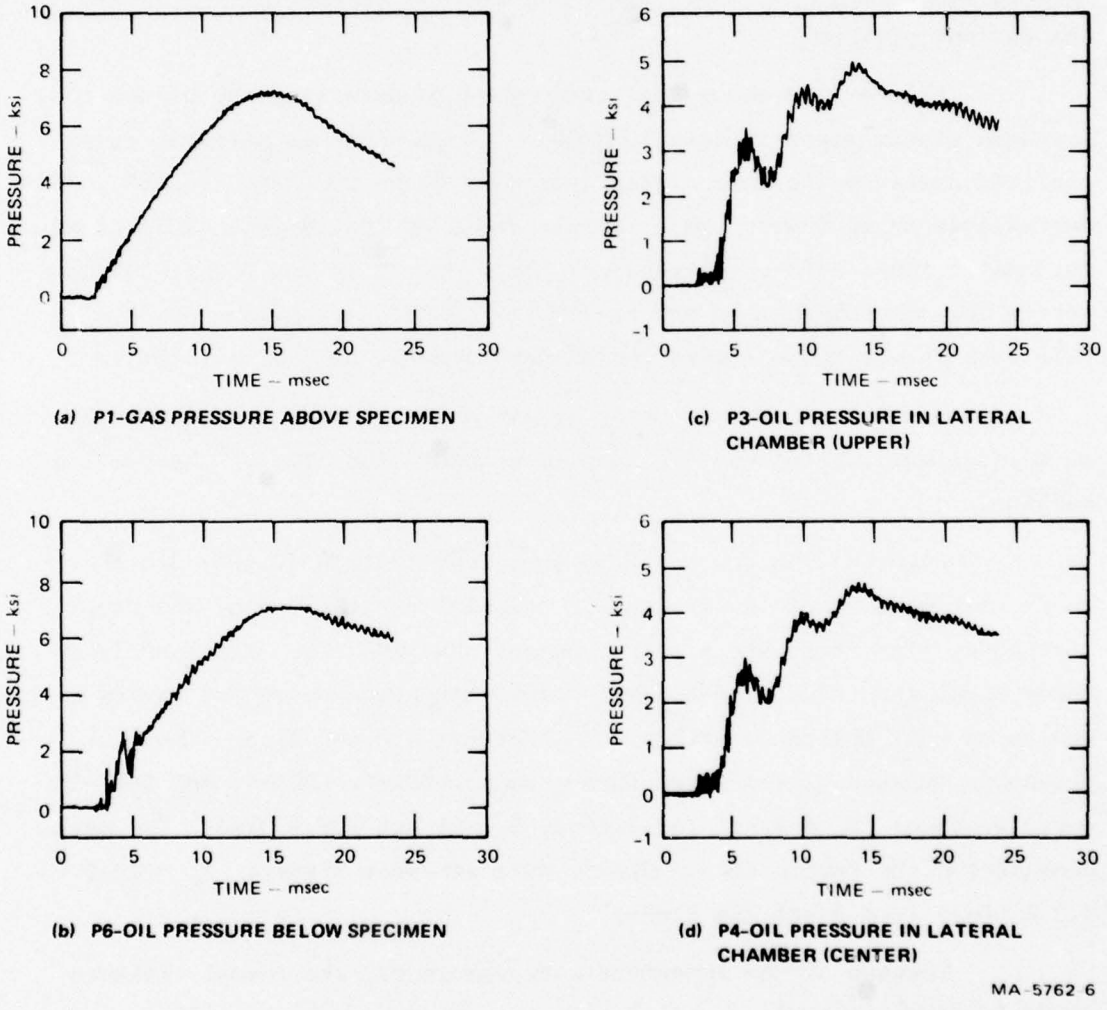

FIGURE 2.47 PRESSURE DATA FROM UNIAXIAL STRAIN TEST LDUX-10

removed entirely. The lateral pressure pulses shown in Figures 2.48(c) and 2.48(d) are from a test in the small testing machine, DUX-74, in which the holes through the specimen receiver plate were constricted. Subsequent tests in the small testing machine showed that when these holes are constricted further, the oscillation is nearly eliminated. A similar modification has been made to the specimen receiver plate in the larger scale testing machine, but we had no rock specimen to perform further tests in the current program.

Figure 2.49 shows the strain gage records from one of the four specimen strain gages in test LDUX-10. The specimen is slightly overconfined, because the hoop strain initially drops to about -0.125%. This corresponds to an inward radial displacement at the surface of 7-1/2 mils (0.2 mm). Then, before the peaks of the pressure pulses occur, the hoop strain returns toward zero and oscillates about a mean value of -0.05%. This corresponds to an inward radial displacement of 3 mils (0.08 mm).

Records of the apparatus strain are presented in Appendix A of this volume, where they are used to estimate the life of the testing machine.

Figures 2.50 through 2.53 show four 12-inch (0.3-m) diameter rocks that were tested under dynamic uniaxial strain loading and then sectioned. The rocks are a tuff simulant, SRI RMG 2C2. The tunnels in these rocks are reinforced with A16061-TO monocoque cylinders having mean radius-to-wall thickness ratios, a/h, between 4.0 and 11.5. The peak pressures in each of the first three tests, LDUX-4, LDUX-5, and LDUX-10, were the same: P_V = 7 ksi (48.3 MPa), P_H = 4 ksi (27.6 MPa). The peak pressures in the fourth test, LDUX-9, were somewhat higher: P_V = 10.5 ksi (72.4 MPa), P_H = 7 ksi (48.3 MPa).

Because of the imperfect rock specimens, the tunnel closures in the first three tests do not follow the expected trend, namely, that tunnel closure should increase as the strength of reinforcing structure decreases. The weakest structure, tested in LDUX-10, suffered the least closure, less than 1%. The strongest structure, tested in LDUX-4, had a tunnel closure of approximately 3%.

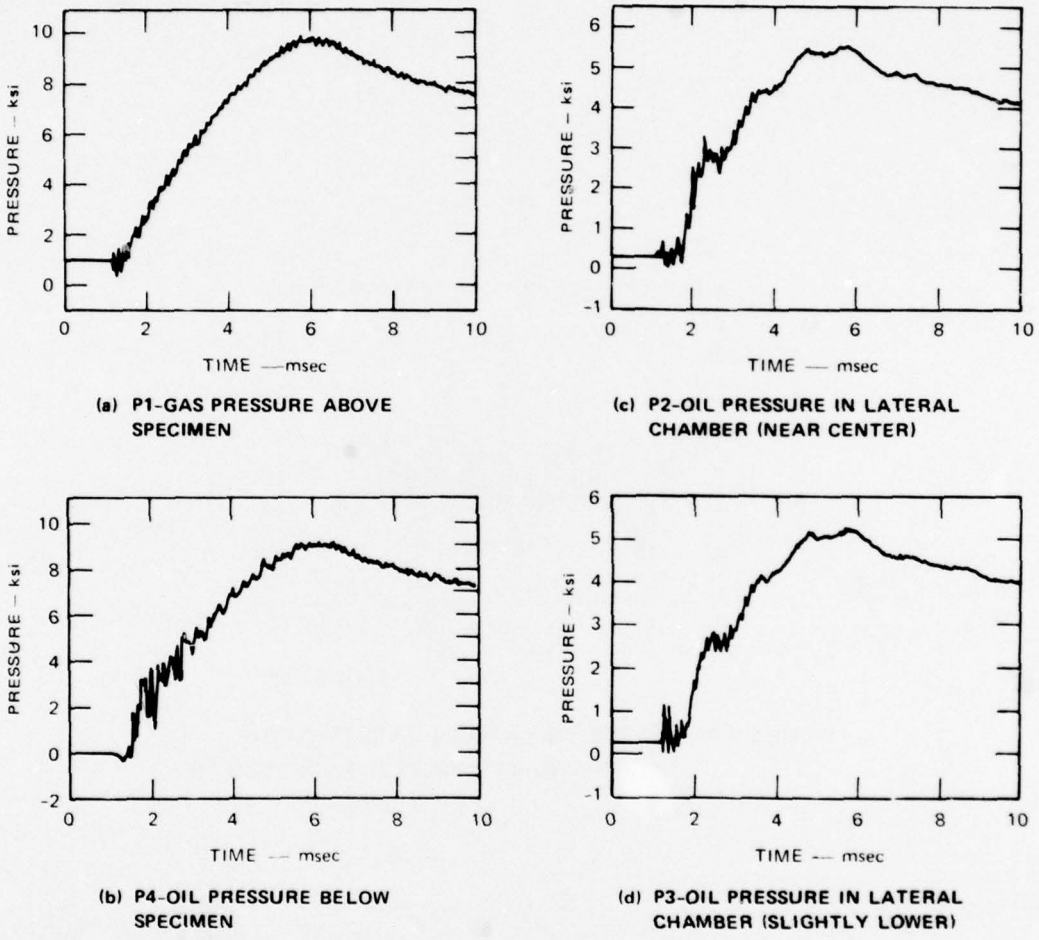

FIGURE 2.48 PRESSURE DATA FROM A UNIAXIAL STRAIN TEST IN THE SMALL TESTING MACHINE, DUX-74, SHOWING IMPROVEMENT OF LATERAL PRESSURE PULSES

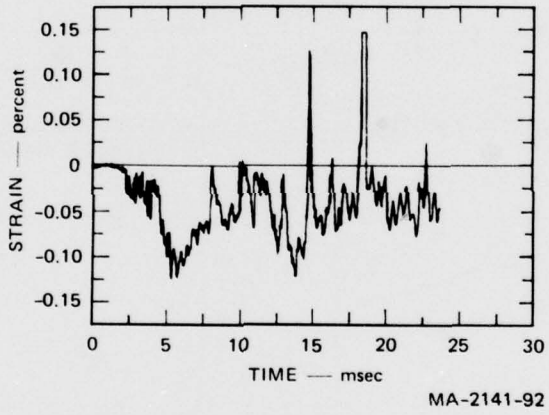

FIGURE 2.49 SPECIMEN LATERAL STRAIN DATA FROM UNIAXIAL STRAIN TEST LDUX-10

MP-4121-142

FIGURE 2.50 SECTIONED SPECIMEN FROM UNIAXIAL STRAIN TEST LDUX-4
(P_V = 7 ksi, P_H = 4 ksi, $\Delta D_V/D_V$ = 2.83%, $\Delta D_H/D_H$ = 1.23%)

MP-4121-143

FIGURE 2.51 SECTIONED SPECIMEN FROM UNIAXIAL STRAIN TEST LDUX-5
(P_V = 7ksi, P_H = 4ksi, $\Delta D_V/D_V$ = 18.4%, $\Delta D_V/D_H$ = 7.98%)

MP-4121-144

FIGURE 2.52 SECTIONED SPECIMEN FROM UNIAXIAL STRAIN TEST LDUX-10 (P_V = 7 ksi, P_H = 4 ksi, $\Delta D_V/D_V$ = 0.82%, $\Delta D_H/D_H$ = -0.77%)

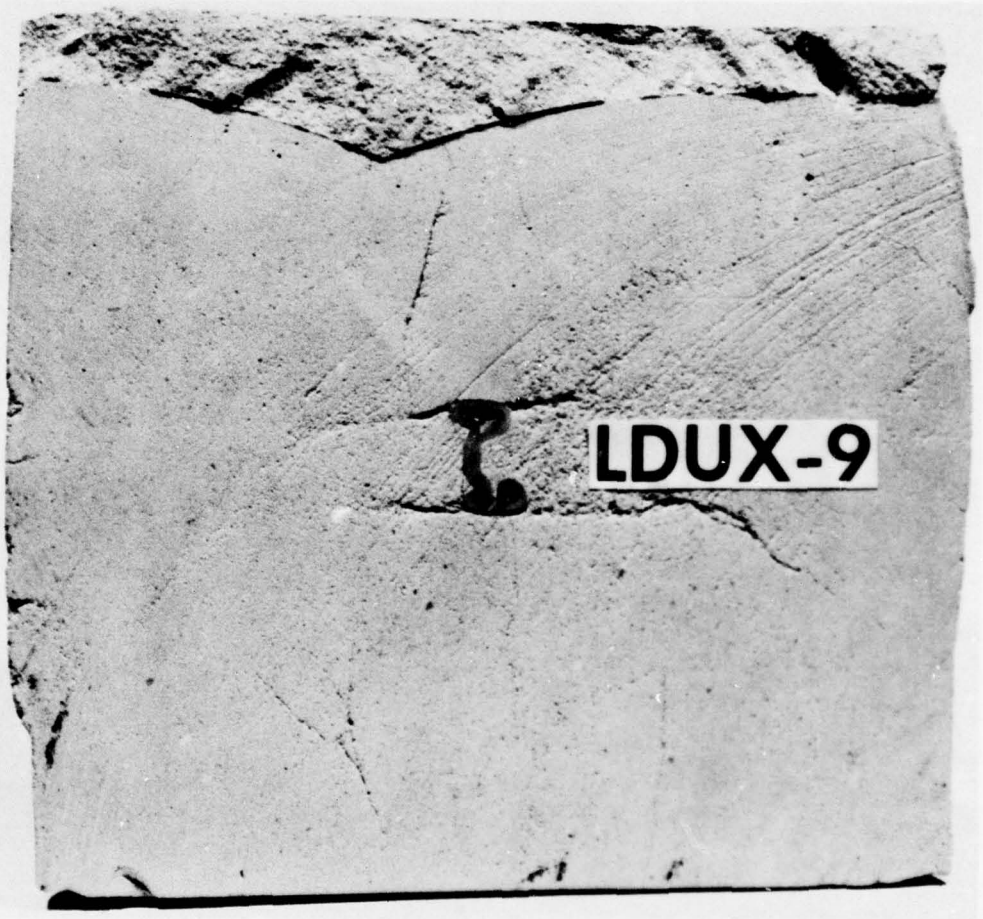

MP-4121-145

FIGURE 2.53 SECTIONED SPECIMEN FROM UNIAXIAL STRAIN TEST LDUX-9 (P_V = 10.5 ksi, P_H = 7 ksi, $\Delta D_V/D_V$ = 38.7%, $\Delta D_H/D_H$ = 100%)

In Section 2.2 we described the technique used to make these specimens. The SRI RMG 2C2 grout was cast around a mandrel. When the specimens cured, the mandrels were removed, leaving a 2-inch (50-mm) diameter tunnel cavity through the specimen. However, because of shrinkage during the curing period, the specimens developed cracks near the mandrel. These cracks, which are evident in all four of the sectioned rocks shown, are believed to have influenced the tunnel closure. The influence of flaws is especially evident when comparing the tunnel closures shown in Figures 2.52 and 2.53. The tunnel reinforcing structures in LDUX-9 and LDUX-10 were of equal strength, but the closure varied from less than 1% to total closure. The difference in the tunnel closure is attributed to the fairly large cracks which weakened the rock tested in LDUX-9. In the future we will drill the tunnels into solid grout specimens, as we have been doing successfully for the smaller testing machine. The contribution for pre-existing flaws to the tunnel closure in LDUX-9 indicates the need for a study of the influence of joints on the response of deep-base structures.

3. MACHINE DESIGN AND OPERATION FOR STATIC TESTING*

3.1 APPROACH

In the last chapter, the individual machine components and the stacking sequence used for the two dynamic-test machine configurations were discussed. For the static configuration, the same stacking sequence and machine parts are employed, even though the loading techniques are very different. One additional ring is needed; its function and position in the stack will be discussed in the next section.

The dynamic tests are fired with all personnel under cover in the bunker, for obvious reasons. The static tests also are performed with all personnel in the bunker, but for a somewhat different reason. Normal test procedures present no hazards, but the possibility of an O-ring failure at high pressure [up to 30 ksi (0.21 GPa)] necessitates that all personnel be under cover during a test. During testing of the ultimate capability of our small static machine, a burst O-ring sliced completely through a plasterboard witness plate. The instrumentation and controls used for this remote testing mode will be described in the last section of this chapter.

Figure 3.1 shows several of the standard loading paths that are possible with the testing machine in the static configuration. One possible load path, denoted as isotropic, is the one for which the vertical and lateral pressures are increased at the same rate, i.e., the stress state is hydrostatic. This simulates the symmetric pressure from end-on loading of a deep-based structure. Another possible load path, denoted as uniaxial strain, is the one for which the vertical and lateral pressures are such that the radial displacement on the lateral surfaces of the specimen is zero. This simulates the side-on loading of a deep-based structure, in which the strain field in the rock is nearly uniaxial. A third possible path, denoted as triaxial, is one for which the loading is isotropic initially, and then the lateral pressure is held constant and the vertical pressure is increased. This load path is the same as that followed in the standard triaxial test of geomechanics. The final load path shown, denoted

---

*The hydraulic system and the remote control and data acquisition unit for static testing were paid for with SRI International capital funds.

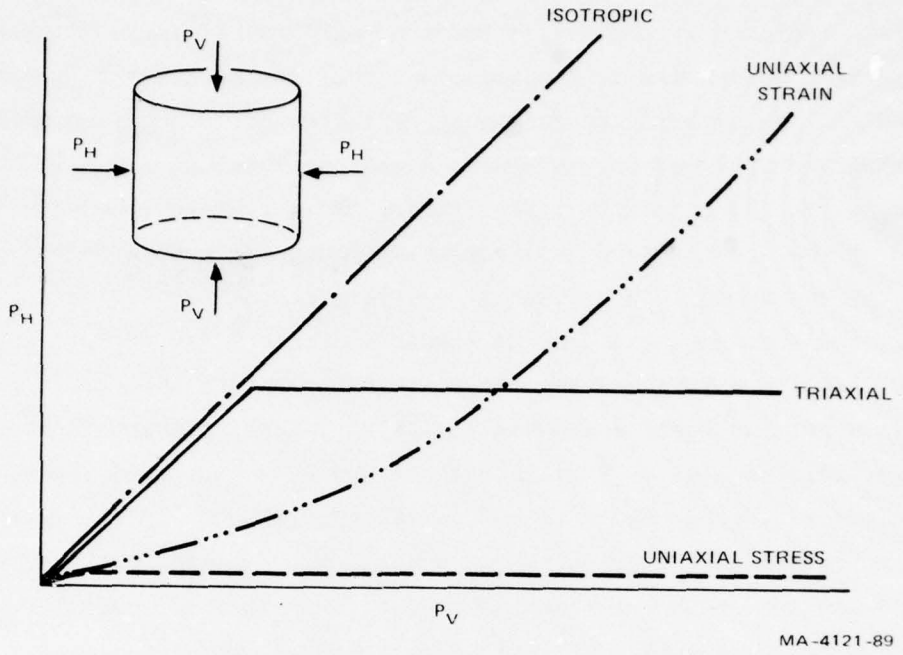

FIGURE 3.1 SCHEMATIC SHOWING SEVERAL STANDARD LOAD PATHS FOR STATIC TESTS

as uniaxial stress, is one in which the vertical pressure is increased while the lateral pressure is held at zero. This load path is a special case of the triaxial load paths, i.e., one in which the isotropic loading portion has been eliminated.

For all but uniaxial strain loading, the load path is well determined before the test starts, and the operator simply controls the lateral and vertical pressure pumps manually. For uniaxial strain loading, the load path is determined during the test by the deformation of the specimen. If, for example, at some point the specimen is underconfined, i.e., the lateral surface of the specimen has undergone an outward radial displacement, then the lateral confining pressure must be increased until the radial displacement is reduced to zero.

For uniaxial strain loading in our machine, the vertical and lateral pressures may be controlled either manually or automatically. For manual control, the outputs of two of the strain gages mounted on the specimen are fed into BLH model 1200A digital strain indicators. The output of

the strain indicators is averaged and then used to deflect a pointer-and-scale meter. A positive deflection means that the specimen is under confined and the lateral pressure must be increased; a negative deflection means that the specimen is overconfined and the vertical pressure must be increased. In the automatic control mode, the outputs of the strain gages mounted on the specimen are fed into the BLH digital strain indicators just as in the manual control mode. However, in addition to deflecting a meter, the average output of the strain indicators is fed into a comparator circuit, which compares the averaged output of the strain gages with the upper and lower allowable limits of lateral strain selected before starting the test. If neither limit has been exceeded, the pumps continue operating as they were before the comparison. If one of the limits is exceeded--for example, the upper limit, indicating that the radial expansion of the specimen is greater than desired--then the vertical pressure pump is stopped and the lateral pressure pump is allowed to continue. When the lower limit on lateral strain is reached, the lateral pressure pump is stopped and the vertical pump is started. In this way, the lateral and vertical pressures increase so that the load path in the $P_H - P_V$ plane oscillates between two curves that bound the uniaxial strain load path from above and below. It is necessary that the upper and lower limits be small so that the deviations from uniaxial strain do not significantly influence the tunnel deformation.

3.2 MACHINE ASSEMBLY FOR STATIC TESTING

An assembly drawing of the testing machine in the static triaxial configuration is shown in Figure 3.2. For the most part, the machine parts and stacking sequence are the same as for the two dynamic configurations. The only difference is that there is a new plate that replaces the lateral chamber reducer ring and the Bellofram assembly, which are at the top of the lateral chamber in the dynamic isotropic configuration. This change is necessary because of the difference in loading techniques between the static and dynamic tests. The new part, the static top vertical/lateral seal plate, part 27, is shown in Figure 3.3. This plate has two functions. The first is that, in conjunction with the copper cap and O-ring

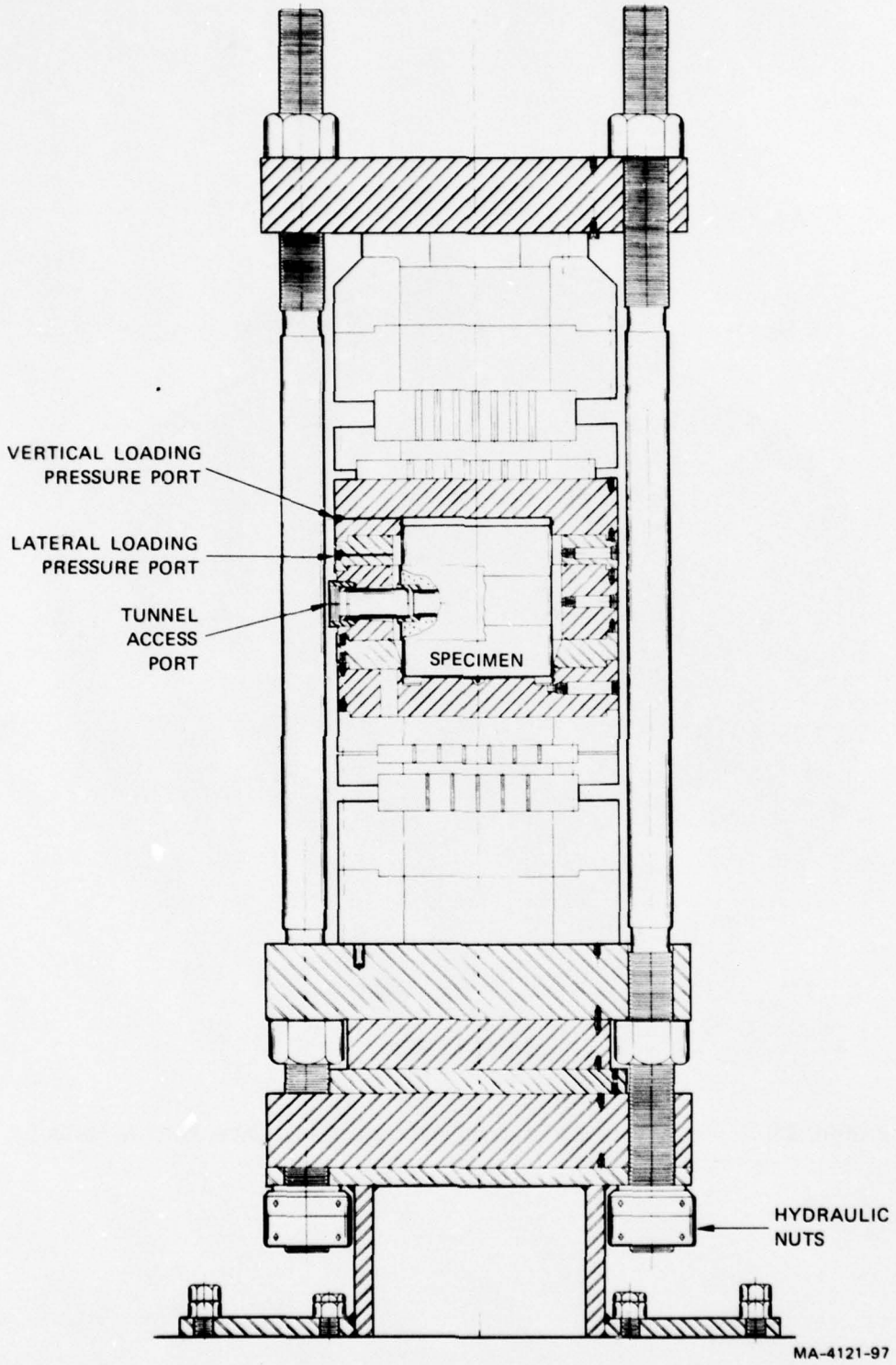

FIGURE 3.2 CROSS SECTION OF THE TESTING MACHINE IN THE STATIC TRIAXIAL CONFIGURATION

MP-4121-146

FIGURE 3.3 STATIC TOP VERTICAL/LATERAL SEAL PLATE, PART NUMBER 27

shown, it seals the vertical loading fluid from the lateral loading fluid. Its second function is to provide for the application of the vertical loading pressure through the small, 1/8-inch (3.2-mm) diameter port shown in Figure 3.4. The lateral pressure is applied through a similar port in the lateral chamber ring.

After the testing machine has been assembled, the pressure lines from the hydraulic system are connected to their respective ports in the upper two rings of the lateral chamber. The hydraulic system is mounted on a cart for mobility on the test pad. The cart and testing machine are shown in Figure 3.5. The hydraulic system can be controlled from the cart, but only to a limit of 5 ksi (35 MPa) by safety switches that cannot be overridden by a remote operator in the bunker until the local operator at the cart relinquishes control.

3.3 INSTRUMENTATION AND TEST PROCEDURES

The instrumentation used in the static tests is much the same as that used in the dynamic tests. The major change is that different pressure gages are used because of the long duration of the static tests. The time constant of the charge amplifiers that are used in conjunction with the pressure gages in the dynamic tests is much too short for use in static applications. Therefore, strain gage rather than piezoelectric pressure cells are used to measure the pressures applied to the specimen in the static tests.

Figure 3.6 gives a block diagram of the remote control and data acquisition system. The bunker contains power supplies and amplifiers for the instrumentation, data recording and display units, and an oil pressure control panel (all of which will be discussed later), as well as an air regulator to control the air pressure applied to the hydraulic pumps. Outside the bunker, on the cart, there is another air regulator that is used to control the air pressure supplied to the pumps when the hydraulic system is being operated from the cart. The two pumps on the cart are Sprague S-216C air-driven, reciprocating hydraulic pumps with

MP-4121-147

FIGURE 3.4 1/8-INCH DIAMETER PORT IN THE STATIC TOP VERTICAL/LATERAL SEAL PLATE USED TO APPLY VERTICAL LOADING PRESSURE

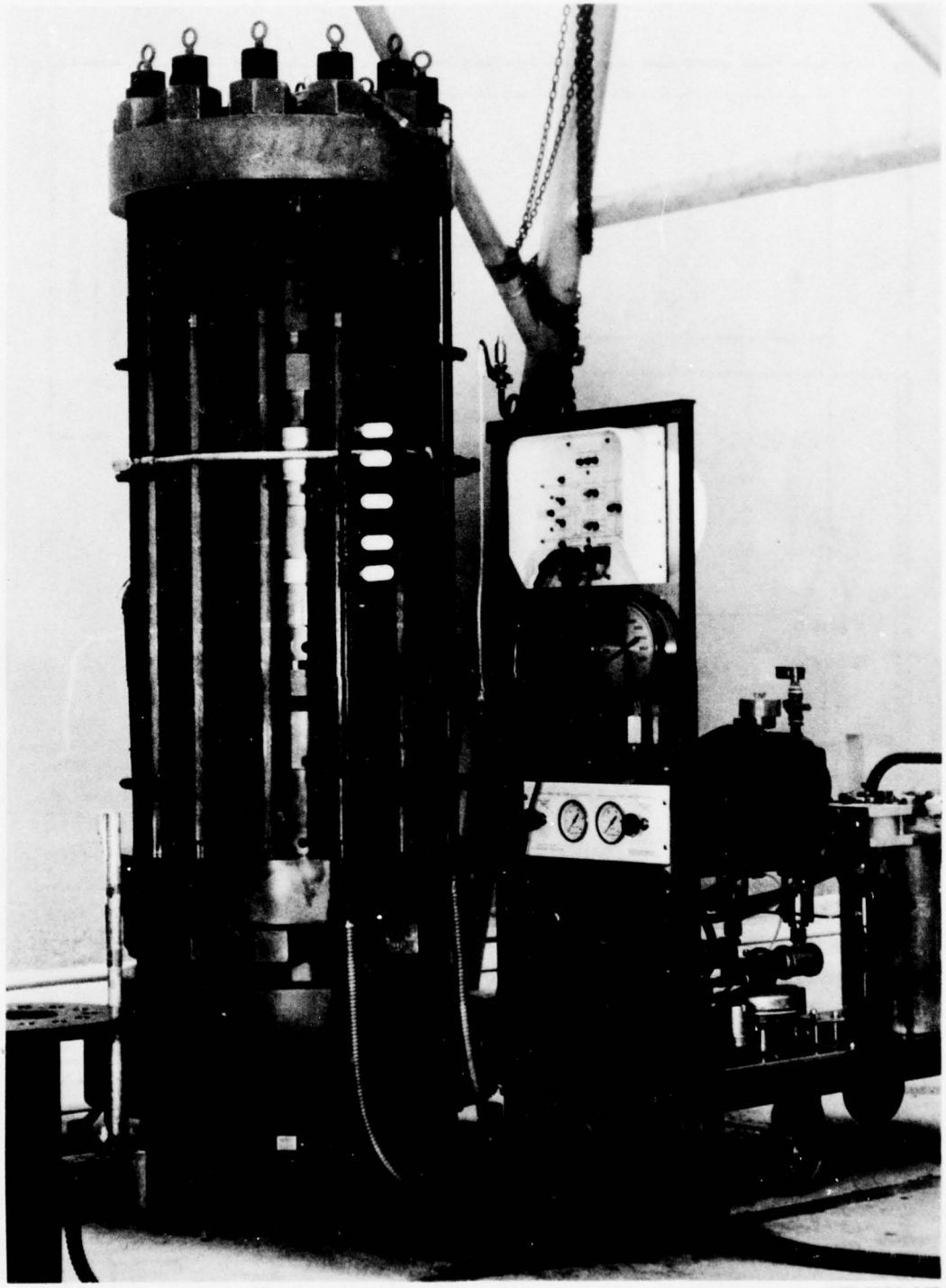

MP-4121-148

FIGURE 3.5 TESTING MACHINE WITH CART CONTAINING HYDRAULIC SYSTEM THAT SUPPLIES VERTICAL AND LATERAL PRESSURES

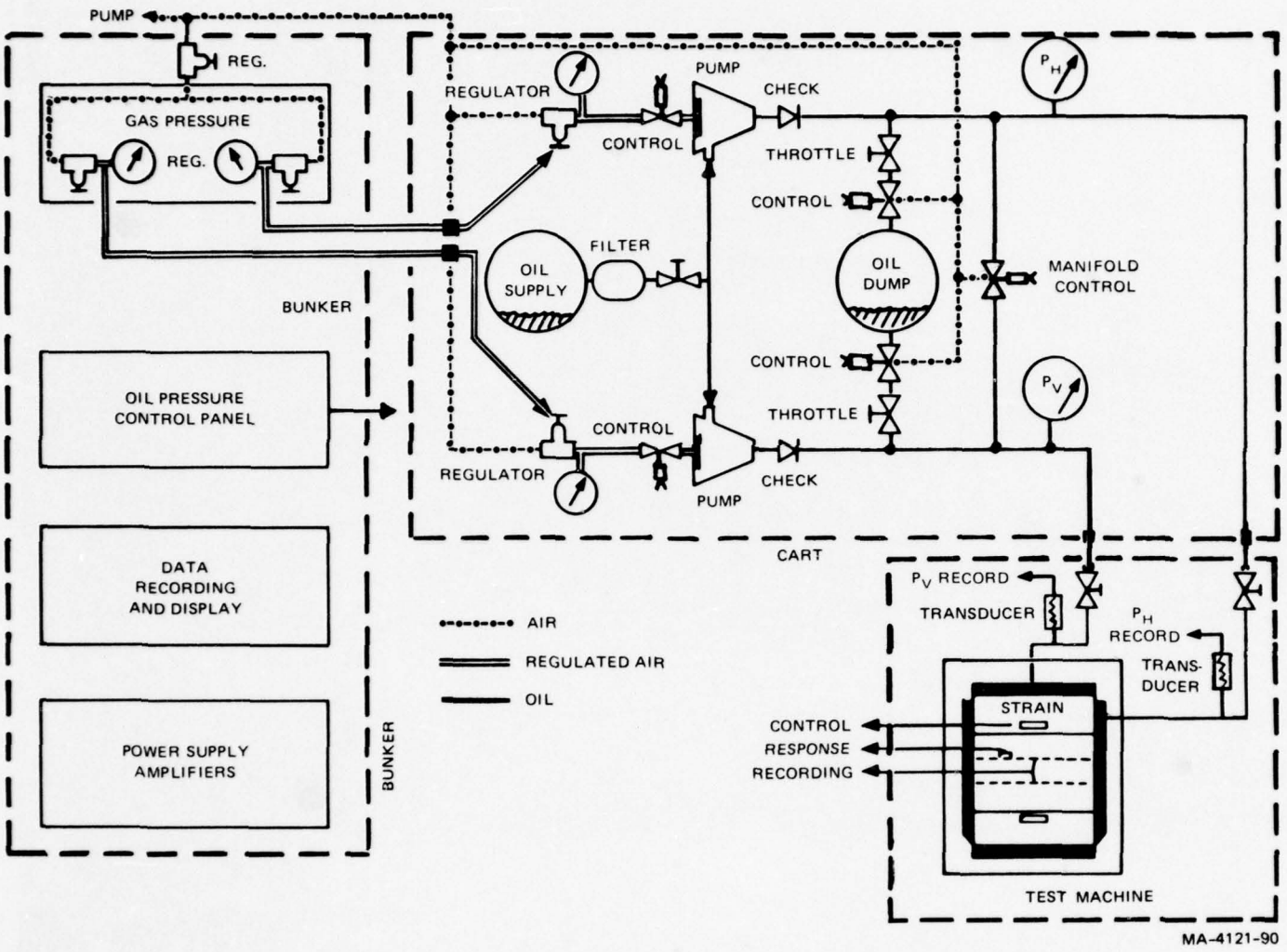

FIGURE 3.6 BLOCK DIAGRAM OF THE REMOTE CONTROL AND DATA ACQUISITION SYSTEM FOR STATIC TESTING

a multiplication ratio of 300:1. These pumps are capable of supplying pressures up to 30 ksi (0.21 GPa) with a 100-psi (0.7-MPa) line pressure at the test site.

The schematic of the hydraulic system is also shown in Figure 3.6. The two air-driven hydralic pumps are mounted on the cart as previously mentioned. The pumps share a common 10-gallon oil reservoir that is also mounted on the cart. Pressures are transmitted from the pumps to the testing machine by standard 65,000-psi (0.45-GPa) pressure tubing. The pressure in the vertical and lateral pressure supply lines is determined by standard dial gages mounted on the cart. Electronic pressure transducers mounted on the testing machine are used to measure the pressures actually applied to the specimen.

The lateral and vertical pressure supply lines can be tied together by a solenoid-pneumatic, piston-type valve that is remotely activated. In this way, either one or both pumps can be used to apply isotropic loading to the specimen. To perform a triaxial test this valve is initially open and the vertical and lateral pressures are the same. When the desired level of confining pressure is reached, the valve is closed and, if both pumps are operating, the lateral pressure pump is stopped. The vertical pressure pump continues to operate, increasing the vertical pressure to complete the test.

To relieve the pressure on the specimen, a solenoid-pneumatic, piston-type valve is opened in each line, and the high-pressure oil is released into a common 5-gallon dump mounted on the cart. The flow rates through these valves are controlled by throttles so that the unloading can be controlled. This is especially important if the loading on the specimen is to be cyclic, because the unload path can be selected and automatically controlled as well as the load path.

Figure 3.7 shows a schematic diagram of the remote control and data acquisition system. This includes the power supplies and amplifiers for the instrumentation and the data recording and display units. The loading pressures are controlled through the pressure control panel in either

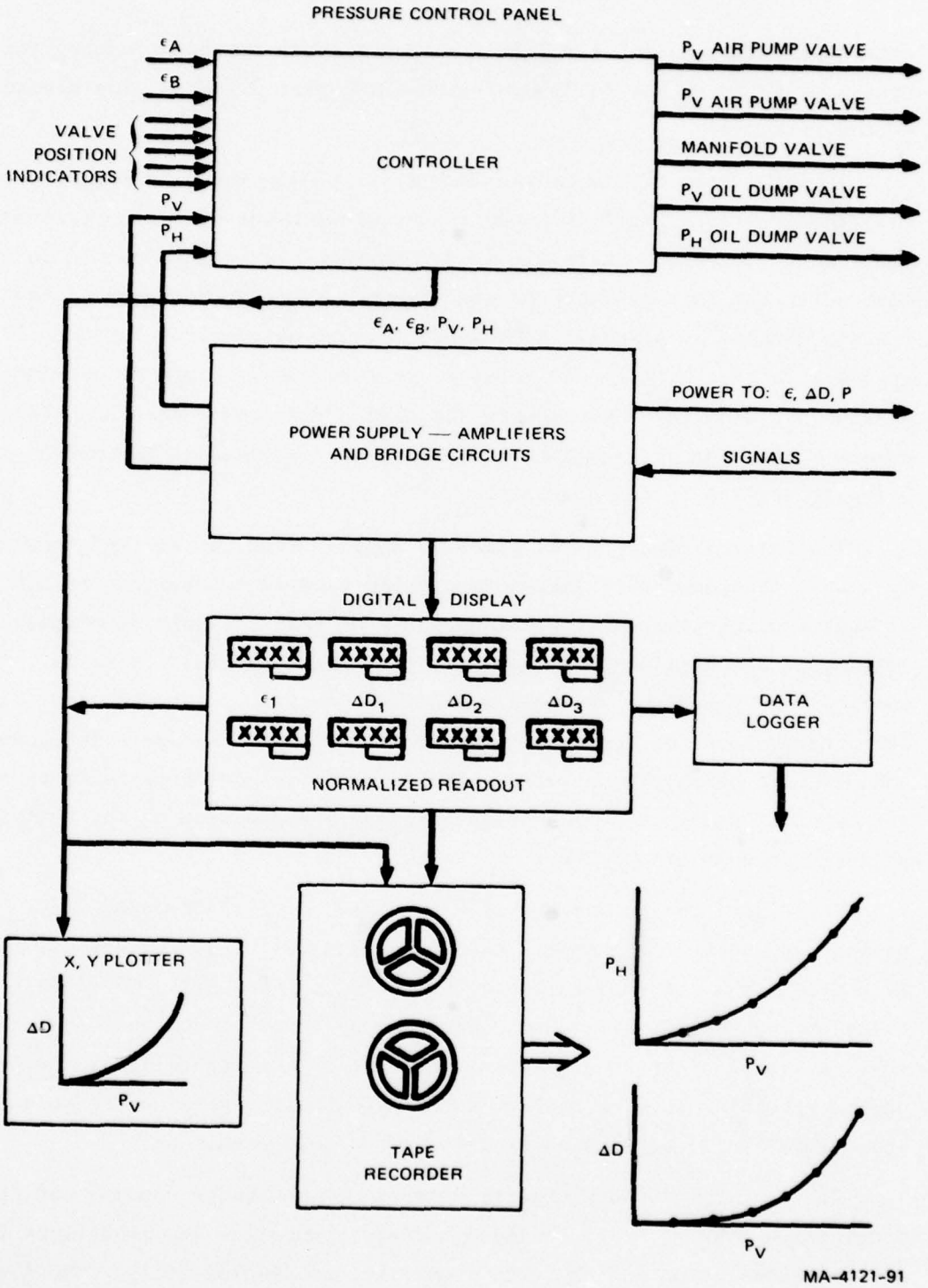

FIGURE 3.7 SCHEMATIC DIAGRAM OF THE REMOTE CONTROL AND DATA ACQUISITION SYSTEM

the automatic or manual mode. Figure 3.8 shows a photograph of the control panel. If the test is being run in the manual mode, the operator increases the pressures simultaneously or independently. If the loading path is to produce uniaxial strain in the specimen, the operator must watch the meter in the center of the panel and control the pressures so that the needle does not deflect far from its null position. If the test is being run in the automatic mode, the pressures applied to the specimen increase along the load path required for uniaxial strain. Should the objectives of a particular test require that after a certain point the load path deviate from uniaxial strain loading, the automatic control can be overridden and the pressures increased manually.

Data from the test are handled in several ways. Data are displayed by meters in normalized digital form (up to 16 channels) for evaluation by the operator as the test proceeds. The data are recorded in analog form on tape (up to about 30 channels). From here the data can be digitized and reduced for complete analysis later. Limited data may also be recorded in analog form using an X,Y plotter. Typically, this might be the applied lateral pressure or the tunnel closure as a function of the applied vertical pressure. Data are recorded in digital form with a data-logger that prints out the data (up to 20 channels) at regular intervals or at the command of the operator.

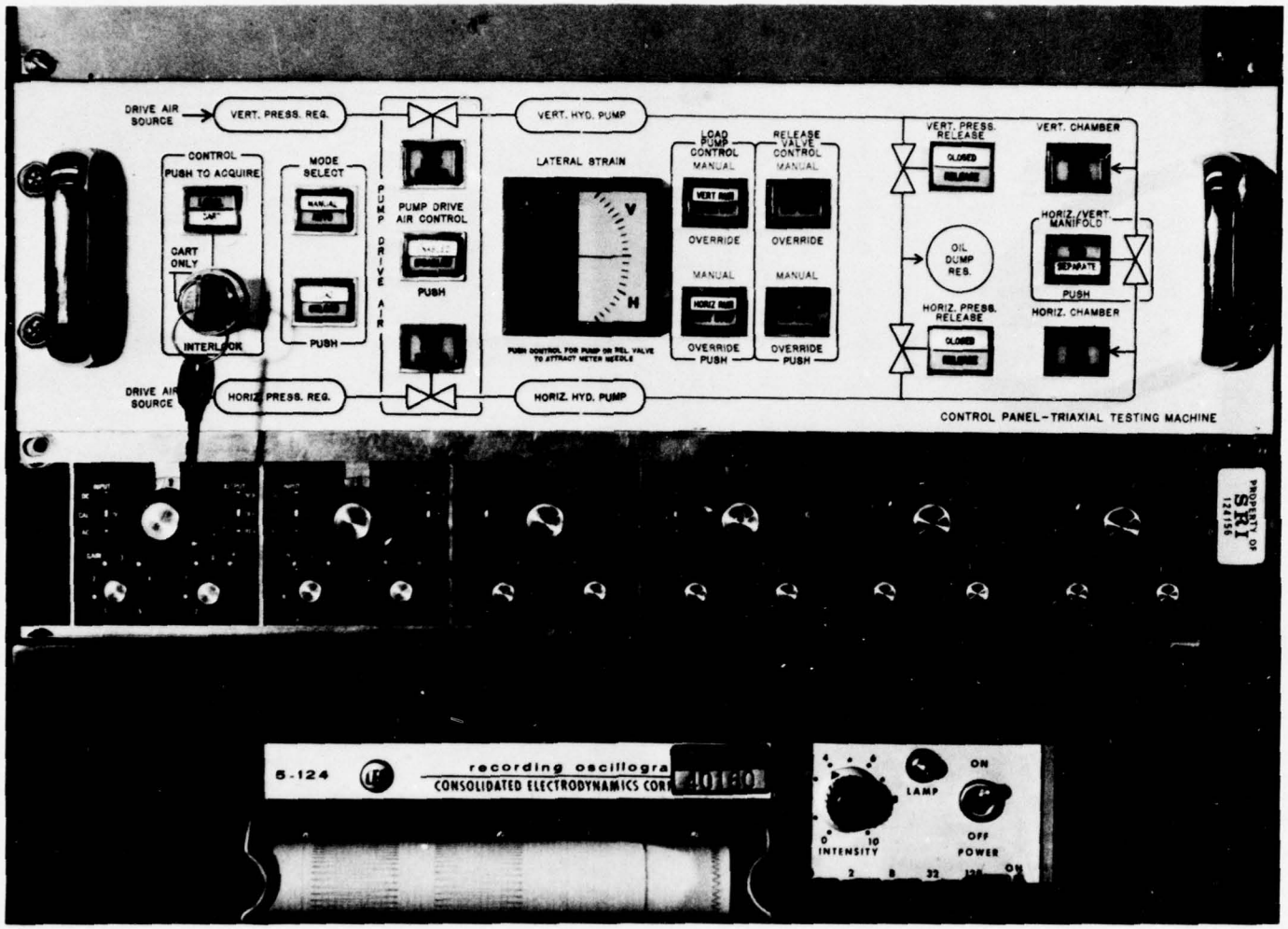

MP-4121-149

FIGURE 3.8 PRESSURE CONTROL PANEL

APPENDIX A

MEASURED MACHINE STRAINS AND ESTIMATED CAPABILITIES

A.1 INTRODUCTION

This appendix presents a summary of several of the larger-scale testing machine capabilities. The first to be discussed is an estimate of the life of the testing machine based on records of strain in the machine during several dynamic tests. The second capability is the pressure that can be applied to the specimen in a dynamic triaxial test as a function of the mass of the explosive charges. Finally, the peak vertical and lateral pressures that can be applied to the specimen in a static test are estimated.

A.2 MEASURED MACHINE STRAINS

Strain gage records from gages mounted on the testing machine during a dynamic calibration uniaxial strain test, LDCUX-2, are shown in Figures A.1 and A.2. The peak vertical and lateral pressures applied to the specimen in this test are 5 ksi (34.5 MPa) and 1.6 ksi (11.0 MPa), respectively. The records shown in Figure A.1 are from the two strain gages mounted in the center of the upper surface of the top end plate. The zero level for the testing machine strain gages in the dynamic tests is the strain induced by the preloading. For the two gages whose output is shown in Figure A.1, the zero corresponds to a tensile strain of 0.092%, determined from static readings taken before and after the machine preloading sequence. Therefore, the peak strain in the center of the upper surface of the top end plate during the test is about 0.2%. This corresponds to a maximum stress of about 60 ksi (0.91 GPa), safely below the 100-ksi (0.69-GPa) yield stress of the T-1 steel of which the plate is made. Results from several tests indicate that the strains in excess of the static 0.092% prestress vary linearly with the applied vertical pressure, P_V, as is expected for linear elastic response. Assuming this trend continues to higher pressures, the top plate will not yield for applied vertical pressures less than 11.2 ksi (77.2 MPa).

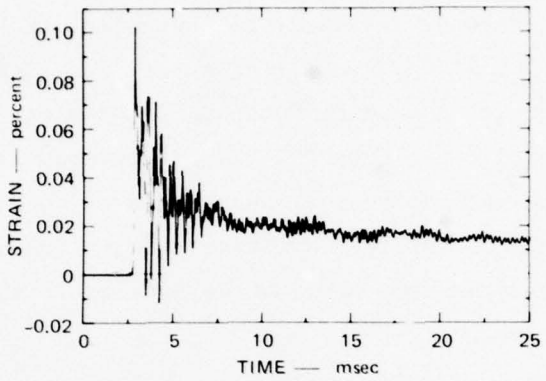

(a) STRAIN GAGE 11 — MOUNTED IN CENTER OF UPPER SURFACE OF THE TOP END PLATE

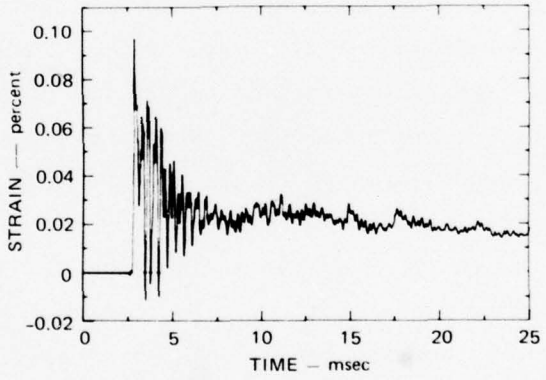

(b) STRAIN GAGE 12 — MOUNTED IN CENTER OF UPPER SURFACE OF THE TOP END PLATE

MA-4121-82

FIGURE A.1 STRAIN GAGE RECORDS FROM LDCUX-2. GAGES MOUNTED IN CENTER OF UPPER SURFACE OF THE TOP END PLATE (P_V = 5 ksi, P_H = 1.6 ksi)

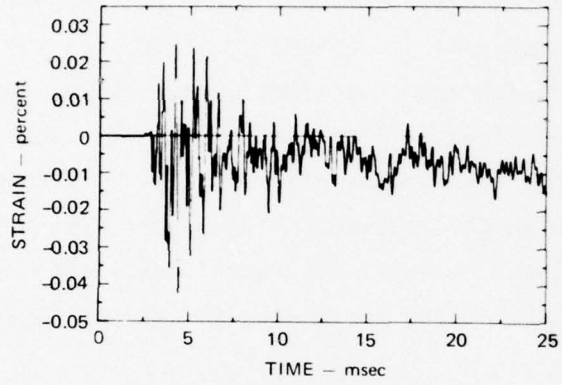

(a) STRAIN GAGE 9 – MOUNTED NEAR TOP OF STUD

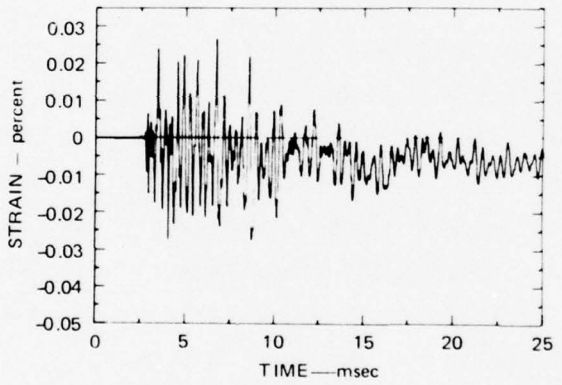

(b) STRAIN GAGE 10 – MOUNTED NEAR BOTTOM OF STUD

MA-4121-83

FIGURE A.2 STRAIN GAGE RECORDS FROM LDCUX-2. GAGES MOUNTED AT OPPOSITE ENDS OF SAME STUD (P_V = 5 ksi, P_H = 1.6 ksi)

The strain gage records shown in Figure A.2 are from gages mounted at opposite ends of a single stud. The zero level for these records is the static strain induced by pre-tensioning the studs, 0.15%, determined from readings taken before and after the machine preloading sequence. The peak strain reached in the stud, then, is about 0.2%. This corresponds to a maximum stress of 60 ksi (0.41 GPa) in the stress-relieved diameter length of the stud, well below the 180-ksi (1.24-GPa) yield stress of the 4340 steel used to make the studs. Results from several tests indicate that the dynamic component of the strain in the studs varies linearly with the applied vertical pressure, as did the strain in the top end plate. However, at the 11.2-ksi (77-MPa) limit for elastic response in the top end plate, the stress in the studs is only 80 ksi (0.54 GPa).

A.3 ESTIMATE OF MACHINE LIFE

Analysis of similar strain data from this and other tests suggests that, in addition to the stresses in the top end plate, low cycle fatigue of the studs is a limiting constraint on operating pressures. As just described, the stud loading consists of the static pre-tension plus an oscillatory stress induced by the explosions in the charge chambers. Since the maximum stress in the studs is well below the yield stress of 180 ksi (1.24 GPa), any failure would be produced by fatigue at the stress concentrations in the threaded lengths.

The peak dynamic stresses determined from the strain records vary linearly with applied vertical pressure, as expected. About five cycles of stress were near the maximum value in each test. The remainder of the 100 or so oscillations had peaks less than half the maximum value. Assuming a desired lifetime of 500 tests, the total number of cycles at the maximum dynamic stress σ_D is 2500 and the number of cycles at less than half the maximum dynamic stress is 50,000. When we plot the two points σ_D, 2500 and 0.5 σ_D, 50,000 on a stress versus cycles-to-failure diagram for high strength steel, we find that low cycle fatigue at 2500 cycles is by far the more critical condition over high cycle fatigue from the 50,000 low-stress oscillations.

Figure A.3 shows a Goodman diagram for 4340 steel with σ_{ult} = 185 ksi, (1.28 GPa). Assuming that the low cycle fatigue limit is 0.8 σ_{ult} and that the stress concentration factor at the bolt threads is k = 3.5 (a reasonable value for American National threads), then the operating point defined by the 45-ksi (0.31-GPa) static stress and the dynamic stress 3.5 x 33 ksi (0.23 GPa) = 115.5 ksi (0.8 GPa) lies on the low cycle fatigue limit. As mentioned in the previous paragraph, the vertical loading pressure that corresponds to a dynamic stress of 33 ksi (0.23 GPa) is 11 ksi (76 MPa). Therefore, the machine can be operated indefinitely (perhaps a thousand or so shots) at the 11-ksi (76-MPa) level.

A.4 EXPLOSIVE REQUIREMENTS

The explosive used to provide the loading pressures in the dynamic tests is a low-density mixture of PETN and microspheres, 9 to 1 by weight. Microspheres are tiny, inert plastic spheres that are mixed with the PETN to slow the rate of detonation and reduce the initial explosive pressure from more than 200 kbar (20 GPa) down to about 7 kbar (0.7 GPa). The PETN/microsphere mixture is packed into cylindrical paper canisters to a density between 0.235 mg/mm^3 and 0.245 mg/mm^3. The amount of explosive that must be used to obtain a specified loading pressure is shown in Figure A.4 for both the vertical and lateral charge chambers.

The solid symbols in Figure A.4 are results of computer simulations of the explosive gases flowing from the charge chamber, through the orifice plate, into the mixing chamber, through the baffle plate, and finally loading the specimen. The results indicate that the peak pressure obtained increases linearly with the charge mass for both chambers, and that the peak lateral pressure is slightly higher than the peak vertical pressure for the same size explosive charge.

The open symbols in Figure A.4 are results from two dynamic uniaxial strain tests, LDUX-9 and LDUX-10. Results from the first eight tests are not plotted because in those tests the area of the unconstricted holes through the orifice plates was much larger than that of the constricted holes in the last two tests. The calculated pressures are for the current

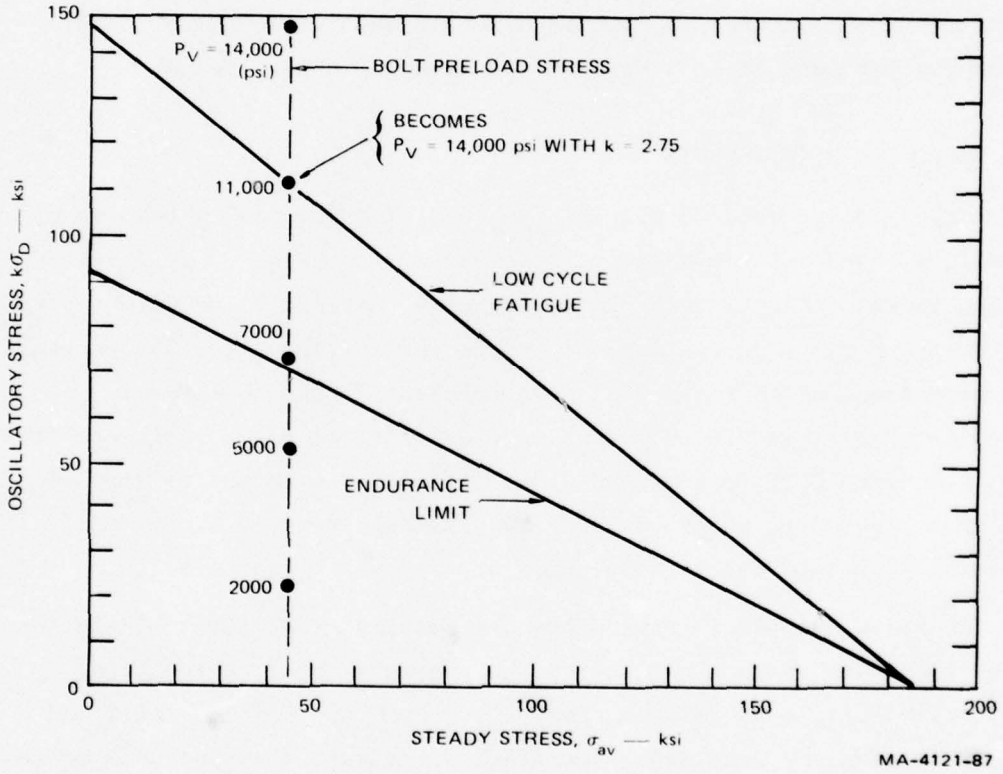

FIGURE A.3 GOODMAN DIAGRAM FOR 4340 STEEL, σ_{ult} = 185 ksi. STRESS CONCENTRATION FACTOR, k = 3.5

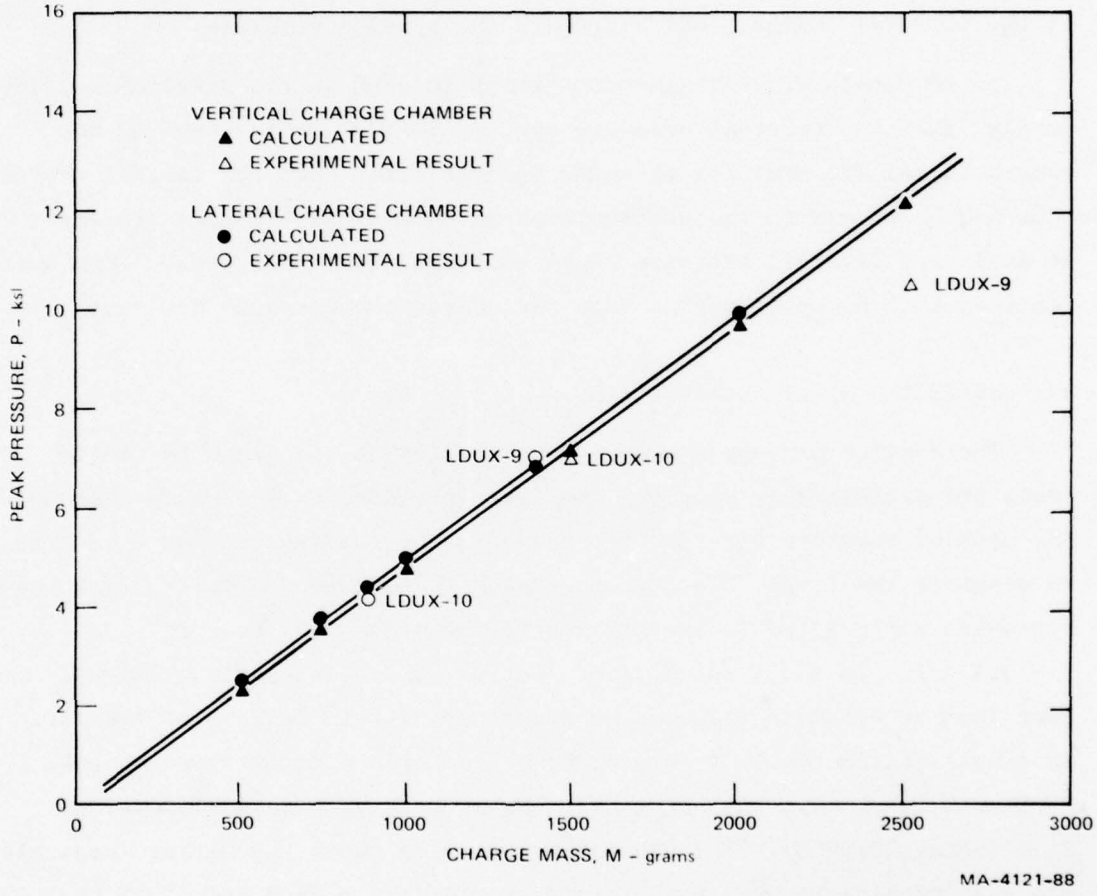

FIGURE A.4 CALCULATED AND EXPERIMENTAL PEAK DYNAMIC PRESSURES AS A FUNCTION OF EXPLOSIVE CHARGE SIZE FOR BOTH THE VERTICAL AND LATERAL CHARGE CHAMBERS.

hole configurations in the orifice plates and vent rings, and to compare these calculated pressures with those obtained in the first eight tests is not valid. Agreement between the calculated pressures and the experimental results is very good except for the vertical pressure in LDUX-9, where the experimental result is about 15 percent lower than the calculated pressure. The difference is attributable to observed venting of the vertical chamber, which reduced the applied pressure.

To be consistent with the constraint imposed in the previous section, namely, that the vertical pressure applied to the specimen should not exceed 11 ksi (76 MPa) for extended machine life, then the largest charge that may be placed in the vertical charge chamber is 2.28 kg. Further, to achieve a vertical pressure equal to 1 kbar (100 MPa), the charge mass required is 3.00 kg, assuming that the charge chamber does not vent.

A.5 ESTIMATED STATIC CAPABILITIES

The maximum pressures that can be applied to specimens in static tests are estimated by equating the force provided by the studs that hold the machine together with the force due to the loading pressures tending to separate the rings. The force holding the machine together after the hydraulic nut preload is transferred to the mechanical nuts is $F = 3.4 \times 10^6$ lb (15×10^6 N) (see Section 2.3). The maximum lateral test chamber pressure that can be contained by this force (for example, in a hydrostatic test) is determined by the area circumscribed by the O-rings between test chamber rings. These O-rings have a diameter of 14.2 inches (0.36 m). The chamber pressure to burst the O-ring (separate the test machine rings) is therefore $p = 4F/\pi D^2 = 21.8$ ksi (0.15 GPa). If the test is performed with the hydraulic nuts still pressurized, the reaction force is 20% larger, so that the bursting pressure is increased to 26.2 ksi (0.18 GPa). However, in either case, we would use a safety factor of 1.25 (remote machine operation), so that the operating pressures are 17.4 ksi (0.12 GPa) with mechanical nuts and 21.0 ksi (0.15 GPa) with the hydraulic nut pressure maintained.

For uniaxial strain and triaxial tests, the required lateral chamber pressure is usually much less than the vertical chamber pressure, so that vertical pressure is the controlling limit. The vertical chamber O-rings are at the 12-inch (0.3-m) diameter of the test rock; therefore, the vertical chamber burst pressure is $4F/\pi D^2$ = 30.5 ksi = 2.1 kbar (0.21 GPa). Thus, static uniaxial strain tests to the 2-kbar level are within the machine's capability. This assumes, of course, that the lateral confining pressure does not exceed the 1.2- or 1.5-kbar (0.12- or 0.15-GPa) limit of the lateral chamber.

APPENDIX B

MACHINE PARTS

This appendix contains a list of all machine parts, the part numbers, the drawing numbers, and a few other pieces of similar information. Figure B.1 shows an assembly drawing of the testing machine in the dynamic triaxial configuration. Each machine component is identified by its part number, which may then be used to find information regarding that part in one of the two parts lists included in this appendix. The first of these lists (Table B.1) includes parts numbered 5 through 59; the second (Table B.2) includes parts 100 through 112. The parts contained in the first list were fabricated especially for this testing machine, whereas the parts contained in the second list are commercially available.

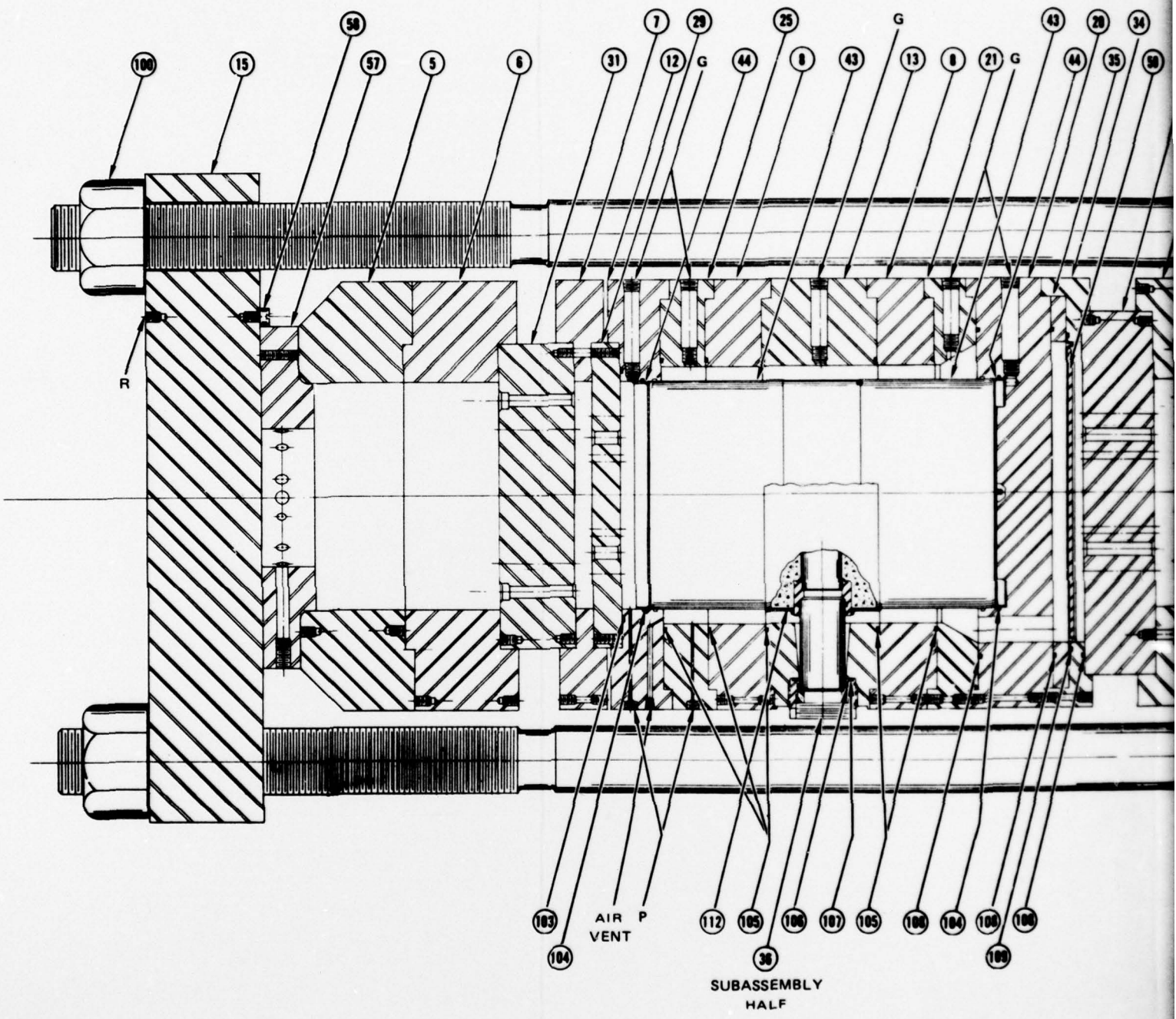
100
15
58
57
5
6
31
7
29
12
G
44
25
8
43
G
13
8
21
G
43
44
20
35
34
30
R
103
104
AIR VENT
P
112
105
36
106
107
105
108
104
108
109
108
SUBASSEMBLY HALF

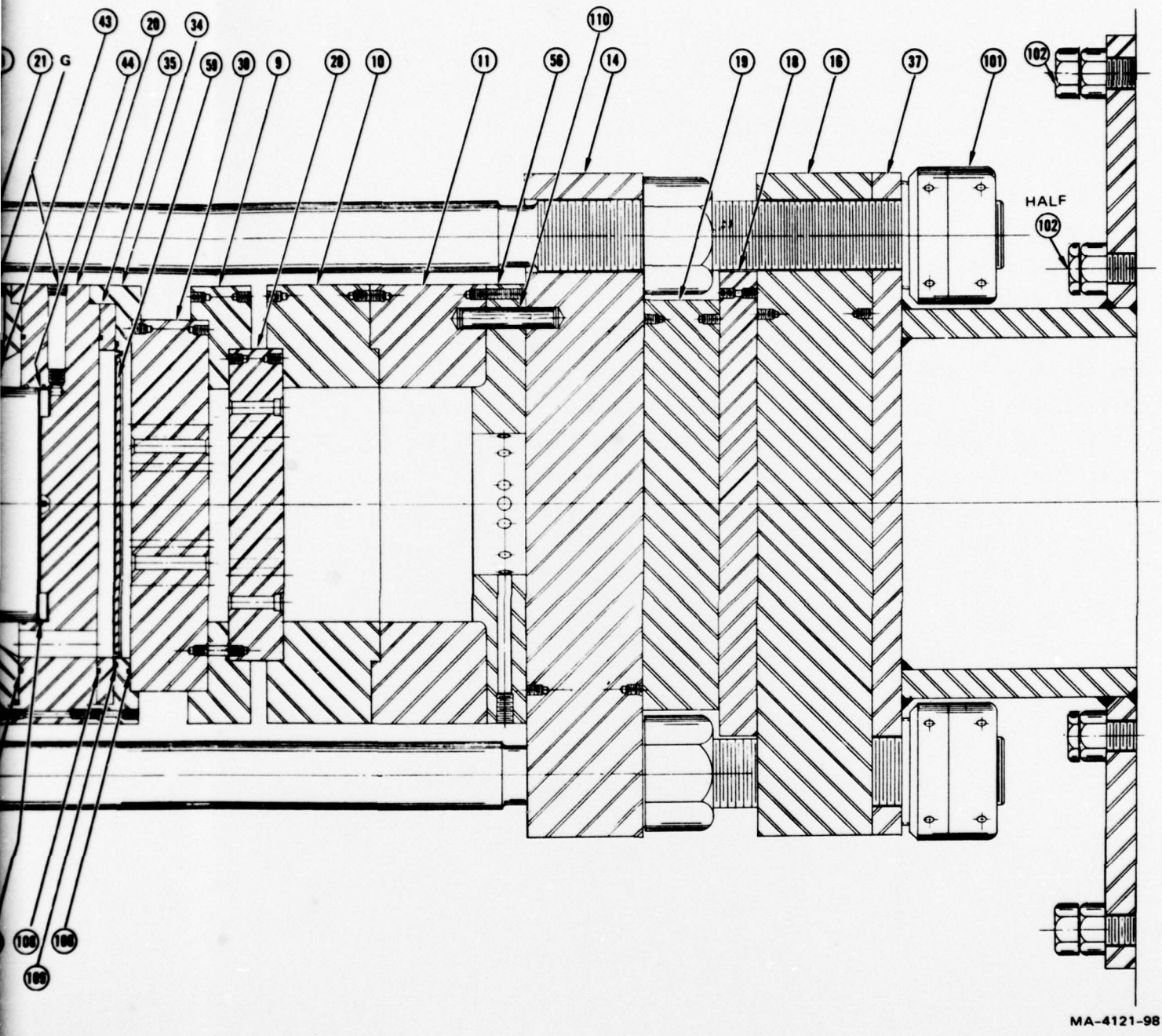

FIGURE B.1 ASSEMBLY DRAWING OF TESTING MACHINE IN THE DYNAMIC TRIAXIAL CONFIGURATION WITH PART NUMBERS INDICATED.

Table B.1. Large Tester Parts List--Special Parts

Part Name	Part Number	Drawing Number	Quantity	Material	Heat Treatment or Yield Strength
Upper Vertical Charge Chamber Ring	5	D-3743-5	1	4142 Steel	R_c 30-32
Lower Vertical Charge Chamber Ring	6	D-3743-6	1	4142 Steel	R_c 30-32
Vertical Mixing Chamber Ring	7	D-3743-7	1	4142 Steel	R_c 30-32
Lateral Chamber Spacer Ring	8	D-3743-8	2	4142 Steel	R_c 30-32
Lateral Mixing Chamber Ring	9	D-3743-9	1	4142 Steel	R_c 30-32
Upper Lateral Charge Chamber Ring	10	D-3743-10	1	4142 Steel	R_c 30-32
Lower Lateral Charge Chamber Ring	11	D-3743-10	1	4142 Steel	R_c 30-32
Specimen Vertical/Lateral Sealing Ring	12	D-3743-12	1	4142 Steel	R_c 30-32
Lateral Chamber Tunnel Ring	13	D-3743-13	1	4142 Steel	R_c 30-32
Bottom End Plate	14	D-3743-14	1	T-1 Steel	σ_y = 100 ksi
Top End Plate	15	D-3743-15	1	T-1 Steel	σ_y = 100 ksi
Spool End Plate	16	D-3743-16	1	T-1 Steel	σ_y = 100 ski

Part Name	Part Number	Drawing Number	Quantity	Material	Heat Treatment or Yield Strength
Backup Nut Spacer Plate, Lower	18	D-3743-18	1	10-15-1020 Steel	---
Backup Nut Space Plate, Upper	19	D-3743-19	1	10-15-1020 Steel	---
Specimen Receiver Plate	20	D-3743-20	1	4140 Steel	R_c 30-32
Lateral Chamber Reducer Ring	21	D-3743-21	1	T-1 Steel	σ_y = 100 ksi
Lateral Chamber Adaptor Close-off Ring	23	D-3743-23	1	T-1 Steel	σ_y = 100 ksi
Lateral Chamber Top Ring	25	D-3743-25	1	4142 Steel	R_c 30-32
Static Top Vertical/ Lateral Seal Plate	27	D-3743-27	1	4140 Steel	R_c 30-32
Lateral Chamber Orifice Plate	28	D-3743-28	1	4340 Steel	R_c 32-37
Vertical Chamber Baffle Plate	29	D-3743-29	1	ALMAR 18-300	σ_y = 300 ksi
Lateral Chamber Baffle Plate	30	D-3743-30	1	4340 Steel	R_c 32-37
Vertical Chamber Orifice Plate	31	D-3743-31	1	4340 Steel	R_c 32-37

Part Name	Part Number	Drawing Number	Quantity	Material	Heat Treatment or Yield Strength
Stud	33	D-3743-33	15	4340 Steel	σ_y = 180 ksi
Bellofram Ring	34	D-3743-34	1	T-1 Steel	σ_y = 100 ksi
Bellofram Clamping Ring	35	D-3743-35	1	4142 Steel	R_c 30-32
Assembly Mounting Pad	37	D-3743-37	1	1015-1020 Steel	---
Specimen Copper Cap	43	A-3743-43	30	Copper	---
Copper Sealing Cup	44	A-3743-44	30	Copper	---
Stud Alignment Ring	45	D-3743-45	1	Al 5052	H32
Aluminum Dummy Specimen	46	C-3743-46	1	Aluminum	---
Entry Portal	48	C-3743-48	2	4142 Steel	---
Tunnel Retaining Ring	49	C-3743-49	2	Brass	---
Tunnel Entry Tube	50	C-3743-50	2	ALMAR 18-300	σ_y = 300 ksi
Rock Specimen End Fitting	51A	C-3743-56A	1	ALMAR 18-300	σ_y = 300 ksi
Rock Specimen End Fitting	51B	C-3743-56B	5	ALMAR 18-300	(1) σ_y = 300 ksi 4 σ_y = 250 ksi
Photographic Mirror Support	53	D-3743-53	1	Al 6061	T6

Part Name	Part Number	Drawing Number	Quantity	Material	Heat Treatment or Yield Strength
Hydraulic Nut Washer	54	C-3743-54	30	T-1 Steel	σ_y = 100 ksi
Lateral Chamber Vent Ring	56	D-3743-56	1	T-1 Steel	σ_y = 100 ksi
Vertical Chamber Vent Ring	57	D-3743-57	1	T-1 Steel	σ_y = 100 ksi
End Plate Aligning Pin	58	A-3743-58	3	Mild Steel	---
Bellofram Protector Plate	59	C-3743-59	6	Al 6061	T6

Table B.2. Large Tester Parts List--Commercial Parts

Part Name	Part Number	Drawing Number	Quantity	Supplier
Mechanical Nuts	100		12	
Hydraulic Nuts	101		12	Terra Tek, Inc.
Anchor Stud Nuts	102		12	
O-Ring 2-279	103	D-3743-12	1	Parker
O-Ring 2-278	104	D-3743-12	4	Parker
O-Ring 2-280	105	D-3743-8, -13, -25	3	Parker
O-Ring 2-229	106	C-3743-48	4	Parker
O-Ring 2-232	107	C-3743-48	2	Parker
O-Ring 2-283	108	D-3743-34	3	Parker
Bellofram	109	----	1	Parker
Centering Dowel	110	----	4	
O-Ring Special Cut	111	D-3743-23	1	Parker
Wilson Seal	112	----	1	

DISTRIBUTION LIST

DEPARTMENT OF DEFENSE

Assistant to the Secretary of Defense
Atomic Energy
ATTN: Executive Assistant

Defense Advanced Rsch. Proj. Agency
ATTN: TIO

Defense Documentation Center
Cameron Station
12 cy ATTN: DD

Defense Intelligence Agency
ATTN: DB-4C2, T. Ross
ATTN: RDS-3A

Defense Nuclear Agency
ATTN: RAEV
ATTN: DDST
ATTN: STVL
3 cy ATTN: SPSS
4 cy ATTN: TITL

Field Command
Defense Nuclear Agency
ATTN: FCPR
ATTN: FCTMOF

Field Command Test Directorate
Test Construction Division
Defense Nuclear Agency
2 cy ATTN: FCTC, J. LaComb

Joint Strat. Tgt. Planning Staff
ATTN: NRI-STINFO, Library

Livermore Division, Field Command, DNA
Department of Defense
Lawrence Livermore Laboratory
ATTN: FCPRL

Under Secretary of Defense for Rsch. & Engrg.
Department of Defense
ATTN: Strategic & Space Systems (OS)

WWMCCS System Engineering Org.
2 cy ATTN: T. Neighbors

DEPARTMENT OF THE ARMY

Chief of Engineers
Department of the Army
ATTN: DAEN-MCE-D
ATTN: DAEN-RDM

Construction Engineering Rsch. Lab.
Department of the Army
ATTN: CERL-SL

Deputy Chief of Staff for Ops. & Plans
Department of the Army
ATTN: MOCA-ADL

Deputy Chief of Staff for Rsch. Dev. & Acq.
Department of the Army
ATTN: DAMA-AOA-M

DEPARTMENT OF THE ARMY (Continued)

U.S. Army Ballistic Research Labs
ATTN: DRDAR-BLE, J. Keefer
ATTN: DRXBR-X, J. Meszaros
ATTN: DRXBR-BLE, W. Taylor
ATTN: Technical Library

U.S. Army Cold Region Res. Engr. Lab.
ATTN: S. Blouin

U.S. Army Communications Command
ATTN: Technical Reference Division

U.S. Army Engineer Center
ATTN: ATSEN-SY-L

U.S. Army Engineer Dist., Omaha
ATTN: MROED-D, C. DiStefano

U.S. Army Engineer Div., Huntsville
ATTN: HNDED-SR
3 cy ATTN: C. Huang

Harry Diamond Laboratories
Department of the Army
ATTN: DELHD-NP

U.S. Army Engineer Div., Ohio River
ATTN: ORDAS-L

U.S. Army Engr. Waterways Exper. Station
ATTN: J. Day
ATTN: G. Jackson
ATTN: J. Ballard
ATTN: L. Ingram
ATTN: Library
ATTN: W. Flathau
ATTN: J. Drake
ATTN: P. Mlakar

U.S. Army Nuclear & Chemical Agency
ATTN: Library

DEPARTMENT OF THE NAVY

Civil Engineering Laboratory
Naval Construction Battalion Center
ATTN: H. Haynes
ATTN: S. Takahashi
ATTN: R. Odello
ATTN: Code L08A
ATTN: L51, W. Shaw

Naval Cmd., Control & Communications
ATTN: OP-943

Naval Electronic Systems Command
ATTN: PME 117-21A, B. Kruger

Naval Facilities Engineering Command
ATTN: E. Violett
ATTN: Code 09M22C

Naval Postgraduate School
ATTN: Code 2124

DEPARTMENT OF THE NAVY (Continued)

Naval Research Laboratory
ATTN: Code 2627

Naval War College
ATTN: Code E11

Strategic Systems Project Office
Department of the Navy
ATTN: NSP-43

Naval Surface Weapons Center
ATTN: Code F31

DEPARTMENT OF THE AIR FORCE

Air Force Institute of Technology, Air University
ATTN: Library

Air Force Systems Command
ATTN: DLCA, Maj Celec

Air Force Weapons Laboratory
ATTN: DE, M. Plamondon
ATTN: NT, D. Payton
ATTN: SUL

Deputy Chief of Staff
Research, Development, & Acq.
Department of the Air Foce
ATTN: AFRDQSM

Deputy Chief of Staff
Programs & Analyses
Department of the Air Force
ATTN: PACSM

Foreign Technology Division, AFSC
ATTN: NICD, Library

Space & Missile Systems Organization/MN
Air Force Systems Command
ATTN: MNNH
ATTN: MNN

Strategic Air Command/XPFS
Department of the Air Force
ATTN: NRI-STINFO, Library

U.S. Air Force/XO
ATTN: XODC

DEPARTMENT OF ENERGY

Department of Energy
Library Room G-042
ATTN: Doc. Con. for Classified Library

Lawrence Livermore Laboratory
ATTN: Doc. Con. for H. Heard
ATTN: Doc. Con. for L-96, L. Woodruff
ATTN: Doc. Con. for Tech. Info. Dept. Library
ATTN: Doc. Con. for L-21, D. Oakley

Los Alamos Scientific Laboratory
ATTN: Doc. Con. for B. Killian
ATTN: Doc. Con. for J. Johnson
ATTN: Doc. Con. for L. Germaine
ATTN: Doc. Con. for Reports Library

DEPARTMENT OF ENERGY (Continued)

Oak Ridge National Laboratory
Union Carbide Corporation-Nuclear Division
X-10 Laboratory Records Department
ATTN: Doc. Con. for Technical Library

Sandia Laboratories
Livermore Laboratory
ATTN: Doc. Con. for Library & Sec. Class. Div.

Sandia Laboratories
ATTN: Doc. Con. for 3141
ATTN: Doc. Con. for L. Hill

OTHER GOVERNMENT AGENCIES

Department of the Interior
Bureau of Mines
ATTN: Technical Library

Department of the Interior
U.S. Geological Survey
Special Projects Center
ATTN: W. Twenhofel
ATTN: R. Carroll
ATTN: D. Snyder

Department of the Interior
U.S. Geological Survey
ATTN: D. Roddy

DEPARTMENT OF DEFENSE CONTRACTORS

Aerospace Corporation
ATTN: P. Mathur
ATTN: Technical Information Services

Agbabian Associates
ATTN: M. Balachanda
ATTN: C. Bagge
2 cy ATTN: M. Agbabian

Applied Theory, Inc.
2 cy ATTN: J. Trulio

Avco Research & Systems Group
ATTN: Library, A830

The BDM Corporation
ATTN: Corporate Library

The Boeing Company
ATTN: K. Friddell
ATTN: T. Berg
ATTN: H. Leistner
ATTN: R. Dyrdahl
ATTN: Aerospace Library
ATTN: J. Wooster

California Institute of Technology
ATTN: D. Anderson

California Research & Technology, Inc.
ATTN: Library
ATTN: K. Kreyenhagen
ATTN: S. Shuster

University of California
ATTN: R. Goodman
ATTN: N. Cook

DEPARTMENT OF DEFENSE CONTRACTORS (Continued)

Calspan Corporation
ATTN: Library

Civil/Nuclear Systems Corporation
ATTN: J. Bratton

University of Dayton
Industrial Security Super., KL-505
ATTN: H. Swift

University of Denver
Colorado Seminary
Denver Research Institute
ATTN: Sec. Officer for J. Wisotski

EG&G Washington Analytical Services Center, Inc.
ATTN: Library

Electromechanical Sys. of New Mexico, Inc.
ATTN: R. Shunk

Eric H. Wang
Civil Engineering Rsch. Fac.
The University of New Mexico
ATTN: G. Leigh
ATTN: N. Baum

Foster-Miller Associates, Inc.
ATTN: J. Hampson for E. Foster

Franklin Institute
ATTN: Z. Zudans

General Electric Co.-TEMPO
Center for Advanced Studies
ATTN: DASIAC

IIT Research Institute
ATTN: R. Welch
ATTN: M. Johnson
ATTN: Documents Library

University of Illinois
Consulting Services
ATTN: W. Hall
ATTN: A. Hendron
ATTN: N. Newmark

Institute for Defense Analyses
ATTN: Classified Library

J. H. Wiggins Co., Inc.
ATTN: J. Collins

Kaman AviDyne
Division of Kaman Sciences Corp.
ATTN: Library

Kaman Sciences Corporation
ATTN: Library

Lockheed Missiles and Space Co., Inc.
ATTN: Technical Information Center
ATTN: T. Geers

Massachusetts Institute of Technology
ATTN: W. Brace

DEPARTMENT OF DEFENSE CONTRACTORS (Continued)

Merritt CASES, Inc.
ATTN: J. Merritt

City College of New York
Dept. of Civil Engineering
ATTN: C. Miller

Northwestern University
The Technology Institute
ATTN: T. Belytschko

Pacifica Technology
ATTN: G. Kent

William Perret
ATTN: W. Perret

Physics International Company
ATTN: C. Vincent
ATTN: D. Orphal
ATTN: E. Moore
ATTN: Technical Library
ATTN: F. Sauer

R&D Associates
ATTN: C. Knowles
ATTN: D. Rawson
ATTN: C. MacDonald
ATTN: Technical Information Center
ATTN: J. Lewis
ATTN: D. Shrinivasa
ATTN: R. Port

R&D Associates
ATTN: H. Cooper

The Rand Corporation
ATTN: A. Laura

Science Applications, Inc.
ATTN: Technical Library

Science Applications, Inc.
ATTN: Technical Library

Southwest Research Institute
ATTN: W. Baker
ATTN: A. Wenzel

SRI International
ATTN: B. Holmes
ATTN: G. Abrahamson
ATTN: H. Lindberg
ATTN: P. Senseny

Systems, Science & Software, Inc.
ATTN: D. Grine
ATTN: W. Wray
ATTN: R. Duff
ATTN: C. Archembeam
ATTN: Library
ATTN: T. Bache

Terra Tek, Inc.
ATTN: H. Pratt
ATTN: Library

DEPARTMENT OF DEFENSE CONTRACTORS (Continued)

Tetra Tech, Inc.
ATTN: Library

Texas A & M Research Foundation
ATTN: A. Rychlik

Texas A & M University System
c/o Texas A & M Research Foundation
ATTN: J. Handin

TRW Defense & Space Sys. Group
ATTN: Technical Information Center
ATTN: P. Huff
ATTN: P. Dai

TRW Defense & Space Sys. Group
San Bernardino Operations
ATTN: E. Wong

DEPARTMENT OF DEFENSE CONTRACTORS (Continued)

Universal Analytics, Inc.
ATTN: E. Field

Weidlinger Associates
Consulting Engineers
ATTN: M. Baron
ATTN: I. Sandler

Weidlinger Associates
Consulting Engineers
ATTN: J. Isenberg

Westinghouse Electric Corporation
Marine Division
ATTN: W. Volz